AALBORG UNIVERSITY
DENMARK

Characterization of fluorescein-labelled PVP-based polymeric nanocarriers & their uptake in mammalian cells.

Student report for short master thesis in the Nanotechnology

Students:

Name: Tushar Kumar, study number: 20177336

Name: Daniel Ameljan, study number: 20171765

Supervisor: Leonid Gurevich, Ph.D

AALBORG UNIVERSITY
STUDENT REPORT

Department of Materials and Production
Skjernvej 4, 9220 Aalborg East
Denmark

Abstract

Nanocarrier drug delivery systems are receiving increased attention as a new approach in medicine, particularly in cancer therapy. Nanocarriers offer many advantages compared to conventional drug delivery systems, such as protection of the drug load from degradation, increased drug efficacy and reduced toxicity hence minimizing side effects. In this master thesis we investigate self-assembly ability of amphiphilic block copolymer poly-N-vinyl-2-pyrrolidone modified with acrylic acid (PVP-OD AA 12kDa) containing thiooctadecyl-terminated block and its potential use as a platform for drug delivery. In order to fundamentally understand physiochemical properties of PVP-OD-AA, polymer was studied by FTIR spectroscopy and solvent compatibility was investigated. The results obtained from solvent compatibility study revealed ethanol as the best solvent for the polymer dissolution and subsequent modification via EDC/NHS chemistry. Furthermore, for conjugation of fluorescent dye to the acrylic acid present in the polymer structure, EDC/NHS chemistry was implemented with different activation strategies. For polymeric micelle preparation, three different methods, namely dialysis, direct dissolution and cosolvent evaporation were employed. DLS results showed a size distribution of 97nm (PdI 0,530), 168,6 (PdI 0,114) and 105,6nm (PdI 0,172) for direct dissolution, cosolvent and dialysis method respectively. PVP based polymeric micelles can be used to elucidate the uptake mechanism by mammalian cells, as the polymer will be fluorescently labelled so its fate upon cellular uptake can be studied independently from that of the hydrophobic load.

Title:

Characterization of Fluorescein-labelled PVP-based polymeric nanocarriers & their uptake in mammalian cells

Field:

Nanobiotechnology

Project period:

September 2020 – January 2021

Participants:

Daniel Ameljan & Tushar Kumar

Supervisor: Leonid Gurevich

Page numbers: 94

Date of completion: 31-03-2021

Table of contents

1. Introduction

Over the past decades, nanotechnology has gone through impressive progress and found its invaluable applications in industry and medicine. Due to the recent rise and development of precisely controlled polymerization techniques, such as atom transfer radical polymerization (ATRP) and reversible addition-fragmentation chain transfer (RAFT), various block copolymers with carefully selected properties have been synthesized and their potential application in biomedical fields, especially in formation of novel drug delivery systems is incessantly studied.

Precise control over synthesis of various polymers and their structure gave an access to open new possibilities for drug delivery. Polymeric based drug delivery systems have revolutionized approach in battling various diseases and allowed to overcome limitations of traditional drug delivery methods, by protecting the encapsulated drug from degradation, control over its release and distribution, enhancing its efficiency and bioavailability, reducing unwanted side effects and most importantly allowing precise targeting to tissues of interest [1].

Among all polymeric drug delivery systems, polymeric micelles have been receiving a special attention due to their unique core-shell structure, which allows incorporation of highly hydrophobic drugs without necessity of any chemical modification with their simultaneous protection from unwanted interactions with biological compounds. Polymeric micelles are defined as core-shell nanoparticles formed by self-assembly process of block or graft copolymers in a selective solvent [1]. Possibility of tailoring constituent blocks of polymeric micelles gives a prominent chance for constructing sophisticated drug delivery systems with smart functionalities. By conjugation of specific ligands, such as antibodies, peptides and fluorescent molecules, polymeric micelles can serve as multifunctional platform for targeted drug delivery and molecular imaging.

The main aim of this master thesis is to study the self-assembly ability and creating fluorescently labelled nanocarriers based on novel amphiphilic block copolymer, poly-N-vinyl-2-pyrrolidone, modified with acrylic acid and thiooctadecyl serving as a hydrophobic block (PVP-OD-AA, figure 1). Produced nanocarriers will be used to elucidate the uptake mechanism by model mammalian cells. Since polymer will be fluorescently labelled, its fate upon cellular uptake can be evaluated independently from that of the hydrophobic load, which also is chosen to be fluorescent, but in a different range.

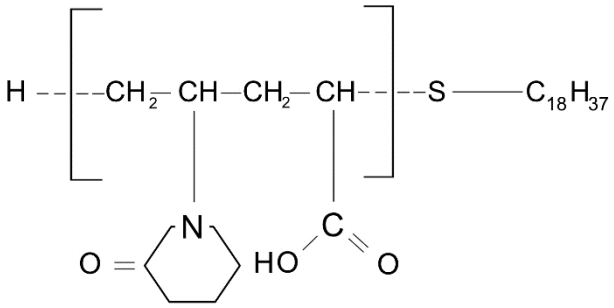

Figure 1: PVP-OD-AA block copolymer.

1.1 Polymeric micelles

Polymeric micelles (PMs)(Figure 1.1) are defined as nanoparticles with a dynamic core-shell structure, formed by spontaneous self-assembly process of amphiphilic block or graft copolymers in selective solvents above their CMC (critical micelle concentration) value. Usually, they exhibit a spherical shape in the size range of 10-100nm, nonetheless cylindrical or vesicular supramolecular structures can be formed as well. The main phenomenon behind micelle formation is minimization of interfacial free energy of block copolymers placed in a solvent with contribution of various driving forces such as hydrophobic interaction, π- π interaction, electrostatic forces and even polymer-metal complex formation [1]. Self-assembly process of polymeric micelles is usually a result of hydrophobic interaction between hydrophobic segment of block copolymer with surrounding water molecules, nonetheless formation of micelles by electrostatic interactions (usage of charged polymer with oppositely charged molecules – poly-ion complex micelles), complexation via hydrogen bonding [2] and metal-ligand interactions [3] have been reported as well, where all approaches were described as non-covalent methods for micelle formation [4].

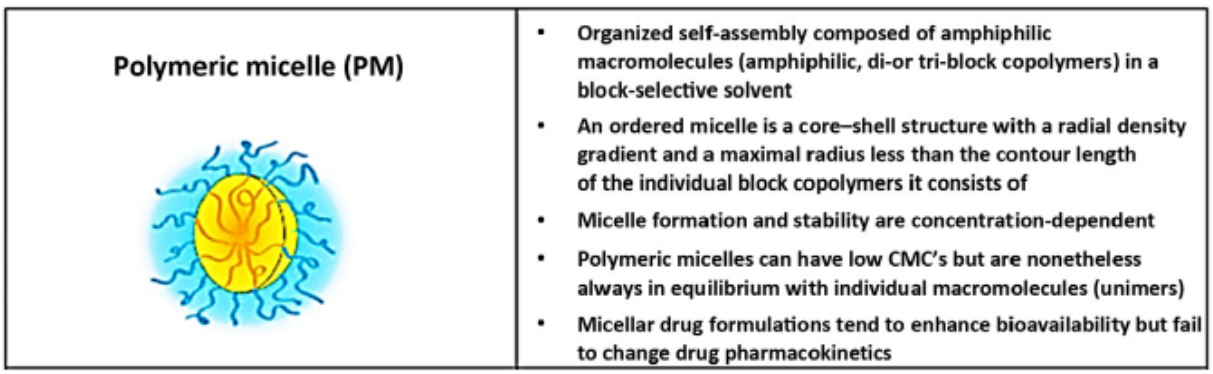

Figure 1.1: General characteristics of polymeric micelles. Adapted from [5].

Amphiphilic di-block copolymers (ABC's) structure is divided in two regions within the same molecule - namely hydrophobic and hydrophilic segment, which exhibit different physical and chemical properties and therefore are capable of undergoing phase separation as a consequence of chain behaviour in solvents that particularly dissolve one of the blocks [6]. If concentration of the amphiphilic copolymer in aqueous solution reaches or exceeds the CMC value, hydrophobic part of ABC's starts to assemble in order to minimize the contact area with surrounding water molecules [4]. As a consequence, so-called "hydrophobic core" is created, whereas hydrophilic segment is positioned between the core and external aqueous environment, forming a shell. This hydrophilic shell works as an interface between the surrounding aqueous environment and hydrophobic segment and therefore stabilizes the newly established structure [6]. Removal of hydrophobic part of polymer chain from the aqueous environment and reestablishment of hydrogen bond network in water results in decrease of the free energy of the system and leads to the phenomenon of spontaneous formation of supramolecular core-shell nanostructures, called polymeric-micelles (Figure 1.2) [4,6]. Both components of polymeric micelles, it is hydrophobic core and hydrophilic shell are characterized by different properties and different interaction with a solvent. Compared with micelles created from typical surfactant molecules, they exhibit much better thermodynamic and kinetic stability and lower CMC values [1].

Polymeric micelles, because of their remarkable core-shell structure, offer a promising approach for drug delivery system of highly hydrophobic compounds with poor bioavailability. Core of the micelle is used as a segment to entrap the hydrophobic drug, whereas corona is responsible for protection from Reticuloendothelial system (RES), for example by preventing opsonization and therefore ensuring long circulation time in the body [1].

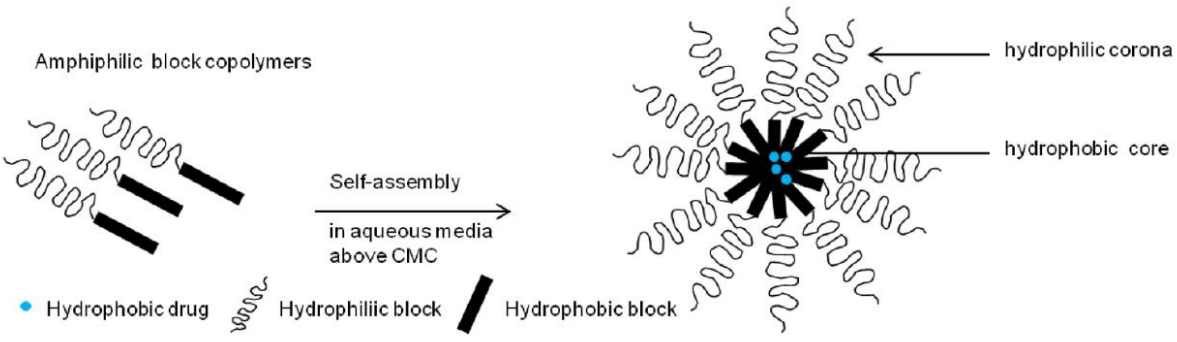

Figure 1.2: Process of self-assembly and drug encapsulation of amphiphilic block copolymers in aqueous environment. Adapted from [7].

As mentioned before, the inner hydrophobic core allows incorporation of weakly water-soluble molecules, which results in their better stability and increase in bioavailability [1]. Recent studies showed that incorporation of hydrophobic drug into the polymeric micelle

core results in increase of water-solubility of particular drugs even to thousands fold [8]. One of the main reasons behind this phenomenon is presence a hydrophobic compartment, where drugs can be incorporated by chemical conjugation, ionic interactions or physical entrapment (caused by hydrophobic effect). The mechanism of drug incorporation is dependent on physiochemical features of the polymer and properties of used drug [9]. For example, Burt, H and co-workers [10] successfully incorporated anticancer drug paclitaxel (PTX) into a polymeric micelle based on poly(D,L-lactide)-MePEG di-block copolymer, which leaded to one thousand fold increase in PTX solubility in the aqueous environment.

1.1.1 Critical micelle concentration

Before reaching CMC value, polymer chains exist in the solution as unimers, nonetheless at or above CMC, they start to self-assemble into micelles and both micelles and unimers are present in the solution [1]. Below the CMC, the increase of amphiphilic polymer concentration leads to increase in number of amphiphilic molecules on air-water interface. When concentration of ABC's reaches CMC, both the solution and interface are saturated with unimers. Even though individual polymer chains in the micelle are in dynamic equilibrium, PM's exhibit superior thermodynamic and kinetic stability compared to other drug delivery system [1]. In comparison to nanoparticles, which exhibit static and stable structure, micelles display a dynamic structure – surfactants or amphiphilic copolymers forming a micelle can be freely exchanged with unimers / free surfactant present in the solution. [11]

Micellization process can be described by standard change in the free energy of the system:

$$\Delta G^{\circ}_{\mathrm{mic}} = RT \ln(\mathrm{CMC}) \qquad (1.1)$$

R – gas constant; *T*- temperature of the system; *CMC* – critical micelle concentration

For polymeric micelles CMC value is around 1000-fold lower than for typical surfactant molecules, that is why even if they are highly Diluted below the CMC, PM's shows way slower dissociation into unimers (kinetic stability) caused by molecular effect and entangling of the micelle core-forming polymers [1].

In order to achieve a thermodynamically stable PM's, the copolymer concentration should be above the CMC value. The CMC value is dependent on the hydrophilic-lipophilic balance (HLB) of block-copolymer used. Increase of the hydrophobic block with hydrophilic part kept constant, leads to lower CMC values. In comparison to micelles formed from

traditional low-molecular weight surfactants (CMC 10^{-3} – 10^{-4} M), PM's display very low CMC values (10^{-6} – 10^{-7} M), allowing them to preserve a micellar structure even upon high Dilution [6]. Kinetic stability is usually taken into consideration, when concentration of block-copolymer is reduced below the CMC value. Since drug delivery conditions are nonequilibrium, kinetic stability of polymeric micelles plays more important role than their thermodynamic stability. Compared to micelles assembled from low molecular weight surfactants, the kinetic stability of polymeric micelle is way higher for the stiff/bulky inner core structure, which leads to slower disassembly rate of PMs at concentrations below CMC. Consequently, it allows polymeric micelles to preserve structural integrity and prevent drug leakage for longer time, hence enhancing the bioavailability [4].

1.1.2 Polymeric micelles as drug delivery systems

Drug delivery system (DDS) is defined as formulation that allows introduction of therapeutic agent into the body with increased efficacy and safety. Among all DDS, polymeric based drug delivery systems received special attention due to development of controlled and very precise polymerization techniques, such as ATRP and RAFT, which allows creation of various block copolymers suitable for biomedical applications [12]. Polymeric drug delivery systems are divided in three basic categories, namely colloidal carriers (for example micelles, polymeric nanoparticles and nanogels), polymer-drug conjugates and polymeric hydrogels. Although there is no universal system, which could be efficiently used for various classes of therapeutic agents, polymeric micelles seems to be in the centre of attention for drug delivery applications. This is mainly because of their unique core-shell structure, which allows incorporation of highly hydrophobic drug into the micellar core, with simultaneous maintenance of water solubility due to the hydrophilic shell. As a drug delivery system, PM should be resistant to rapid dissociation upon Dilution and preserve a stable core-shell structure, before reaching targeted location. Polymeric micelles are well known for their structural, thermodynamic and kinetic stability, which are a consequence of the entanglement of polymer chains in the hydrophobic core [4,13].

PMs are designed to obtain following crucial parameters in targeted drug delivery:

- Solubilization of hydrophobic drugs inside the core
- Controlled release of a drug
- Targeting a desired cell type or tissue/organ
- Exhibit biocompatibility, biodegradability and low toxicity.

Additional advantage of PM's over other drug delivery system is possibility of tailoring multifunctional polymeric micelles for simultaneous drug delivery, targeting and imaging.

These desired properties can be achieved by surface modification, usage of different monomers acting as building-blocks and varying block copolymer length ratio. This strategy might be extremely beneficial in order to battle complicated diseases like cancer, where a multi-facet approach is required [1,7,14]

1.1.3 Targeting strategies of polymeric micelles

When first polymeric drug delivery systems were formulated, it was believed that only one targeting strategy is possible, namely receptor-mediated approach (Figure 1.3). As a consequence of this belief, many systems based on conjugation of ligands, antibodies or peptides to outer shell of polymeric micelles were developed [14]. This strategy of battling various diseases with use of drug delivery systems is called “active targeting”, nonetheless recent studies presented other possibility. It was observed, that nanoparticles, polymeric micelles and polymer-drug conjugates exhibit prolonged circulation time in the blood and might passively accumulate in tumor cells, even without targeting ligands conjugated to them. Unregulated and aberrant growth of tumor vasculature in order to satisfy increasing demand of oxygen and nutrients makes endothelial cells loosely aligned with considerable gaps between them, leading to their high permeability. Additionally, growing tumor cells tend to compact lymph vessels, leading to their collapse and as a result lymphatic drainage from tumor cells is almost entirely supressed [7]. These two phenomena allows various nanoparticles not only to penetrate into tumor tissue, but also retain there, since decreased lymphatic drainage cannot remove them efficiently. This passive targeting strategy is based on EPR (Enhanced permeability and retention) effect and it leads to accumulation of nanoparticles in tumors with simultaneous increase in therapeutic index and decrease in undesirable side effect [14].

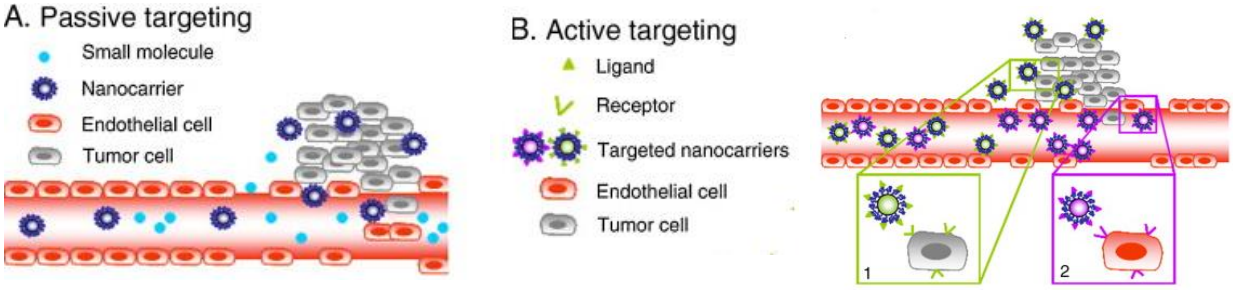

Figure 1.2: Illustrious comparison of passive targeting via EPR effect and active targeting with ligands. Adapted from [15].

1.2 Selection of polymers

Amphiphilic block copolymers are the Lego bricks for polymeric micelles containing distinct hydrophilic and hydrophobic block domains. The physicochemical properties of block copolymers directly influence the properties and in vivo interaction of polymeric micelles. For drug delivery purpose, a block-copolymer used for formation of micelles should:

- Spontaneously self-assemble in water
- Enhance drug solubility by several orders of magnitude
- Provide high loading efficiency
- Remain stable upon Dilution
- Biocompatible and non-toxic
- Be possible to produce on larger scale [11].

The structure of polymeric micelles based on the entropic driven micellar theory, exemplifies the inner core and the exterior corona arrangement of hydrophobic and hydrophilic segments of block copolymers respectively. Hydrophilic block represents the surface properties involved in disposition, distribution, and fate of the micelle in the body, whereas the hydrophobic core carries the biologically active moieties. It is worth to mention that critical micelle concentration (CMC) value of polymeric micelles is affected by the hydrophilic/hydrophobic balance of the block domains with taking the molecular weight of the copolymer into account [16].

Selection of polymeric blocks depends on the ideal characteristics of polymeric micelles (low toxicity, biocompatibility, targetability etc) and also the physicochemical properties of the active drug load. The most commonly utilized amphiphilic copolymers in polymeric micelles self-assembly includes di-block (A–B), triblock (A–B–A), and graft copolymers (Figure 1.3 and Table 1.1) [5].

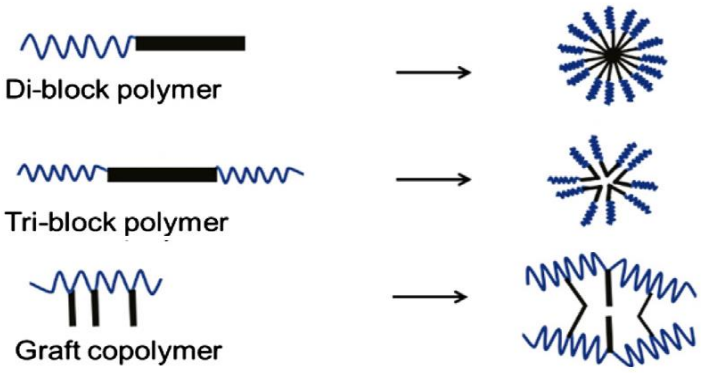

Figure 1.3: Representation of typical amphiphilic copolymers [5].

Table 1.1: Possible structures and few examples of amphiphilic copolymers [17]

Types of micelle-forming copolymers	Representation of structure[a]	Examples of copolymers
Block copolymers	Di-block AAAAAAABBBBBB	Poly(styrene)-b-PEO
	Tri-block AAAABBBBBAAAA	PEO-b-PPO-b-PEO
Graft copolymers	AAAAAAAAAAAA B B B B B B B	Stearic acid-grafted-chitosan oligosaccharide

1.2.1 Corona: The Hydrophilic Block Domain

The hydrophilic block domain of a copolymer controls the surface properties of the polymeric micelles which includes stealth behaviour in blood circulation and provides sites for surface modifications. It contributes to the stealth behaviour of the micelles by preventing the opsonization and uptake by reticuloendothelial system, and thus provides longer circulation time. The most commonly used polymers for the hydrophilic block belong to the polyether category such as polyethylene glycol (PEG) and polyethylene oxide (PEO). PEG has been the most widely used hydrophilic block for the construction of polymeric micelles involved in drug delivery. The meritorious properties of FDA approved PEG such as biocompatibility, stealth nature, multiple hydroxyl groups and non-toxic label makes it an excellent choice for corona. In the context of cancer therapeutics, PEG has been extensively used as a hydrophilic block for the delivery of drugs such as doxorubicin (DOX), paclitaxel (PTX) as well as camptothecin (CPT) [18].

Apart from the stealth behaviour, the hydrophilic block plays an important role in micellar stability in vivo in the presence of serum proteins as it has been observed that polymeric micelles become unstable in the vicinity of proteins [5]. It was observed that the introduction of PEG groups decreased the adsorption of plasma protein to micelles [19]. In addition to PEG, other polymers used for the hydrophilic block part are mentioned in table 1.2.

Table 1.2: List of most commonly used hydrophilic polymers for polymeric micelles preparation [5].

Polymers used for a hydrophilic portion
PEOz
Phosphorylcholine-based polymers
Poly(acrylic acid)
Carboxyl methyl Chitosan
PEO
PVP
PEG
Poly(*N*-isopropyl acrylamide)
Poly(vinyl alcohol)
Poly(vinyl alcohol-covinyloleate)
Oligomeric polyethyleneimine

PEOz, Poly(2-ethyl oxazoline); *PEO*, poly(ethylene oxide); *PVP*, poly(*N*-vinylpyrrolidone); *PEG*, poly(ethylene glycol).

1.2.2 Core: The Hydrophobic block

The hydrophobic block of a copolymer is involved in the overall formation of the micelle and acts a carrier for the active drug moiety. The hydrophobicity of the core forming block influences the CMC value of the micelles as it has been observed that increase in hydrophobicity causes decrease in the CMC [16]. Another important aspect of the design and choice of the hydrophobic block is the compatibility with the active drug load. The hydrophobic block can be tailored based on the desired properties of polymeric micelles with a wide variety of lipophilicity and structures. Some of the commonly used hydrophobic block in the area of cancer therapeutics are mentioned in table 1.3

Table 1.3: List of hydrophobic polymers used for preparation of polymeric micelles [5].

Polymers used for hydrophobic segment
PPO
PLGA
Poly(D,L-lactic acid)
Poly(D,L-lactic-*co*-glycolic acid)
PBLM
Polyester, for example, PCL, poly(lactic acid)
Polyamide, for example, poly (L-lysine), poly(β-amino ester)
PEG–PE
γ-Benzyl-L-aspartate
γ-Benzyl-L-glutamate
Sermine
PASP
Poly(glycolic acid)
PGlu
Phis
PAP

PAP, Poly(L-amino acid); *PASP*, poly(aspartic acid); *PBLM*, poly(*b*-benzyl-L-aspartate); *PCL*, poly (ε-caprolactone); *PEG-PE*, phosphatidylethanolamine; *PGlu*, poly(glutamic acid); *Phis*, poly(histidine); *PLGA*, poly(lactic-*co*-glycolic acid); *PPO*, poly(propylene oxide).

1.2.3 Poly(N-vinyl-2-pyrrolidone) polymer

In our study, we have tried to explore the remarkable self-assembly property of amphiphilic block copolymer based on 1-Vinyl-2-pyrrolidinone and acrylic acid (obtained as a courtesy of research group of Prof. Shtilman at Mendeleev University, Moscow)(Figure 1.4). PVP modified with acrylic acid offers a great possibility for functionalization with biomolecules and fluorescent dyes.

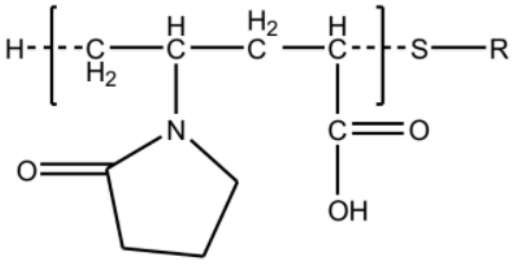

Figure 1.4: Block copolymer based on 1-Vinyl-2-pyrrolidinone and acrylic acid

The amphiphilic thiooctadecyl terminated poly-N-vinyl-2-pyrrolidone (PVP-OD) used in this study was synthesized by radical polymerization of N-vinyl-2-pyrrolidone using azobisisobutyronitrile (AIBN) as radical chain initiator and octadecyl mercaptan as chain transfer agent (Figure 1.5). It has been observed that free radical polymerization leads to atacticity in vinyl polymers exhibiting mainly amorphous arrangement unless the side group is small or polar in nature [20]. It can be interpreted that PVP-OD might be atactic with slight crystallinity due to the presence of polar pyrrolidone moiety. This information is crucial in understating the interaction of polymer chains with different solvents as the tacticity influences the solubility dynamics of a polymer in solution. Another important aspect of amphiphilic self-assembly is critical micellar concentration and in our case DPHT fluorescence spectroscopy was performed to evaluate the CMC value for PVP-OD 12KDa ~ 1.0 mmol/L [21].

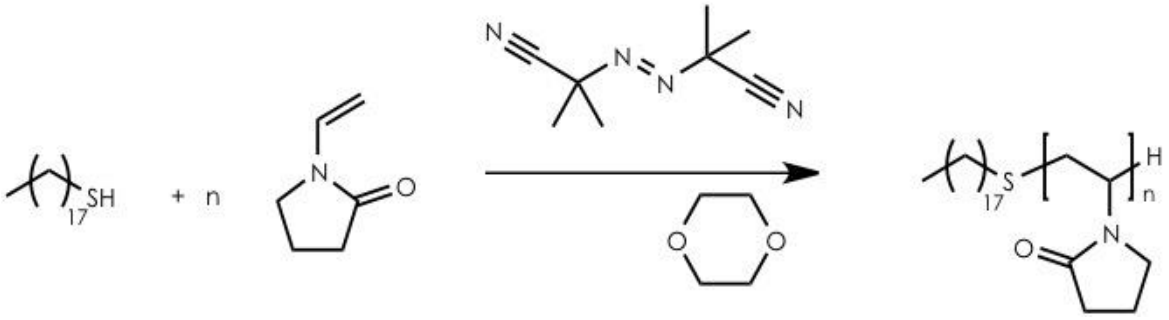

Figure 1.5: Radical polymerization of N-vinyl-2-pyrrolidone using AIBN as radical chain initiator and octadecyl mercaptan as chain transfer agent [22].

Apart from PEG (as mentioned in the Selection of polymers chapter), Polyvinylpyrrolidone (PVP) is a preferrable choice for the corona in polymeric micelles involved in drug delivery. PVP commonly known as polyvidone or povidone, is a water-soluble polymer prepared mainly by free radical polymerization of N-vinylpyrrolidone in the presence of AIBN as an initiator as depicted in figure 1.5.

"Dry PVP is a light flaky hygroscopic powder and readily absorbs up to 40% of water by its weight. In solution, it has excellent wetting properties and forms films, which makes it good as a coating or an additive to coatings" [23]. PVP has a historical significance as it was used as a blood plasma expander for trauma victims during world war II. In pharmaceutical industry, it has been used as a binder for pharmaceutical tablets and upon oral administration it simply passes through the body.

"PVP is a bulky, non-toxic, non-ionic polymer with C=O, C–N and CH_2 functional groups that is widely used in nanoparticle synthesis. The PVP molecule contains a strongly hydrophilic component (the pyrrolidone moiety) and a considerable hydrophobic group (the alkyl group). Water and many non-aqueous liquids are excellent solvents for PVP, as a result of

the highly polar amide group within the pyrrolidone ring and apolar methylene and methine groups in the ring and along its backbone" [24].

PVP has a positive effect on the self-assembly process of anionic hydrocarbon amphiphiles as it improves the arrangement of molecules in the polymer-surfactant complex and reduces the standard free energy of formation of the complex in aqueous medium [25]. Amphiphilic PVP derivatives have been shown to undergo spontaneous aggregation with the formation of spherical nanosized micellar particles consisting of a hydrophobic core and a hydrophilic shell. PVP-Stear 4000 polymer in water at polymer concentration near CMC value generates 40-50 nm micellar particles by direct dissolution method. PVP-OD 3500 polymer in water at polymer concentration close to CMC value generated 50-60 nm micellar particles by emulsion method (Figure 1.6) [16].

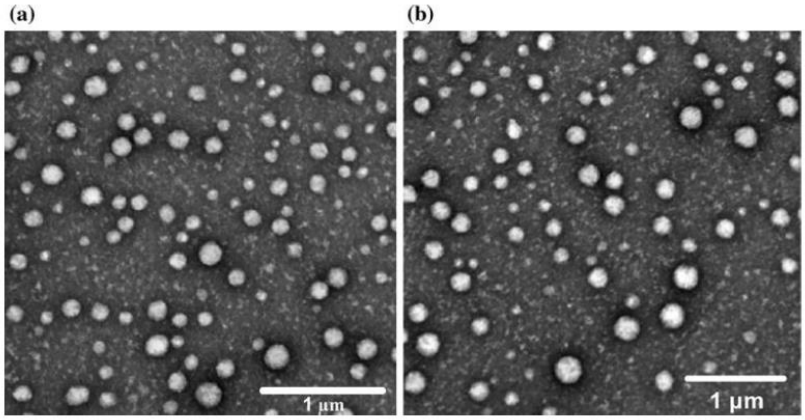

Figure 1.6: Transmission electron micrographs: a) nanoparticles prepared from PVP-OD3500; b) PVP-OD3500 nanoparticles loaded with IMC (weight ratio 1:1) [16].

Apart from the conventional polymeric micelle system comprising hydrophilic corona/shell and hydrophobic core, PVP has been used in the construction of novel three-layered onion type micelles owing to the pH-controlled hydrophobicity behaviour of PVP. It has been observed that 'PVP is protonated and soluble in water at low values of pH and deprotonated and fairly hydrophobic at pH higher than 4.8' [26]. The scheme below (Figure 1.7) depicts the formation of onion type micelles employing two different blocks in different pH conditions. The initial phase is marked by the formation of core micelle consisting polystyrene-block-poly(2-vinylpyridine) (PS-b-PVP) where polystyrene forms the core and PVP chains are extended forming corona at pH 4.1. "When the core micelles are mixed with an acidic solution of the molecularly dissolved PVP-b-PEO copolymer and titrated by alkalis, at pH 4.8 the collapsing corona blocks of the core micelles capture the PVP blocks of the PVP-b-PEO polymer and the PEO blocks keep the resulting structure (the onion micelles) in solution. The excess molecules of PVP-b-PEO copolymer form small micelles" [27].

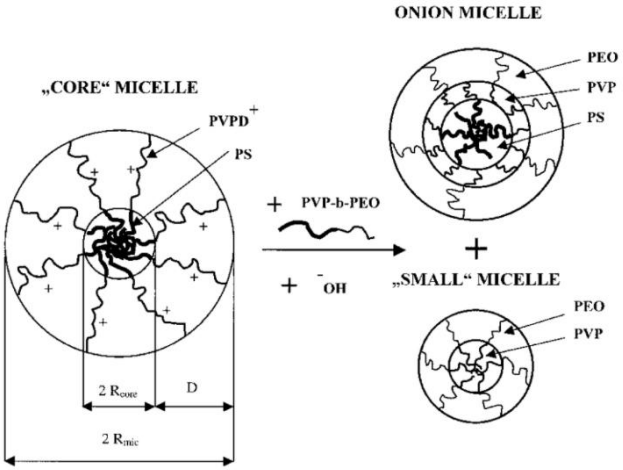

Figure 1.7: Formation of onion type micelles employing two different blocks in different pH conditions [27].

1.3 Polymer-solvent dynamics

One of the most important part of our project work deals with polymer-solvent dynamics; investigating solvent compatibility for amphiphilic PVP polymer modified with acrylic acid containing a long 18 carbon chain hydrophobic block (OD). Obtaining information about solvent-polymer interaction is crucial in order to successfully conjugate 5-Aminofluorescein through acrylic acid group. A polymer chain in solution is dynamic in nature therefore keeps changing its shape incessantly. Terms like *conformation*, *contour length*, *random coil*, *excluded volume* and *radius of gyration* is often used to understand polymer dynamics. *Conformation* is defined as an instantaneous shape of a polymer chain in solution (Figure 1.8). The distance between the ends of a fully extended linear polymer is called *contour length* (Figure 1.9). A fully stretched conformation is highly unlikely in solution and therefore the chain is rather crumpled and takes a conformation of a *random coil* (Figure 1.9).

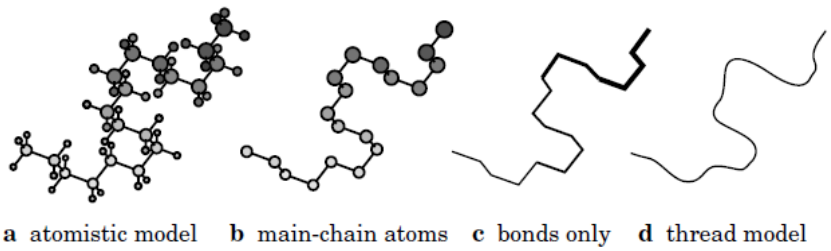

Figure 1.8: Simplification of chain conformation from an atomistic model (a) to main-chain atoms only (b), and then to bonds on the main chain only (c), and finally to a flexible thread model (d) [28].

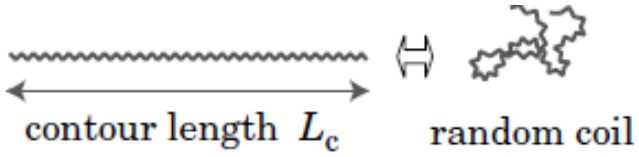

Figure 1.9: A random-coil conformation is pulled to its full length L_c [28].

Two monomers cannot occupy the same space in any real polymer resulting in an excluded zone, where even a part of a monomer cannot overlap with a part of the other monomer. This effect is defined as *excluded volume***.** Excluded volume concept is used to distinguish between an ideal chain and a real chain. In an ideal chain, two or more monomers can occupy the same site (lattice model) whereas a real chain is defined as a regular chain with an excluded volume (Figure 1.10).

The ideal chain does not exist in reality, but we use the ideal-chain model extensively because it allows to solve various problems in polymer solutions in a mathematically rigorous way. We can treat the effect of the excluded effect as a small difference from the ideal chains. Under certain situations, the real chain behaves like an ideal chain such as concentrated solutions, melts, and glasses. The other special case is of a DiIute solution in an ideal solvent called a *theta solvent* [28].

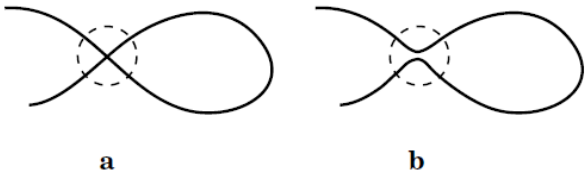

Figure 1.10: Conformations of an ideal chain (a) and a real chain (b) in two dimensions [28].

Linear flexible chains in a random coil conformation depicts that the *end-to-end distance r* (the distance separating the chain ends) (Figure 1.11), will be considerably less than the counter length

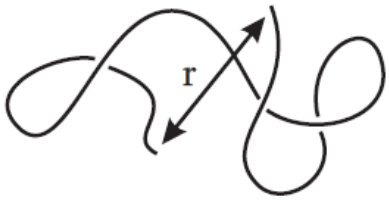

Figure 1.11: Schematic representation of a coiled polymer chain showing the end-to-end distance [29].

The chain conformation keeps changing due to rotation of backbone bonds for an isolated polymer, therefore it is impossible to assign a unique value of *r*. An infinite number of conformations is possible for a single polymer chain so usually an average magnitude of *r* over all possible conformations is computed from the mean of the squares of end-to-end distances and is called the *root mean square* (RMS) end-to-end distance, given by $\langle r^2 \rangle^{1/2}$, where the brackets < > means that the quantity is averaged over time. It is described by a simple equation taking freely jointed chain into consideration [29]:

$$\langle r^2 \rangle_f^{1/2} = n^{1/2} l \quad (1.2)$$

where the subscript *f* indicates freely jointed chain, *n* is the total number of monomeric units and *l* is the length of a monomeric unit.

The highly coiled nature of the polymer is highlighted by the large value of 'n'.

The dimensions of polymer molecules are also described often in terms of the RMS distance of a chain segment from the centre of mass of the molecule.

Using the centre of mass as a reference, the dimensions of polymer molecules are often defined in terms of the RMS distance of a chain segment. It is defined as "the square root of the average squared distance of all the repeating units of the molecule from its centre of mass and is known as the RMS *radius of gyration*, $\langle S^2 \rangle^{1/2}$, given by [Orfino, 1961]" [29]:

$$\langle S^2 \rangle = \langle (1/n) \sum_{i=1}^{n} s_i^2 \rangle \quad (1.3)$$

where s_i is the vector distance from the centre of mass to the *ith* unit of the chain in one particular conformation of the molecule and *n* is the total number of units. The angular brackets denote a linear average over all possible conformations of the molecular chain.

The radius of gyration has huge significance when it comes to defining polymer dimensions by directly measuring the radius of gyration with the help of light scattering, neutron scattering, and small angle scattering experiments, whereas the end-to-end distance is of no use (not directly observable) and also considering the case of branched polymers as they have more than two ends.
In case of high-molecular-weight linear macromolecules that have random coil shapes, $\langle S^2 \rangle^{1/2}$ is uniquely related to $\langle r^2 \rangle^{1/2}$ by equation 1.4 [29].

$$\langle S^2 \rangle^{1/2} = \frac{\langle r^2 \rangle^{1/2}}{\sqrt{6}} \quad (1.4)$$

1.3.1 Concentration Regimes

Each linear polymer chain occupies a volume of a sphere of taking the radius of gyration R_g into account (based on a very simple approximation), as illustrated below (Figure 1.12).

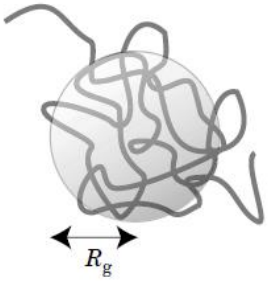

Figure 1.12: Depiction of a polymer chain with a volume approximately of a sphere of radius *R*g [28].

At low concentrations, these spheres are separated from each other and gradually, as the concentration *c* rises up, they become congested and slowly come in contact with each other at the **overlap concentration** (c^*). In this congested state, the spheres pack the whole volume of the solution. Quantitively it is defined by the following equations [29]:

$$c^*\left(\frac{4\pi}{3} R_g{}^3\right) = \frac{M}{N_A}$$

$$c^*\left(\sqrt{2}R_g\right)^3 = \frac{M}{N_A}$$

$$c^*[\eta] = 1 \quad (1.5)$$

where M/N_A is the mass of each chain, with N_A the Avogadro's number. The last equation relies on the intrinsic viscosity of the polymer.

When *c* is below *c** (*c* « *c*), the polymer chains act more or less independently as they are separated from each other. The polymer solution in this condition belongs to the **Dilute regime.** A completely different situation comes into play when the concentration above *c**. This regime is marked by the overlapping of polymer chains leading to the state of entanglement. This solution regime is called **semi-dilute**. The semi-dilute solutions are significantly different from those of an ideal solution due to different thermodynamic

properties. At a low concentration in terms of the volume fraction or the mass concentration deviation takes place in polymer solutions. The existence of the semi-dilute regime is characteristic of the polymer solutions

At a very high concentration (*c***), each segment of the polymer chain does not have a sufficient space available and the solution enters a state called **concentrated** regime [28]. The different concentration regimes are depicted below in Figure 1.13.

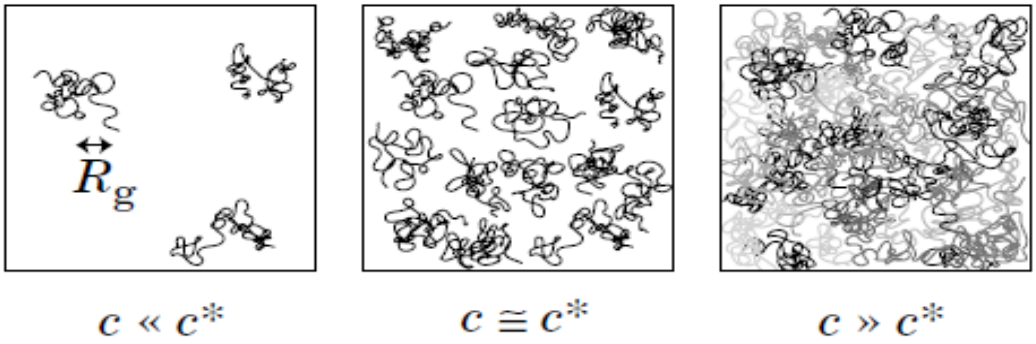

Figure 1.13: Concentration regimes for solutions of linear flexible polymers: dilute solution, *c* « *c**; solution at the overlap concentration *c*=*c**; semi-dilute solution, *c* » *c** [28].

1.3.2 Hansen Solubility Parameter

Polymers are quite stubborn when it comes to dissolution. Consider the classic example of starch being a mixture of amylose and amylopectin. Amylopectin is branched and does dissolve in water, while linear amylose disperses in water. Eventually the amylose-rich fraction settles out as a semisolid (amylose helices come together, crystallize and precipitate) after allowed to sit in water for a day. Synthetic polymers behave in a similar fashion. Amorphous blocks of the polymers are soluble in at least few common solvents whereas the crystalline parts remain insoluble. Polymers are often dissolved with great difficulty as they usually require strong solvent and heat supply [30].

Hansen solubility parameter is used to predict the solubility of polymers in solvents using the simple concept of *like dissolves like.* It was developed by Charles M. Hansen in 1967 on the basis of cohesive energy, E, of a solvent which is broken into three components namely, *dispersion* forces, *permanent dipole–dipole* forces, and *hydrogen bonding*; [31].

$$E = E_D + E_P + E_H \quad (1.6)$$

Cohesive energy can be expressed in terms of latent heat of vaporisation H_V, universal gas constant *R* and absolute temperature *T:*

$$E = H_V - RT \quad (1.7)$$

Cohesive energy is dependent on the size of a molecule therefore it follows a trend that 'bigger molecules in a molecular series have bigger cohesive energies.' It is not useful on its own and thus requires scaling so that molecules in a series are more comparable. This is where the cohesive energy density comes into picture and is obtained by dividing by molar volume *V*:

$$E/V = E_D/V + E_P/V + E_H/V \quad (1.8)$$

The cohesive energy density usually better defined in terms of the solubility parameter δ where $\delta^2 = E/V$. This provides us the classic equation for Hansen Solubility Parameters where the total parameter, δ, is broken into δD, δP and δH for Dispersion, Polar and Hydrogen-bonding:

$$\delta^2 = \delta D^2 + \delta P^2 + \delta H^2 \quad (1.9)$$

The units of solubility parameters are $MPa^{½}$ [32].

The three Hansen parameters is geometrically expressed as a coordinate of a point in the so-called Hansen space or Hansen solubility sphere (Figure 1.14). The closer two points are in their proximity, the more likely the compounds are to dissolve into each other. "In the case of a polymer, only solvents within a certain range will dissolve the polymer. This range is usually an ellipsoid and only solvents within this space are likely to dissolve the polymer in question "[31].

To get an approximate spherical volume of solubility, quite occasionally, the scale of the dispersion axis is doubled. Taking the approximate spherical volume of solubility into consideration, distance of the solvent coordinates (δ_{d2}, δ_{p2}, δ_{h2}) from the centre point (δ_{d1}, δ_{p1}, δ_{h1}) of the solute sphere is given by:

$$R_a^2 = 4(\delta_{d2} - \delta_{d1})^2 + (\delta_{p2} - \delta_{p1})^2 + (\delta_{h2} - \delta_{h1})^2 \quad (1.10)$$

The distance R_a in the equation above can be compared with the solubility radius of the polymer, R_0. If $R_a < R_0$, it increases the probability of a solvent to dissolve the desired polymer. The radius of the solubility sphere is known as the *interaction radius* and the ratio R_a / R_0 the *relative energy difference* (RED) of the system [32].

R_a / R_0 > 1 = indicates that the compound is a non-solvent
R_a / R_0 < 1 = indicates that the compound is a good solvent
R_a / R_0 = 0 – may result in swelling

Hansen and Barton have tabulated the interaction radius and partial solubility parameters for many polymers and solvents which can be used to analyse solvent compatibility for many complex molecules.

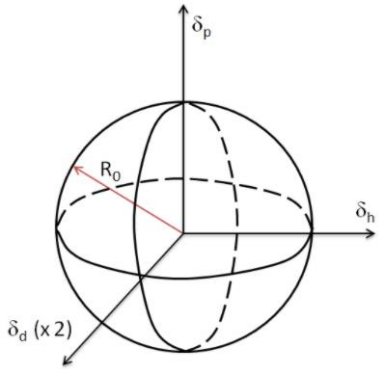

Figure 1.14: Hansen solubility sphere with interaction radius R_0 and three different components [33].

1.4 Preparation methods of drug-loaded polymeric micelles

Generally, there are three main techniques for preparation of drug-loaded polymeric micelles based on different incorporation mechanism:

1) Physical entrapment or solubilization, which is considered as a passive approach, driven by hydrophobic interaction
2) Chemical conjugation of a drug molecule to hydrophobic core of amphiphilic block copolymer by covalent linkage
3) Poly-ionic complexation based on ionic binding [34].

Physical entrapment method is usually preferred over active approaches, particularly for hydrophobic drug molecules. Chemical conjugation or poly-ionic complexation methods requires a specific reactive functional groups on both drug and block copolymer, which implies the necessity of designing a novel system adjusted for chosen incorporation. On the other hand, passive approach of physical entrapment is more forgiving – various drugs might be incorporated into the hydrophobic core just by tailoring the desired structure of the core-forming block [34].

There are various loading methods used for physical incorporation of the drug into the micellar core, such as direct dissolution method ,cosolvent evaporation, dialysis method, oil-in-water emulsification, solid dispersion method, micro-phase separation and even freeze-drying method [5, 34, 35]. Based on the method, solubilization of a drug might occur within assembly process of micelle, or after it. In order to determine the loading capacity of PM's, so called micelle-water partition coefficient is used. Factors such as structure of core-forming segment, physiochemical properties of a drug, copolymer composition and its molecular weight were determined to have the biggest influence on loading capacity of

polymeric micelle [34]. All of above mentioned factors are contributing to so-called compatibility parameter between the particular drug and inner core.

For example, calculation of Flory-Huggins parameter was used by Allen's group [36], in order to predict polymer-drug compatibility and it leaded to successful development of the system. Comparison of partial solubility parameters of hydrophobic drug and inner core allowed a prediction that core-forming segment of amphiphilic block copolymer will be compatible with a drug of choice (Ellipticine) and it resulted in increase of drug solubility by 3000 folds in comparison to Ellipticine solubility in water [34, 36]. Level of compatibility between the hydrophobic drug and the core-forming segment also plays an important role in drug release from the micelle: better compatibility results in significant decrease of the drug release rate.

In this section main techniques for passive drug-loading of polymeric micelles will be elaborated, with exclusion of micro-phase separation and freeze-drying method, since they are highly selective and can be used just for narrow range of materials.

1) Direct dissolution method

This technique is regarded as the simplest and most straight-forward method for preparation of drug-loaded polymeric micelles. Both drug and the block copolymer are dispersed in (usually) aqueous solvent and if concentration of ABC reaches CMC or above it results in formation of polymeric micelles (Figure 1.15). Unfortunately, this method is regarded as highly ineffective for copolymer with high molecular weight or with lengthy hydrophobic segment. Another requirement for direct dissolution method is at least partly solubility of drug in water, which is very often not the case (most of drugs used with polymeric micelles are highly hydrophobic). Treating a solution with ultrasounds, stirring or additional heating might improve the solubility and allow micelle fabrication by this technique, nonetheless it was reported that so prepared micelles tend to aggregate and are described as "nonequilibrium micelles", which features mainly depends on the physiochemical properties and morphology of amphiphilic copolymer used [5]. Direct dissolution method was successfully used by Yang et al. [37] in order to incorporate anticancer drug Paclitaxel (PTX) into polylactide/poly(ethylene glycol)(PLA-PEG) micelles and it was found that loading capacity of PMs was depended on stirring time – increase in stirring time resulted in higher loading capacity [37].

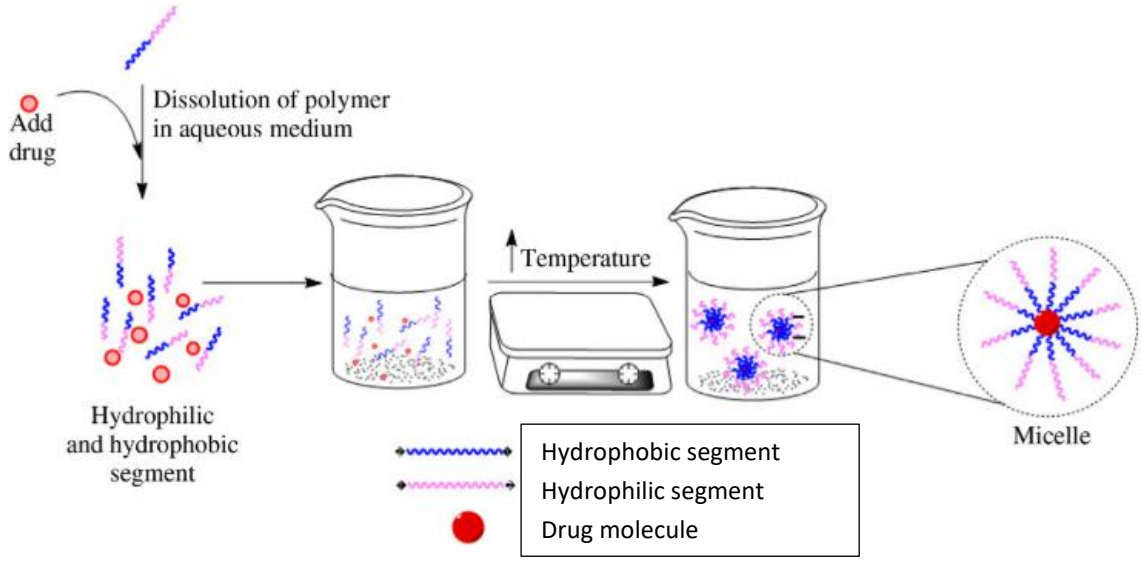

Figure 1.15: Formation of micelles via direct dissolution method [5].

2) Cosolvent evaporation method

Cosolvent evaporation technique is based on the usage of volatile, water-miscible organic solvent, which is capable of dissolution of both polymer and a drug, followed by controlled water addition to extent in which ABC and hydrophobic drug are still dissolved (Figure 1.16). After a complete mixing of the solution containing both organic solvent and water, it is subjected to evaporation until organic phase is fully removed from the mixture. This slow, controlled evaporation of organic solvent leads to simultaneous increase of water content in subjected mixture, resulting in magnification of hydrophobic interaction and therefore allowing a hydrophobic drug to be encapsulated into the micellar core. Cosolvent evaporation method is often described as a "gentler method" of micelle preparation than direct dissolution, since it allows a better control of water content and results in smaller-sized micelles. The main disadvantage of this method is requirement of a good organic solvent capable of full dissolution of both ABC and a drug, since it directly influences the drug loading capacity as well as size and shape of the micelles. Additionally, similarly to the direct dissolution, it was reported that this method cannot be successfully used for ABCs with lengthy and highly hydrophobic core segments, because it results in unstable, non-equilibrium micelles [5].

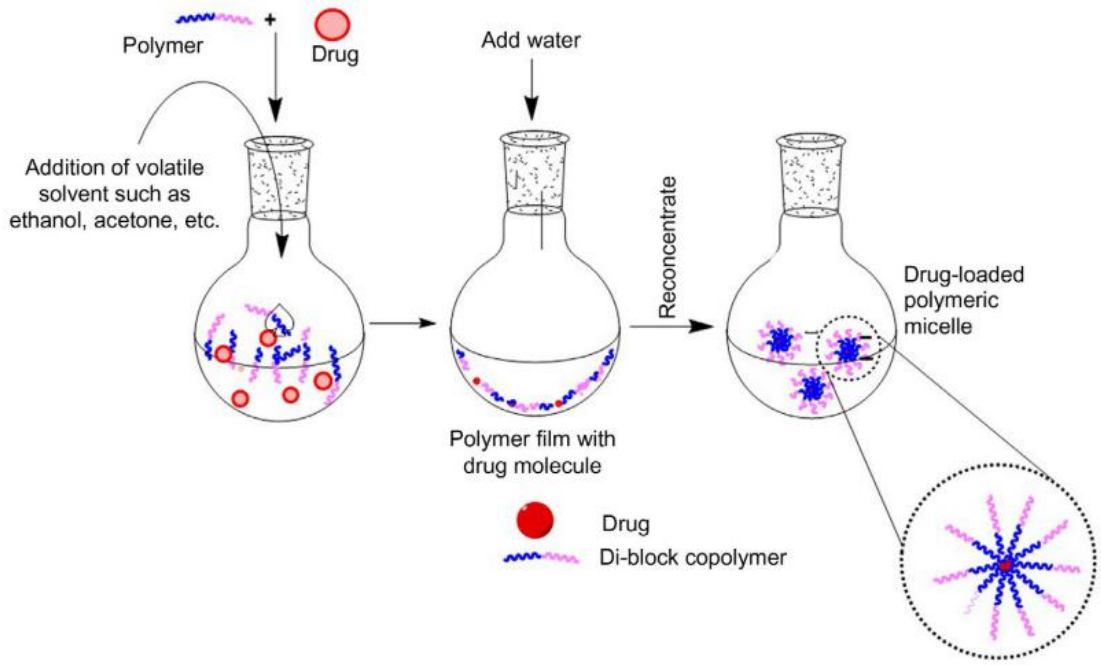

Figure 1.16: Formation of micelles via cosolvent-evaporation method [5].

3) Dialysis method

As name suggests, this technique of micelle preparation is based on dialysis process. Both the drug and the polymer are firstly dissolved in suitable, water-miscible organic solvent, which is capable of solubilizing both hydrophilic and hydrophobic block of the copolymer and vigorously mixed together. Then, so prepared solution is transferred to dialysis bag and subjected to dialysis against excess of water. During the dialysis process, water gradually enters and replaces organic solvent present in dialysis bag and therefore triggers the self-assembly of the ABCs into micelles (Figure 1.17). Permeability of the dialysis membrane should be carefully selected in order to prevent leakage of the micelles from the bag, but simultaneously allow non-loaded drug to be removed during the dialysis [34]. For example, Chen at al. [38] developed penta-block polymeric PEG-b-(poly(2-(diethylamino) ethyl methacrylate)-b- poly (hydroxyethyl methacrylate)-g-folic acid) micelles as a platform for anticancer drug delivery of doxorubicin, which was loaded by dialysis method. Obtained micelles exhibited particle size around 120nm with drug loading content around of 21% and entrapment efficiency of 48% [5,38].

It should be noted that dialysis method is suitable for preparation of micelles from ABC's with lengthy hydrophobic segment and it's more suited for laboratory-scale production rather than large scale production [5].

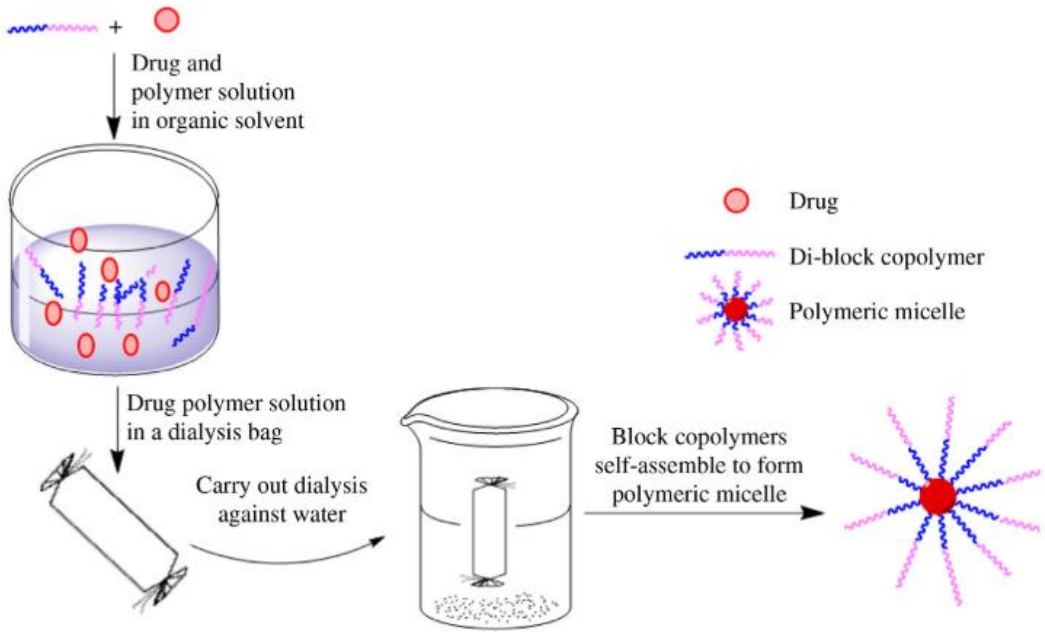

Figure 1.17: Formation of micelles via dialysis method [5].

4) Oil-in-water emulsification (emulsion method)

The first step in emulsion method is selection of water-immiscible solvent, which is capable of dissolving both drug and the polymer. Most commonly used solvents are tetrahydrofuran, chloroform, acetone or a mixture of these solvents [5]. After a complete dissolution of both components, water is slowly added to the mixture under a constant, intense stirring in order to produce emulsion, in which organic solvent establish an internal phase and water forms a continuous phase. The last step is a slow removal of the solvent by evaporation or lyophilization, which allows later reconstitution in order to form micelles driven by self-assembly of the ABCs. This method was used by Woraphatphadung et al. (26) in order to develop pH-sensitive, curcumin loaded polymeric micelles based on N-naphthyl-N,O-succinyl chitosan and N-octyl-N,O-succinyl chitosan for colon-targeted drug delivery [5,39].

5) Solid dispersion method

This technique is based on preparation of solid dispersion by dissolving block copolymer and a drug in suitable organic solvent followed by slow evaporation under reduced pressure. This process leads to formation of polymeric matrix and further preheating followed by addition of water results in generation of drug-loaded-polymer micelles. Single-step solid dispersion method was successfully implemented by Yang et al. [40] for encapsulation of curcumin into MPEG-P(CL-co-TMC) micelles. So prepared micelles exhibited excellent PdI value of 0.11, small particle size (28 nm), encapsulation efficiency around 96% and drug loading of 14%.

1.5 EDC and NHS chemistry

Carbodiimide chemistry is widely used and known as a strategy for labelling or crosslinking of carboxylic acid to various biomolecules containing primary amines through amide bond formation. One of the most popular and versatile approach is based on the usage of 1-ethyl-3-(-3-dimethylaminopropyl) carbodiimide (EDC), which is considered as a zero-length crosslinking reagent, because no part of it is present in a final bond between conjugated molecules [41]. Additionally, it offers many advantages over other cross-linking reagents, such as glutaraldehyde and formaldehyde. High conversion efficiency, moderate condition of the reaction, wide selection of solvents, very good biocompatibility with small influence on the bioactivity of targeted molecules and cleaner final products makes EDC chemistry superior to other carboxylic group activation strategies [42].

As shown on Figure 1.18, EDC (often used in hydrochloride form (EDAC)) reacts with carboxylates and forms an active O-acylisourea intermediate, which is moderately unstable in aqueous solutions (in water environment with pH around 4.75 it manifests a half-life time in the order of few seconds)[3]. Although, if O-acylisourea encounters a primary amine present in the reaction mixture, its fairly prone to its nucleophilic attack and results in formation of amide bond with the targeted carboxylic group and release of EDC by-product, which is a soluble urea derivative. Absence of primary amine in reaction mixtures leads to hydrolysis of O-acylisourea and subsequently regeneration of the carboxylic group with the release of an N-unsubstituted urea [41].

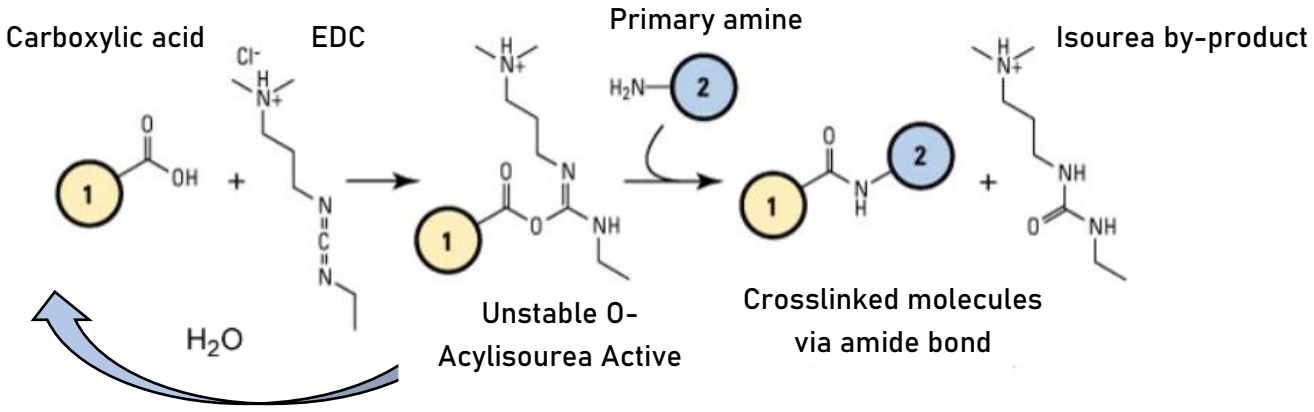

Figure 1:18: General mechanism of EDC chemistry. Molecules (1) and (2) might be proteins, polymers, peptides or any other chemical containing respectively carboxylic group and primary amine [41].

As mentioned above, O-acylisourea is highly unstable in water environment and for that reason N-hydroxysuccinimide (NHS) or its water-soluble derivative, N-hydroxysulfo-succinimide (sulfo-NHS) is often included into EDC coupling protocols. NHS has an ability to convert the O-acylisourea ester into more stable amine-reactive NHS ester (Figure 1.19), leading to the higher coupling efficiency. Moreover, satisfactory stability of the NHS-esters

allows the two-step conjugation approach, in which conditions of the reaction can be firstly adjusted for favouring ester formation and subsequently readjusted in order to improve efficiency of the reaction between the primary amine and the NHS-ester. Even though NHS esters shows better stability than O-acylisourea, they are still prone to hydrolysis in water, although it was shown that reduction in the reaction temperature will slow down the rate of hydrolysis [43].

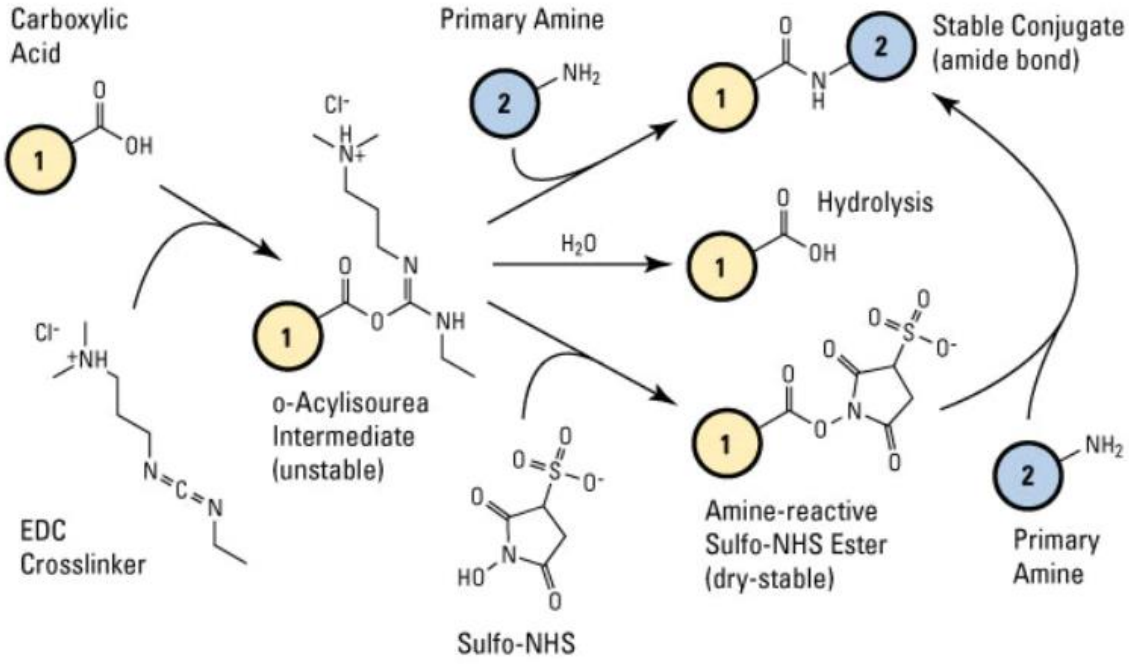

Figure 1.19: General mechanism and possible pathways of crosslinking mechanism with usage of EDC/NHS chemistry [41].

1.6 UV-Vis spectroscopy

UV-Visible spectroscopy is low-cost and facile characterization tool which is frequently employed for the study of nanoparticles. In the basic form of analysis, it measures the intensity of light reflected from a sample and compares it to the intensity of light reflected from a reference material. The reference commonly referred as “blank” assures that the spectral features from the solvent are not included in the sample spectrum. The figure below depicts a double beam instrument which has a single source and a monochromator in combination with a splitter and series of mirrors to get the beam to the sample and the reference as this allows more accurate readings [44].

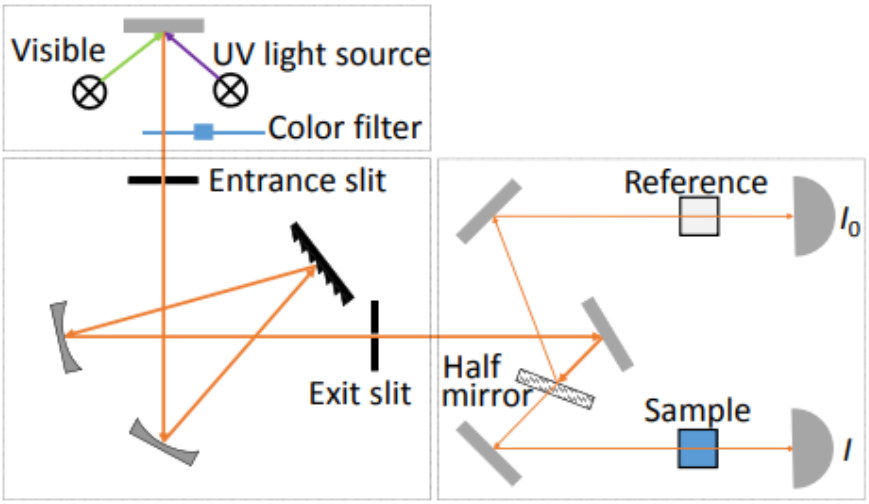

Figure 1.20: Schematic optical diagram of double beam spectrophotometer [44].

The spectroscopical foundation is laid on the principle of Beer- Lambert law which relates the attenuation of light to the material's properties through which the light is propagating. The common formula depicted below describes the relationship between absorbance and concentration of the material under investigation in a given solvent [44].

$$A = \log_{10}\left(\frac{I_o}{I}\right) = \epsilon l c \tag{1.11}$$

A - Absorbance (arbitrary unit)

ε - molar absorptivity of the sample in solution (mol^{-1} L cm^{-1})

l - path length of the cuvette or sample holder

c- concentration of the solution (mol L^{-1})

I_0 - intensity of the light passing through the reference cell

I - intensity of the light passing through the sample cell

Nanoparticles have optical properties that are influenced by size, shape, concentration, agglomeration state and refractive index near the nanoparticle surface, which makes UV-Visible spectroscopy an important tool to identify, characterize and investigate these materials and evaluate the stability of nanoparticle colloidal solutions [45].

1.6.1 Scattering and Absorption

A wide variety of samples have contribution from both scattering and absorption. The contribution of scattering or absorption from the measured extinction spectrum depends on the size, shape, composition and stability of the sample in solution. “As a general rule, smaller particles will have a higher percentage of their extinction due to absorption.” [45]. It has been observed that light scattering by very small gold nanoparticles (2 nm in diameter) is negligible and the optical spectrum is mainly due to photon absorption by the metal (Figure 1.21).

On the contrary, amorphous silica does not absorb photons in the visible spectral range and large silica colloids elastically scatter light (commonly known as Rayleigh scattering) (Figure 1.22).

The curves in figure 1.21 and 1.22 are very similar, but the mechanism for extinction is different, which is depicted in the differences in the visible appearance of the materials [45].

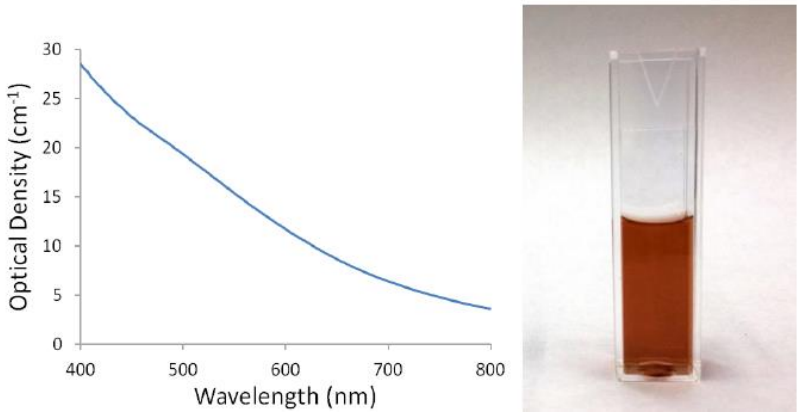

Figure 1.21: The experimental spectrum (left) from 2 nm gold nanoparticles and the Diluted solution (right) appears brownish-red since light is absorbed across the entire visible spectrum **[45].**

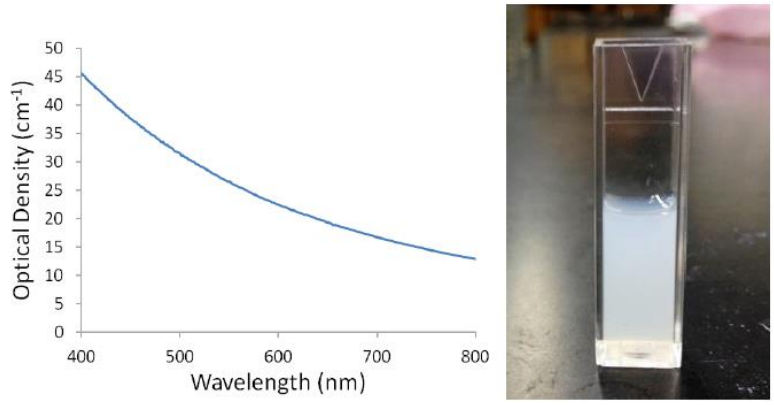

Figure 1.22: The experimental spectrum (left) of 1 um silica and the Diluted solution of colloids (right) appears white since all wavelengths of light are scattered from the particles back toward the observer [45].

1.6.2 Effect of aggregation

UV/Visible spectroscopy can be used as a convenient and efficient characterization technique for monitoring the stability of nanoparticle solutions. The destabilisation of particles results in the decrease in intensity of the original extinction peak; “due to the depletion of stable nanoparticles, and often the peak will broaden or a secondary peak will form at longer wavelengths due to the formation of aggregates.” [45]. For example, Silver nanoparticle (50 nm in diameter) has been monitored to demonstrate the rapid and irreversible change in the extinction spectrum due to agglomeration of nanoparticles [45].

UV-Visible spectroscopy can be used to monitor the stability of polymeric micelles and is interaction with hydrophobic drug involved in intracellular drug delivery. The intracellular drug delivery mechanisms are influenced by the size, composition and stability of the polymeric micelles and its interaction with the hydrophobic drug load. The destabilisation of drug loaded polymeric micelles can result in reduced drug efficacy and unwanted side effects. UV-Visible spectroscopy can be used to monitor the stability of polymeric micelles and its interaction with hydrophobic drug involved in intracellular drug delivery. The mechanism of interaction of curcumin with a novel amphiphilic polymer-Soluplus has been elucidated with the help of UV–vis absorption spectroscopy (Figure 1.23). “Absorption spectroscopy revealed that increasing concentration of the polymer could lead to seclusion of the curcumin molecule and a facilitation of its journey towards a hydrophobic pocket of the polymer. The stability of curcumin could be depicted by the degradation profile which could be investigated via UV–visible spectroscopy.” [46].

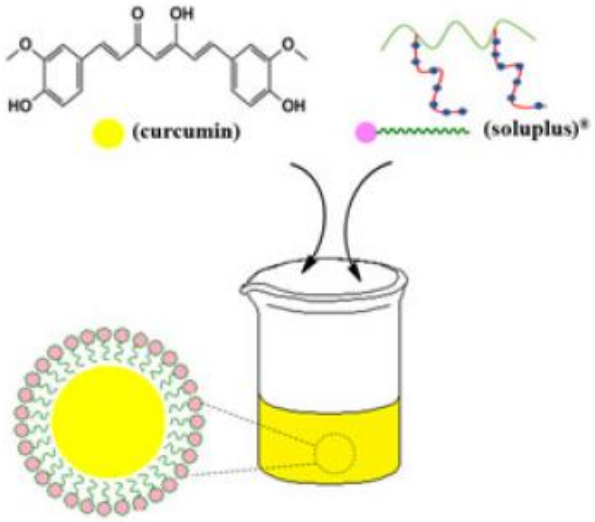

Figure 1.23: Curcumin encapsulated in Soluplus micelles [46].

1.7 Dynamic Light Scattering

Dynamic light scattering (DLS) is one of the most widely used techniques to obtain hydrodynamic size and distribution of particles or nanocarriers in solution based on their diffusion behaviour. In principle, DLS measures the light interference caused by the Brownian motion of nanoparticles in suspension and correlates its velocity (diffusion coefficient) to the size of NPs with the use of Stokes-Einstein equation. DLS also provides an information about size distribution of nanoparticles in form of Polydispersity index (PDI), which is yielded by autocorrelation function. Range of PDI values are situated between 0 and 1, where 0 is considered as very homogenous population of nanoparticles and 1 refers to highly heterogenous population [47].

In this chapter, fundamentals behind DLS and theoretical consideration are presented, based on following references: [47-51].

1.7.1 Brownian motion and hydrodynamic diameter

In order to fundamentally understand principle of DLS, insight in concept of Brownian motion and hydrodynamic diameter has to be elaborated. In 1905 Einstein formed Brownian motion theory, which was named after botanist Robert Brown, who first observed and described this phenomenon in 1827. Einstein established, that particles in solution are constantly bombarded by solvent molecules that surrounds them and this force is causing a random move of particles, where the mean squared displacement of particles caused by Brownian motion is proportional to time. One year later, Einstein included to his theory a discovery from Sir George Stokes, which states that ,"friction exerted by a moving particle is proportional to its radius and to the viscosity of the surrounding solvent molecules" [48]. This leaded to formulation of Stokes-Einstein equation (Equation 1.12), which relates diffusion coefficient of particles with their hydrodynamic diameter and is a main fundation of DLS technique.

$$d(H) = \frac{kT}{3\pi\eta D}$$

Equation 1.12. Stokes-Einstein equation

Where k is Boltzmann's constant, T – absolute temperature, η – viscosity, $d(H)$ – hydrodynamic diameter and D – translational diffusion coefficient.

Translational diffusion coefficient (D) is a parameter which defines the velocity of Brownian motion. Generally, magnitude of Brownian motion is mostly dependable on particle size –

the bigger the particle is, the slower it moves in solution. If translational diffusion coefficient is obtained, it allows to directly calculate the size of a particle in form of hydrodynamic diameter of a sphere with identical translational diffusion speed as the measured particle. It is worth to mention that hydrodynamic diameter actually slightly differs from the real particle size, since it represents ideal sphere. In order to obtain the most realistic hydrodynamic diameter, temperature during the measurement has to be kept constant, since even a slight change in it will directly influence the solvent viscosity and therefore the Brownian motion of measured particles. Other factors that might influence the translational diffusion coefficient and consequently the hydrodynamic diameter are surface structure, shape of nanoparticles and ionic strength of the medium.

1.7.2 DLS principle

Dynamic light scattering is a technique that allows measurement of Brownian motion of particles in solution, caused by bombardment of solvent molecules and translates this motion to the hydrodynamic diameter of particles. In order to do so, sample is illuminated with a laser beam and upon encountering particles present in solution, the light scatters in all possible directions and change in scattering intensity is analysed by the detector [Figure 1.24a]. The scattered light will produce intensity patterns on a detector with regard to either constructive or destructive interference of the scattered light. Destructive phases cancels each other out, whereas constructive phase results in detectable signal. Since particles present in solution are in constant movement due to Brownian motion, this intensity pattern changes continuously every nano- or microsecond. Rate of intensity fluctuation is mainly dependable on the particle size – smaller the particle is the faster it changes (Figure 1.24b).

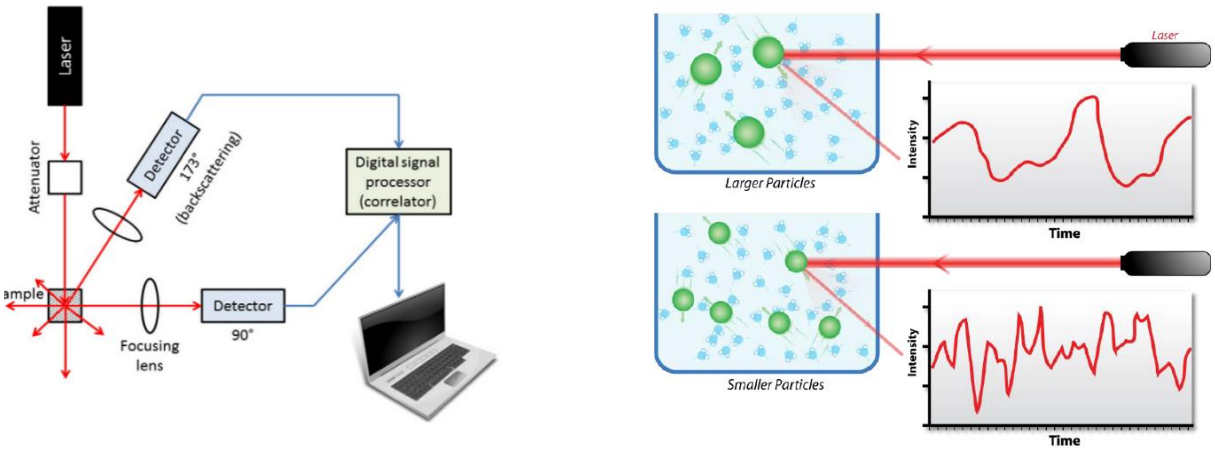

Figure 1.24: a) General scheme presenting the instrumentation of DLS, b) Comparison of intensity fluctuations for smaller and larger particles [Adapted from 50].

As a next step, obtained intensity fluctuation signal is processed by correlator. Correlator is a device that measures the similarity between two signals over a very short period of time (*t+δt)* or only one signal at different time intervals (usually nano- or microseconds). In DLS measurement, the intensity of a first signal at time *t* is compared to its intensity at *t+δt* and within this short time interval a very good correlation is expected. For instance, if we record a signal at *t+2δt* it will also show a reasonable correlation to the initial signal, although not as precise as correlation between *t* and *t+δt.* For that reason it is necessary to record intensity of initial and all subsequent signals, because if time interval *δt* is too long it makes correlation of signals impossible. If there is no correlation between signals then it is indicated by zero (0.00), whereas a perfect correlation is denoted as unity (1.00). Correlation of signals is reducing with time, based on the particle size. For small particles the intensity signal is decaying faster than for the larger ones (Figure 1.25) and slope of correlation function gives indication of sample polydispersity – the stepper the line the more monodispersed the system is.

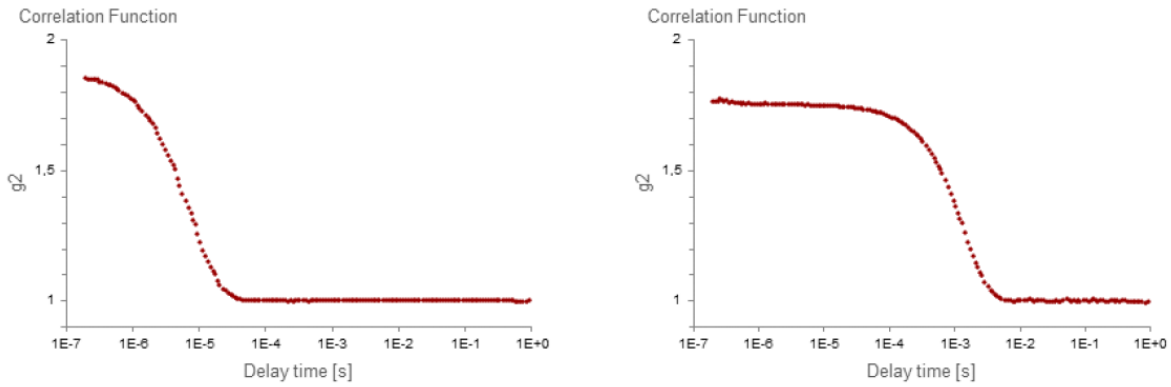

Figure 1.25: Representation of correlation function for small (left) and large (right) particles [Adapted from 50].

1.7.3 Correlation function

Intensity correlation function $G_2(\tau)$ (also called second-order correlation function) is used in DLS measurement in order to describe the motion of investigated particles. It can be expressed in following way:

$$G_2(\tau) = \langle I(t)I(t+\tau)\rangle \quad (1.12)$$

Where, τ is the time lag between the two time points. The $G_2(\tau)$ function can be normalised as:

$$g_2(\tau) = \frac{\langle I(t)I(t+\tau)\rangle}{\langle I(t)\rangle^2} \quad (1.13)$$

Normally, it is impossible to predict how exactly particles moves in solution, although movement of correlated particles can by described by introduction of the electric field correlation function $G_1(\tau)$, which after normalisation is presented as:

$$g_1(\tau) = \frac{\langle E(t)E(t+\tau)\rangle}{\langle E(t)E(t)\rangle} \quad (1.14)$$

Where $E(t)$ and $E(t+\tau)$ are scattered electric fields at time point (t) and ($t+\tau$).

Both correlation functions $g_1(\tau)$ and $g_2(\tau)$ can be combined with each other by Siegert relation, which assumes that photodetector will only note scattered light and counting of photons is arbitrary Gaussian process,

$$g_2(\tau) = B + \beta|g_1(\tau)|^2 \quad (1.15)$$

Where, B corresponds to the baseline of the function and β is the coherence factor that is dependable on the area of detector, optical arrangement and scattering properties of particles.

For monodisperse molecules undergoing a Brownian motion, the electric field correlation function decays exponentially and it is depending on the Decay constant - Γ, (equation 1.16a) whereas in case of polydisperse samples, function $g_1(\tau)$ must not be represented as a singular decay, but rather a distribution of exponential decays (equation 1.16b)

$$g_1(\tau) = e^{-\Gamma\tau} \quad (1.16a) \qquad g_1(\tau) = \int_0^\infty G(\Gamma)e^{-\Gamma_\tau d\Gamma} \quad (1.16b)$$

After inserting equation 1.16a into the equation 1.15 we obtain

$$g_2(\tau) = 1 + \beta e^{-2\Gamma\tau} \quad (1.17)$$

Decay constant Γ is dependable on diffusion behaviour of particles ($D\tau$) and is described by equation:

$$\Gamma = -D_\tau q^2 \quad (1.18)$$

where q is corresponding to Bragg wave vector described as:

$$q = \frac{4\pi\eta}{\lambda} sin(\theta/2) \tag{1.19}$$

with η being a solvent refractive index, λ – wavelength of light and θ is detector angle.

By combining equations for Decay constant and Bragg wave vector with intensity correlation function $g_2(\tau)$ (equation 1.17) we obtain a relationship between the particle movement and measured fluctuations:

$$g_2(\tau) = 1 + \beta e^{-2D_\tau q^2 \tau} \tag{1.20}$$

1.7.4 Information about size obtained from correlation function

Modern DLS instruments are supplied with various software packages that can perform a full data analysis in order to obtain useful information about size and homogeneity of investigated particles. Previously mentioned correlation function (Equation 1.20) contains parameter Dτ, which explains diffusion behaviour of molecules present in solution. By using Stokes-Einstein equation (Equation 1.12), it is possible to directly relate diffusion coefficient to the hydrodynamic diameter of the particles.

Two mainly used approaches for obtaining reliable data on diffusion coefficient from correlation function are called Monomodal distribution and Non-monomodal distribution method. In monomodal distribution analysis a single exponential is fitted into the correlation function and it gives an information about the mean size of particles (z-average) and PDI (polydispersity index) of subjected sample. This method is also called the Cumulants analysis and can be used only for Gaussian distribution of the mean values [48]. On the other hand, non-monomodal distribution does not require assumption about specific type of distribution of diffusion behaviour and by fitting multiple exponential into the correlation function, information about distribution of particle size based on their relative intensities can be obtained. Non-monomodal distribution method gives output in form of intensity size distribution and is most commonly used approach to obtain size information from DLS experiment.

As mentioned before, intensity size distribution is the most commonly used representation of DLS experiment results. Intensity size distribution is defined as a plot of relative intensity of scattered light by particles in different size ranges. But what is the difference between number, volume and intensity distribution, since all of these are used in DLS as data interpretation? Let's consider spherical particles in two populations, equal in number, but with different diameters – 5nm and 50nm. Number distribution will be presented as 2 peaks in the same ratio, since their population number is the same. If we convert number

distribution to volume, then ratio of these peaks will change to 1:1000, since volume of a sphere is equivalent to $4/3\pi(d/2)^3$. Further conversion to intensity distribution will result in a $1:10^6$ ratio between two peaks, because based on Rayleighs approximation, the intensity of scattered light is proportional to d^6. It implies a significant drawback of intensity distribution, because larger particles or contaminants present in sample will mask particles of interest. That is why DLS is considered as a very sensitive method and careful, contaminant-free sample preparation is required in order to obtain reliable data from experiment.

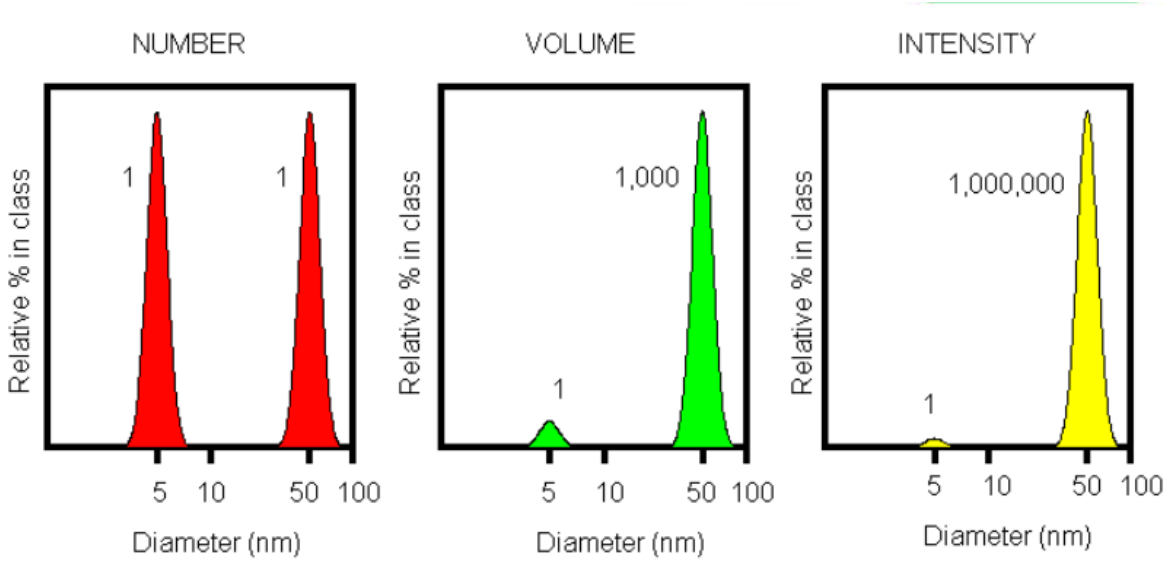

Figure 1.26: Visual representation of two populations of molecules equal in quantity in form of number, volume and intensity distribution [50].

1.7.5 DLS limitations

Even though DLS is a very useful laboratory tool, it possess certain drawbacks, that might result in considerable measurement inaccuracy.

- As mentioned before, DLS experiment is very dependable and sensitive on temperature and solvent viscosity. For obtaining reliable data, temperature has to be kept constant throughout entire experiment and precise solvent viscosity has to be known.
- DLS suffers from low-resolution and very often it cannot distinguish molecules that are similar to each other, for example monomer and dimer.
- It is highly recommended that just transparent sample can be measured, since fluorophores present in the sample might absorb light with the wavelength of the laser. Furthermore, very often fluorescent light might be recorded as noise.
- Since intensity of scattering depends on the d^6 of particles, even small quantity of large aggregates or dust will negatively influence the measurement. It implies a necessity of filtration before performing measurement and precise cleaning of the cuvette.

- Signal obtained from DLS is highly dependable on the size and concentrations of investigated particles, therefore very often it is required to run the experiment with different concentrations in order to optimize and receive reliable data.

1.8 Zeta Potential

Zeta potential, also known as electrokinetic potential is a physical feature exhibited by any particle suspended in colloidal solution. It is defined as the electrical potential at the slipping/shear plane of a colloidal particle and it corresponds to the potential difference between the electric double layer (EDL) of particles and the dispersant layer surrounding them at the slipping plane [49]. Determination of zeta-potential gives an idea about stability of colloidal system and it is a good indication of interaction between colloidal particles. This chapter is based on [47-51] references and it will give an overview about Zeta-potential, its origin and factors which might influence the outcome of measurement.

1.8.1 Electric double layer and slipping plane

If a charged particle is dispersed in solution, it attracts counterions and so-called adsorbed double layer/electric double layer (EDL) is developed on its surface (Figure 1.27). Stern layer (inner layer of EDL) mostly consist of ions with opposite charge to these of the particle, which are strongly bounded to its surface. Outside this layer, it is expected that electrostatic effect caused by particle surface charge is decreasing according to Debye's law – with the distance of every Debye length λ_D, the electric potential is decreasing in magnitude of 1/e. Even though theoretically this effect should extends infinitely, practically it disappears in few nano-meters distance from particle surface. Presence of electrostatic field generated by charged particle results in a creation of outer diffuse layer, which consist of ions with both same and opposite charge. Diffuse layer is considered as dynamic structure, because its composition is dependent on many factors, such as pH, concentration of particles and ionic strength. Diffuse and Stern layer together are forming the electric double layer.

If the charged particle of interest is placed in electric field it will move alongside with its diffuse layer towards oppositely charged electrode. A theoretical plane, which separates the interface between the particles undergoing motion and the dispersant layer surrounding it is called slipping/shear plane and its electric potential corresponds to ζ (zeta) potential.

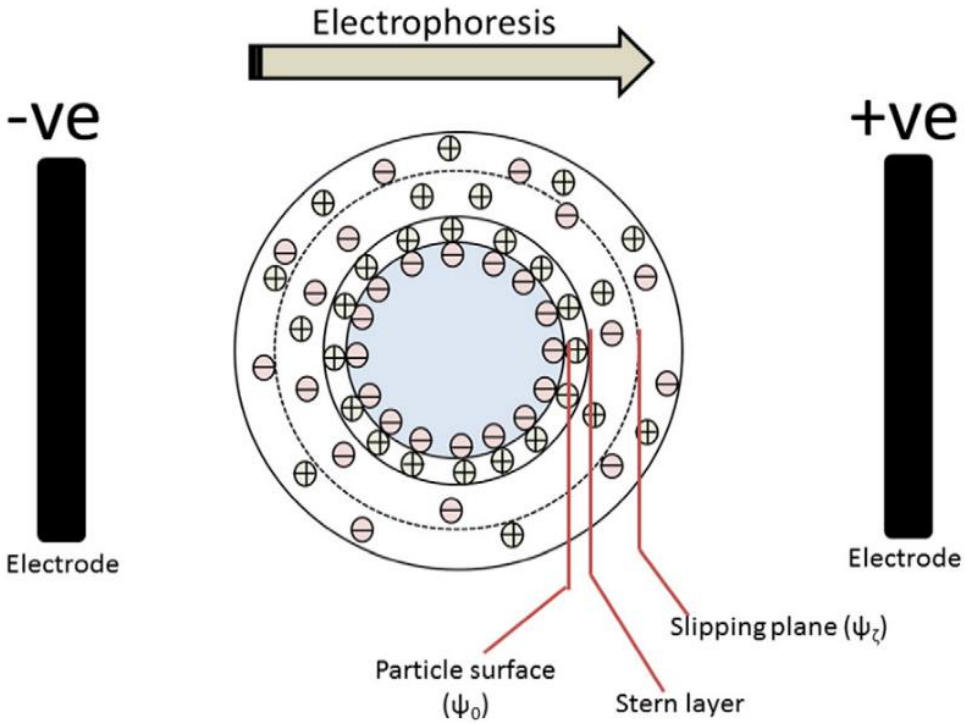

Figure 1:27: Illustration presenting electric double layer which was formed on particle with negative charge [Adapted from 49].

Particle surface potential (ψ_0, also known as Nernst potential) is impossible to measure directly. In dispersion, electrostatic field from particle surface is decreasing with distance, according to equation:

$$\psi = \psi_d e^{-\kappa x} \tag{1.21}$$

Where ψ is a surface potential at distance „x" from Stern layer, ψ_d is potential at Stern Layer and κ is a Debye-Hückel parameter.

If a slipping/shear plane is in close distance to the Stern layer, the $\psi_d \approx \zeta$ and therefore equation 1.21 can be written as:

$$\psi = \zeta e^{-\kappa x} \tag{1.22}$$

Debye-Hückel parameter is mostly dependable on ionic strength, therefore by increasing concentration of electrolytes in solution, the EDL compresses and value of Zeta potential is decreasing.

1.8.2 Determination of Zeta potential

Value of Zeta potential cannot be directly obtained from the measurement and therefore it has to be calculated from theoretical model based on charged particles mobility under the influence of electric field. From equation 1.23, particles electrophoretic mobility (μ_e) can be calculated:

$$\mu_e = \frac{V}{E} \tag{1.23}$$

Where V is particle velocity in (μm/s) and E is strength of electric field in (Volt/cm). Values of both particle velocity and strength of electric field are known and by calculating μ_e, Zeta potential value can be obtained from Henry's equation:

$$\mu_e = \frac{2\varepsilon_r \varepsilon_0 \zeta f(Ka)}{3\eta} \tag{1.24}$$

Where ε_r is relative permittivity, ε_0 is permittivity of vacuum, η is viscosity of the medium and *f(Ka*) is Henry's function.

As presented in equation 1.24, Zeta-potential is dependable on solvent viscosity. Therefore it is crucial to maintain stable temperature during the experiment, since any change in it will directly affect viscosity and subsequently Zeta potential value.

1.8.3 Principle of Zeta potential measurement

If a colloidal solution during electrophoresis is treated with a laser beam, particles present in it will scatter the incident light. Since all charged particles are undergoing motion towards the electrode, the scattered light will have a different frequency compared to the original laser beam. Due to the Doppler effect, shift in the light frequency will be proportional to the speed of moving particles. Generally, in zeta potential experiment (Figure 1.28) a laser beam splits into two separate beams, where one is incident towards the sample , while the other serves as a reference. Comparison and combination of light scattered by the sample and reference beam allows for determination of Doppler shift. From Doppler shift, velocity of particles of interest can be deduced and by usage of equations [1.21-1.24], Zeta potential can be calculated.

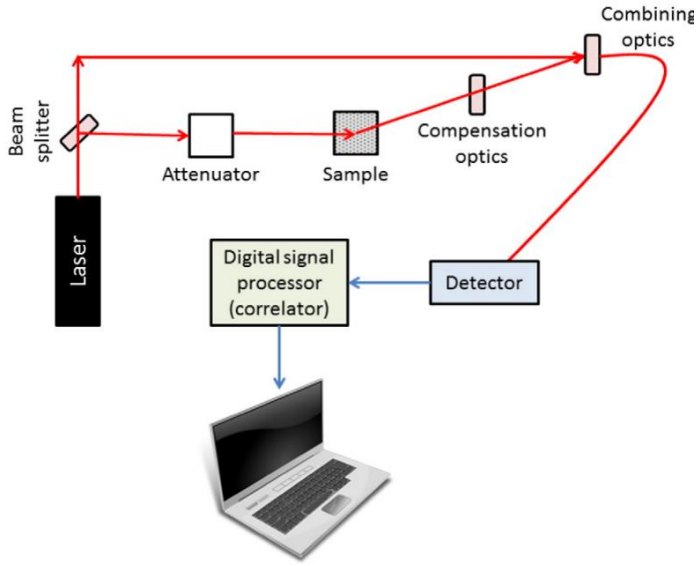

Figure 1.28: General instrumentation used in Zeta potential measurement.

1.8.4 Factors affecting Zeta potential

1) pH

Factor, which has undoubtedly the greatest influence on the outcome of Zeta potential experiment is pH of the sample. Zeta potential changes accordingly to pH – addition of alkali will build-up more negative value, while addition of acid will result in more positive charge. Consequently, in order to obtain reliable information from ZP experiment, pH versus Zeta potential curve should be plotted (Figure 1.29). From this curve the Isoelectric point can be deduced, which corresponds to pH value, where ZP becomes 0. Isoelectric point is important from practical point of view, because it indicates pH value where the colloidal system is expected to aggregate and be the least stable.

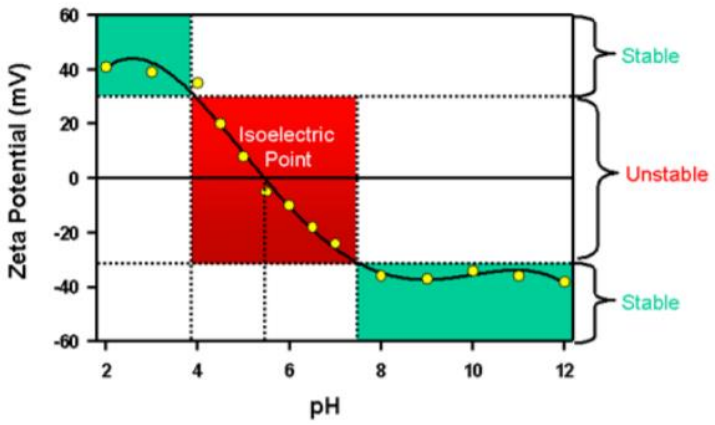

Figure 1.29: Exemplary plot of ZP versus pH. pH value around 5.5 indicates the Isoelectric point, where colloidal system is expected to agglomerate [Adapted from 50].

2) Ionic strength

As presented in equation 1.22, Zeta-potential is influenced by ionic strength. By increasing concentration of electrolytes, the electric double layer is becoming more compact and consequently ZP is decreasing. Valency of ions is also not insignificant – ions with higher valency are compressing EDL more efficiently than monovalent ones resulting in greater decrease of Zeta potential value.

3) Concentration

There is no straightforward correlation between concentration of particles and Zeta Potential, although it is known that both surface adsorption and electric double layer effect determines the outcome of experiment. Generally, it is assumed that for Dilute solutions phenomenon of surface adsorption is dominant and therefore ZP increases with concentration. Nonetheless, if concentration reaches sufficiently high level, the thickness of electric double layer becomes a dominant factor and with increasing concentration decrease in ZP value and stability of system is observed.

1.8.5 Zeta potential and stability of colloidal systems

Zeta potential measurement is widely used in order to determine and predict the stability of colloidal systems. Magnitude of ZP provides information about electrostatic repulsion between particles in the solution. General classification of system stability based on ZP is presented in Table 1.4.

Table 1.4: Expected stability of colloidal system based on ZP value [Adapted from 47].

Zeta potential value (mV)	Stability behavior
0 to ±5	Flocculation or coagulation
±10 to ±30	Incipient instability
±30 to ±40	Moderate stability
±40 to ±60	Good stability
Greater than ±60	Excellent stability

Even though ZP provides indication on colloidal stability, there are other factors that might influence it. According to DLVO theory, which was formulated by Derjaguin, Landau, Verwey and Overbeek, stability of colloidal system is dependable on the contribution of

attractive van der Waals forces and repulsive electrostatic forces originated from EDL. As mentioned before, ZP experiment provides data about magnitude of electrostatic repulsion, but unfortunately it does not give any information about van der Waals attractive forces. Parameter that has significant influence on van der Waals attractive force is Hamaker constant. Generally, if for certain particles Hamaker constant has a low value, then van der Waals attractive force is expected to be weak and electrostatic repulsion indicated with relatively low ZP may be sufficient to maintain a stable colloidal system. Therefore, it is possible to observe stable colloidal solution with low zeta potential value and relatively unstable systems with high ZP. For example, material like colloidal silica even at low ZP value shows excellent stability [51].

2. Materials and methods

2.1 Instrumentation and chemicals

Table 2.1 presents all instruments that were used during this project work, whereas table 2.2 contains information about all chemicals and consumables.

Table 2.1: List of all instruments used.

Instrument	Manufacturer	Description
pH-meter	VWR international	pHenomenal pH 1100L
Vortex	VWR international	MS2 Minishaker
Freeze dryer	Martin Christ GmbH	Alpha 1-4 LD plus
Centrifuge	Eppendorf	5804R
UV-VIS spectrophotometer	Shimadzu	UV-1800
Ultrasonic Bath	Marshall Scientific	Branson 2510
Ultrasonic Processor	SONICS	VC 505 / VC 750
Sonication probe	SONICS	Vibra cell
FTIR	Bruker	Lumos I
Fluorescence Spectrometer	ISS Copenhagen	ChronosDFD
Fluorescent microscope	Zeiss	Observer z1 Axicam mrc5
	Hamamatsu	Digital camera c11440
Rotary evaporator	Ika	RV10 digital
DLS and Zeta-potential	Malvern Instruments	Zetasizer Nano-zs

Table 2.2: List of all consumables and chemicals used in this project work.

Chemicals/Consumables	Manufacturer	Catalog number
PVP-OD 20% AA, 12 kDa	Provided by the research group of Prof. Shtilman at Mendeleev University, Moscow	-
NHS	Sigma-Aldrich	lot #: BCBF5027V
EDC	Sigma-Aldrich	lot #: BCBN0730V
5-Aminofluorescein	Sigma-Aldrich	lot #:MKCG5228
DiIC18	Invitrogen	lot #: 1975524

Pre-Treated, RC Tubing MWCO: 3,5kD Spectra 7 Dialysis Membrane	Spectrum Laboratories Incorporation	lot #: 3288210
Ultracel 10k Centrifugal Filters	Amicon Ultra	lot #: R8JA95767
Ethanol Absolute	Kemetyl	200-578-6
DMSO	Sigma-Aldrich	D2650
DMF	Iris-Biotech GMBH	lot #: 145129B
Acetone	Sigma-Aldrich	34850-1L-M
Cellulose acetate minisart 0.2µm filter	Sartorius	16534-k
Oxyma Pure	Iris-Biotech GMBH	1603117051
DIPEA	Tokyo Chemical Industry	Lot #:YBHACGR

Every chemical was used without any preceding purification. In all experiments, ultrapure water from Milli-Q purification system was used.

2.2 Methods

2.2.1 Solvent selection

In order to determine the most suitable solvent for PVP-OD-20%AA and subsequent conjugation of 5-Aminiofluorescein by EDC/NHS activation chemistry, solubility test was performed. Since PVP-OD-20% is considered as amphiphilic polymer, first solvent of choice was water with distinction on different pH. Therefore 10mg of PVP-OD-20%AA was dissolved in 10ml of acidic, neutral and basic water and the turbidity was assessed. As a comparison, PVP-OD without acrylic acid and PVP-OD-100% AA was also dissolved in water with the same fashion.

As a next step, different organic solvents for solubilization of PVP-OD-20% were examined. 10mg of PVP-OD-20% was placed in 4 separate vessels and 1ml of DMSO, DMF, Ethanol absolute and Acetone was added respectively. For all samples, quantity of organic solvent was increased gradually under heavy stirring until full dissolution of the polymer was observed or after concentration of sample reached 1mg/1ml. Next, regardless of obtained solubility, all solutions were adjusted to 1mg/1ml concentration with subsequent gradual water addition until precipitation or turbidity was observed.

2.2.2 EDC and NHS chemistry

For conjugation of 5-Aminofluorescein to PVP-OD-20%AA polymer EDC and NHS chemistry was performed. Unfortunately, available literature does not offer unequivocal approach for conjugation mechanism and therefore different activation strategies had to be examined. First step of conjugation, which was the same for all protocols, was dissolution of 100mg PVP-OD-20%AA in 40ml of 91% Ethanol under heavy stirring for at least 2h. Subsequently, EDC and NHS was dissolved in 5ml of 91%ethanol each and added in different ratio depending on the protocol (5:2:1 ; 3:3:1 and 2:4:1, which corresponds to molar concentration of EDC:NHS:COO^-) and left for 30minutes under heavy stirring.. After this time, all solutions were added dropwise under stirring to 50mg of 5-Aminofluorescein dissolved in 10ml of methanol respectively, with presence of 16 mM DIPEA, which works as a proton scavenger in amidation reaction. So-prepared solutions were left for overnight stirring and subjected for one week dialysis in 3.5kD dialysis membrane against pH10 adjusted water. After dialysis all samples were completely frozen in liquid nitrogen and submitted for 48 hours lyophilization. Obtained material was examined by UV-VIS and FT-IR spectroscopy in order to get confirmation of 5-Aminofluorescein conjugation to the polymer.

2.2.3 UV-VIS spectroscopy

UV-VIS spectroscopy was used for obtaining information about 5-Aminofluorescein conjugated to the PVP-OD-20%AA polymer. All measured samples were dissolved in ultrapure water and spectra were recorded in spectrum mode with visible range on Shimadzu UV1800.

2.2.4 FTIR

In order to obtain information about chemical structure and confirmation of 5-Aminofluorescein conjugation to PVP-OD-20% polymer, FT-IR spectroscopy was performed. As a starting point, PVP-OD-20%AA was dissolved in ethanol and subjected to freeze drying prior to measurement for examination of possible solvent influence on the polymer structure. As a reference to obtained spectra, PVP-OD without acrylic acid and PVP-OD-100%AA were measured by FT-IR as well. To minimalize the possible water peak, all non-modified polymer samples were dissolved in deuterium water and freeze dried before subjecting to FT-IR. All the polymer samples were placed on a motorized stage and the spectra were recorded in Attenuated total reflectance (ATR) mode. All the FT-IR spectra were recorded by Bruker Lumos 1 spectrometer and were processed and analysed by a free software - Bio-Rad Know It All.

2.2.5 Fluorescence spectroscopy

For evaluation of 5-Aminofluorescein and PVP-OD-20%AA crosslinked with 5-Aminofluorescein emission profile, fluorescence spectroscopy was performed on ChronosDFD spectrometer with excitation wavelength of 490nm. All samples were dissolved in HPLC grade water with concentration ~0.1mM. Emission spectra were obtained on PC1 with 300W Xenon lamp.

2.2.6 Nanocarrier production

In order to create and evaluate characteristics of various PVP-OD based nanocarriers, three different approaches, namely direct dissolution, dialysis and co-solvent evaporation method were implemented. As a reference to PVP-OD-5-AF nanocarriers, dialysis and co-solvent evaporation protocol was repeated, but PVP-OD-20%AA was used instead.

Direct dissolution method

For understanding the general polymer behaviour and micelle formation 12kDa PVP-OD-5-AF polymer was prepared in the following way:

2mg of PVP-OD-5-AF was dissolved in 2ml of ultrapure water, by stirring the solution at the room temperature for 1 hour. Then, solution was transferred to plastic tube and placed in styrofoam container filled with ice for overheat prevention and subjected to 10 minutes sonication with pulse 1s on, 2s off, 40% amplitude. Prior to DLS measurement, polymer solution was pushed through 0.2µm cellulose filter.

Cosolvent evaporation method

10mg of PVP-OD-5-AF and 10 mg of PVP-OD-20AA were gradually added under heavy stirring to 10ml of 91% Ethanol respectively and mixed for at least 2 hours. After this time, 1ml of DiI dye was dissolved in 1ml of absolute ethanol and slowly added to each polymer solution. So-prepared solution was left for 2 hours of mixing and subsequently 10ml pH-10 adjusted chromatography grade water was added and stirred for 4 hours. As the next step, entire solution was subjected to rotary evaporation at 40°C until approximately 5ml of solution remained. After complete evaporation, entire solution was transferred to plastic tube and placed in styrofoam container filled with ice for overheat prevention and subjected to 10 minutes sonication with pulse 1s on, 2s off, 40% amplitude. Before subjecting to DLS, solution was pushed through 0.2µm cellulose filter.

Dialysis method

10mg of PVP-OD-5-AF and 10mg of PVP-OD-20%AA was slowly added and dissolved in 10ml of 91% Ethanol respectively and left for 2h of stirring. Then, 1mg of DiI was dissolved in absolute ethanol and added to both mixtures each. After additional 2h of mixing, 10ml of pH-10 adjusted chromatography grade water was added to each solution and heavily

stirred for 4h. Then, both solutions were transferred to 3.5kD dialysis membranes and subjected to dialysis for 3 days with regular water exchange. After complete dialysis entire solution was transferred to plastic tube and placed in styrofoam container filled with ice for overheat prevention and subjected to 10 minutes sonication with pulse 1s on, 2s off, 40% amplitude. Prior subjection to DLS, solution was pushed through 0.2µm cellulose filter.

2.2.7 DLS and Zeta potential

The hydrodynamic size and zeta-potential of various PVP-OD based nanocarriers was obtained by usage of Zetasizer nano-zs from Malvern Instruments. All data was analysed with help of official Zetasizer software.

2.2.8 Fluorescence microscopy

For determining the uptake possibility of produced nanocarriers by mammalian cells, fluorescence microscopy was performed. This experiment was carried out in Health Care Department of Aalborg University by our student colleague Miquel Santos Llinàs under the guidance and supervision of Associate Professor Pablo Pennissi, to whom we express sincere gratitude for the invaluable help. All the images were obtained by usage of Zeiss inverted microscope and the experiment was performed in following way:

- Cell culture of Fibroblast CRL2429 was seeded on the borosilacate cambered slides in a density of approximately 5000 cells/cm^2 and incubated at 37°C for 6 days. After this time, growth medium in form of DMEM with 10% FCS (fetal bovibe serum) and 1% penicillin was removed.
- As a next step, 0.45ml of micelle solution with concentration of 1mg/1ml was added and incubated at 37°C for 30minutes.
- Slides were washed twice with PBS and analysed by fluorescent microscope.

For obtaining pictures by fluorescence microscopy the growth medium was changed to DMEM + 1% horse serum + 1% penicillin and pH of the samples was adjusted to 10.

3. Results & Discussion

The following sections will describe the results obtained during this master thesis work and also provide an insight into the discussion of relevant aspects. Firstly, the polymer chemistry was investigated by means of FTIR analyses, CMC study and solvent optimization of the PVP-OD 20%AA polymer. Furthermore, we evaluated the polymer's conjugation with 5-Aminofluorescin dye via the EDC/NHS route with the help of UV-Visible spectroscopy, Fluorescence spectroscopy and FTIR spectroscopy. Finally, the polymeric micelles were produced by cosolvent evaporation, dialysis and direct dissolution method and their size and charge distribution were obtained using Zetasizer instrument.

3.1 FTIR analysis of the polymer

Initially, we performed the FTIR spectroscopy to analyse the different chemical groups present in the polymer with varying degree of carboxylation (PVP-OD with 0%, 20% and 100% acrylic acid). All the polymer samples were subjected to FTIR instrument in ATR mode and spectra were processed and analysed with the help of Bio-Rad Know It All software (Section 2.2.4). Obtained polymer spectra are presented in figures 3.2 - 3.6.

The polymer samples were provided as a courtesy of research group of Prof. Shtilman from Mendeleev University, Moscow but information about molecular weight distribution and other spectroscopic data was not included (Figure 3.1). In our study, we have focused on PVP-OD 20%AA polymer (12kDa) keeping in mind that this level of carboxylation should be sufficient for efficient crosslinking reaction with primary amines, such as 5-Aminofluorescein used in this project work.

In order to identify the main chemical vibrations associated with PVP polymer, we have correlated the spectral data obtained from FTIR measurements with the existing polymer database using the Bio-Rad KnowItAll software. The idea behind using polymer with varying degree of carboxylation was to identify the position of the most significant functional group i.e. -COOH belonging to the acrylic acid part of the polymer, as this group will be modified by conjugation of 5-Aminofluorescin dye via EDC/NHS chemistry.

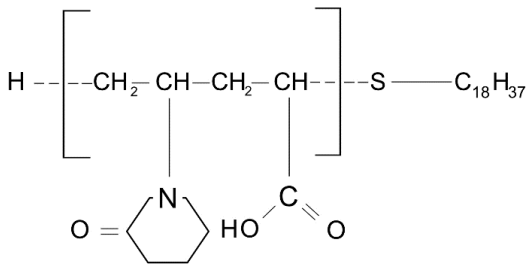

Figure 3.1: General structure of the amphiphilic block copolymer based on 1-Vinyl-2-pyrrolidinone and acrylic acid.

Table 3.1 summarizes the results obtained from the comparative study of FTIR spectra in correlation to the reference spectra present in the Bio-Rad KnowItAll software database. (Figures 3.2-3.5) The observed anomalies have been mentioned in the comment section of Table 3.1 which is further elaborated and explained.

Table 3.1: Summary of results obtained from FTIR analysis with reference spectra.

	Type	**Bond**	**Range(cm^{-1})**	**Mode**	**Comment**
1.Polymer reference [Fig. 3.2]	PVP	CH_2 CH_2 C=O CH_2 CN	2950-2910 2920-2840 1690-1640 1490-1420 1290-1250	Anti-symmetric Symmetric Stretching Deformation Stretching	The tertiary amide poly (vinyl pyrrolidone), PVP, shows a strong C=O absorption band near 1660 cm^{-1}. Other characteristic features are the medium intensity CH_2 deformation bands near 1420 cm^{-1} and the C-N doublet near 1280 cm^{-1}.
	Type	**Expected Bond**	**Observed value (cm^{-1})**	**Expected mode**	**Comment**
2.Polymer measured [Fig. 3.2]	PVP-OD (12KDa)	CH_2 CH_2 C=O CH_2 CN	2918 2894 1655 1422 1287	Anti-symmetric Symmetric Stretching Deformation Stretching	All the characteristic chemical vibrations are present and positionally, well within the range provided in the reference.
	Type	**Bond**	**Range (cm^{-1})**	**Mode**	**Comment**
3. Polymer reference) [Fig. 3.3]	Poly (acrylic acid)	OH C=O CH2 C-O C-O	3200-2500 1720-1700 1480-1440 1260-1230 1185-1165	Stretching Stretching Deformation Stretching Stretching	This spectrum is dominated by the intense C=O stretching mode absorption band near 1710 cm^{-1}. The broad hydrogen-bonded carboxylic acid -OH stretching band extending from about 3500 to 2400 cm^{-1} is another very characteristic feature.
	Type	**Expected Bond**	**Observed value (cm^{-1})**	**Expected mode**	**Comment**
4. Polymer measured	PVP-OD 100%AA	OH C=O	3150 1701	Stretching Stretching	The OH stretch appears as a shoulder not an

[Fig. 3.3]	(12KDa)	CH2 C-O C-O	1455 1244 1171	Deformation Stretching Stretching	intense peak due to the masking effect of water present in the sample. C=O stretch at 1655cm^{-1} which appeared in PVP-OD is not observable in this sample (PVP-OD 100%AA).
	Type	**Bond**	**Range (cm^{-1})**	**Mode**	**Comment**
5. Polymer reference [Fig. 3.4]	PVP	CH_2 CH_2 C=O CH_2 CN	2950-2910 2920-2840 1690-1640 1490-1420 1290-1250	Anti-symmetric Symmetric Stretching Deformation Stretching	The tertiary amide poly (vinyl pyrrolidone), PVP, shows a strong -C=O absorption band near 1660 cm^{-1}. Other characteristic features are the medium intensity CH_2 deformation bands near 1420 cm^{-1} and the C-N doublet near 1280 cm^{-1}.
	Type	**Expected Bond**	**Observed value (cm^{-1})**	**Expected mode**	**Comment**
6. Polymer measured [Fig. 3.4]	PVP-OD 20%AA (12KDa)	CH_2 CH_2 C=O CH_2 CN	2918 2849 1646 1422 1284	Anti-symmetric Symmetric Stretching Deformation Stretching	All the characteristic chemical vibrations are present and positionally, well within the range provided in the PVP reference. * Appearance of small peak at 1716 cm^{-1} might come from C=O stretch present in acrylic acid group of PVP-OD 20%AA.
	Type	**Bond**	**Range (cm^{-1})**	**Mode**	**Comment**
7. Polymer reference [Fig. 3.5]	Poly (acrylic acid)	OH C=O CH2 C-O C-O	3200-2500 1720-1700 1480-1440 1260-1230 1185-1165	Stretching Stretching Deformation Stretching Stretching	This spectrum is dominated by the intense C=O stretching mode absorption band near 1710 cm^{-1}. The broad hydrogen-bonded carboxylic acid -OH stretching band extending from about 3500 to 2400 cm^{-1} is another very characteristic feature.

	Type	Expected Bond	Observed value (cm^{-1})	Expected mode	Comment
8. Polymer measured [Fig. 3.5]	PVP-OD-20%AA (12KDa)	OH C=O CH2 C-O C-O	3154 1716 ------- ------- 1171	Stretching Stretching ---------- ---------- Stretching	The OH stretch appears as a shoulder not an intense peak due to the masking effect of water present in the sample. CH_2 stretching and C-O deformation band which was present in PVP-OD 100%AA sample doesn't appear in this sample (PVP-OD 20%AA). *Appearance of intense peak at 1646 cm^{-1} might come from C=O stretch present in pyrrolidone ring of PVP-OD 20%AA.

The comparative analysis between different reference spectra and measured polymer samples revealed the following anomalies:

- One of the main characteristic features of carboxylated PVP-OD is the presence of -OH stretching band extending from about 3500 to 2400 cm^{-1}. Nonetheless, the OH stretch appears as a shoulder not an intense peak and this can be explained by the masking effect of water molecules. Water exhibits two types of strong vibrations; stretching vibration of O–H appears at 3500–3000 wavenumber, meanwhile that of O–D is normally detected at 2600–2300 cm^{-1} [52]. PVP is highly hygroscopic in nature and thus retains 40% of water by its weight (described in section 1.2.3)**.** Due to the presence of water in the PVP sample by virtue of its intrinsic property, the OH stretch which should appear as an intense peak seems to be diminished.

We tried D_2O treatment of PVP-OD 20%AA sample so that the stretching water peak near 3500-2400 cm^{-1} might shift to higher vibration as in ideal scenario the heavier isotope should be the sole contributor. This doesn't seem to be working and only results in the appearance of a bump near 2500 cm^{-1} in carboxylated PVP-OD samples. This complication can again be attributed to the hygroscopic nature of the PVP polymer. As advised by our FTIR expert, it's extremely hard to devoid the water effect if the material under investigation is hygroscopic and if possible, the instrumentation setup might require a protective desiccator covering while performing FTIR measurement.

- The other very important characteristic feature of carboxylated PVP-OD is the presence of two prominent C=O stretching mode absorption bands; intense C=O stretching band from acrylic acid part of carboxylated PVP-OD, near 1710 cm^{-1} and a strong C=O absorption band from pyrrolidone ring part of carboxylated PVP-OD, near 1660 cm^{-1}. These peaks exhibit positional fluctuation which is depicted in Figure 3.6

For PVP-OD and PVP-OD 20%AA sample, the pyrrolidone ring associated C=O peak appears at 1655 cm^{-1} and 1646 cm^{-1}, respectively. This shift can be explained by the introduction of acrylic acid group in the close vicinity of pyrrolidone ring in PVP-OD polymer which can induce a change by affecting the strength of molecular interactions thus effecting the vibrational frequency of C=O group present in the pyrrolidone ring.

In case of PVP-OD 100%AA sample, there is a prominent intense peak at 1701 cm^{-1} and C=O stretch from pyrrolidone ring which appeared at 1655 cm^{-1} and 1646 cm^{-1} (PVP-OD and PVP-OD 20%AA respectively) is not observable in this sample.

The comparison among all the three spectra (Figure 3.6) reveals that the C=O stretch at 1716 cm^{-1} in PVP-OD 20%AA and C=O stretch at 1701 cm^{-1} in PVP-OD 100% AA are associated with acrylic acid part of the polymer (also in accordance with the poly acrylic acid reference spectrum). The positional peak shift in these samples can be “directly correlated with the level of specific molecular interactions, such as hydrogen bonding and dipole–dipole interactions. The apparent frequency shift of C=O stretching band under concentration change can be attributed to the gradual weakening of such interactions” [53]. The different level of carboxylation is a major factor when it comes to the C=O acrylic acid absorption band position. It also appears that the C=O absorption band from the pyrrolidone part of the polymer might overlap with the C=O acrylic acid absorption band in PVP-OD 100% AA sample, which explains its disappearance depicted in figures 3.3 and 3.6

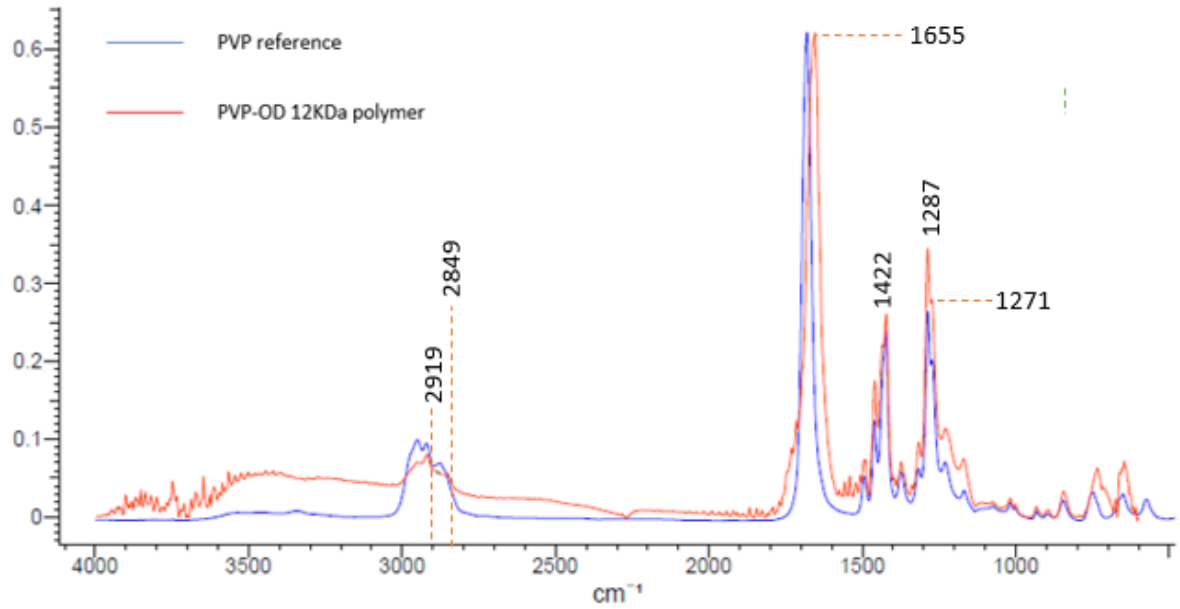

Figure 3.2: Comparative IR spectra of Poly (vinyl pyrrolidone) reference and PVP-OD 12KDa without acrylic acid polymer (all the significant peaks have been marked; refer to table section 1&2)

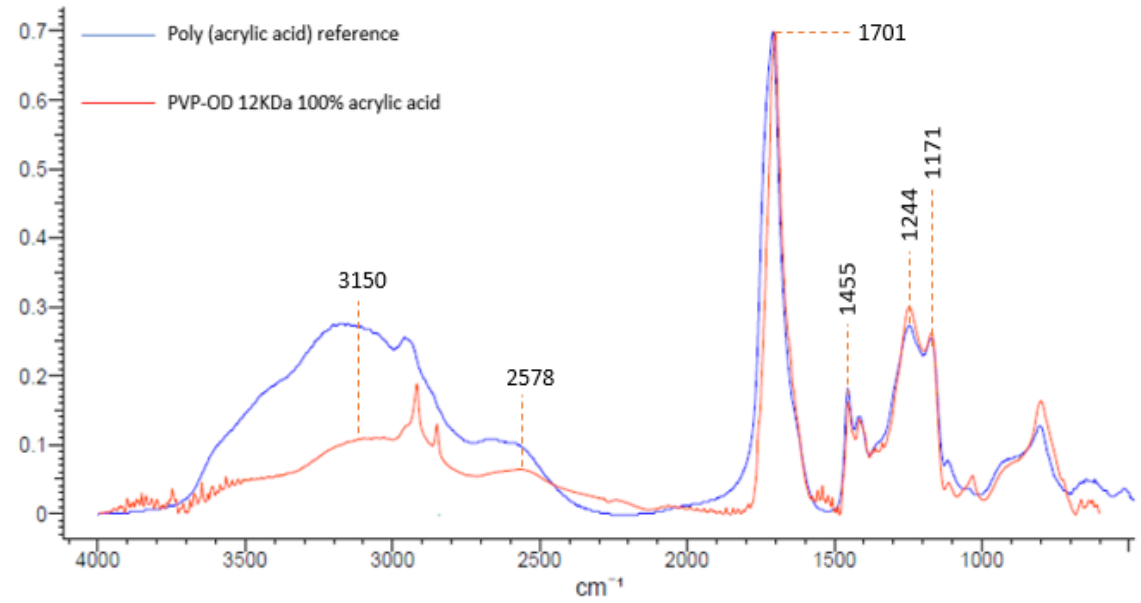

Figure 3.3: Comparative IR spectra of Poly (acrylic acid) reference and PVP-OD 100% acrylic acid polymer (all the significant peaks have been marked; refer to table section 3&4; *D_2O peak at 2578 cm^{-1}).

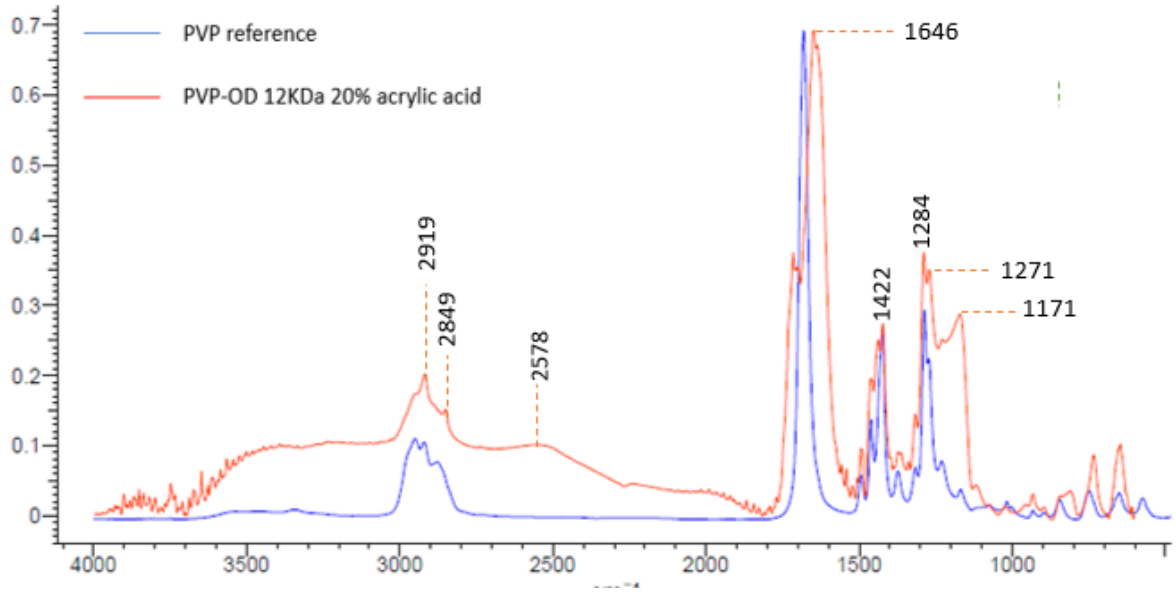

Figure 3.4: Comparative IR spectra of Poly (vinyl pyrrolidone) reference and PVP-OD 20% acrylic acid polymer (all the significant peaks have been marked; refer to table section 5&6; *D_2O peak at 2578 cm^{-1}).

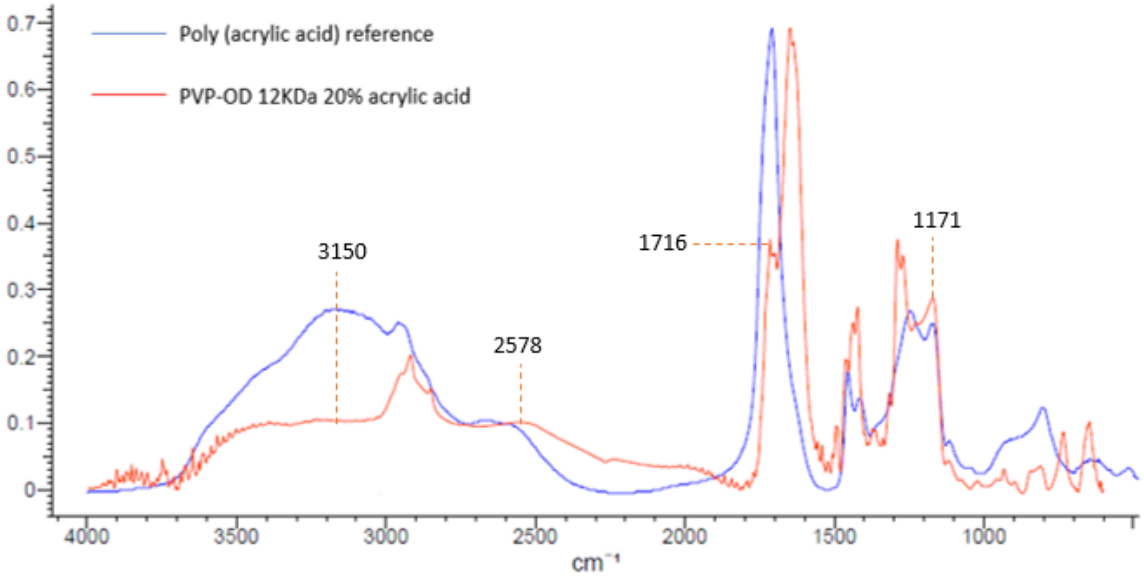

Figure 3.5: Comparative IR spectra of Poly (acrylic acid) reference and PVP-OD 20% acrylic acid polymer (all the significant peaks have been marked; refer to table section 7&8; *D2O peak at 2578 cm-^{1}).

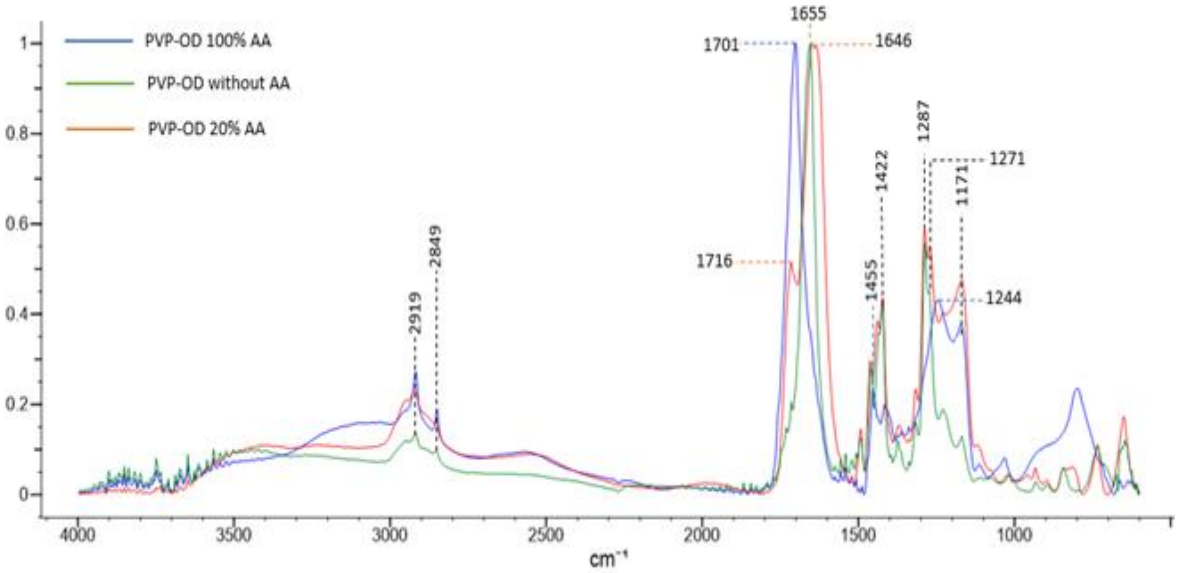

Figure 3.6: Overlay spectra of PVP-OD without acrylic acid, PVP-OD 20%AA and PVP-OD 100%AA (all the significant peaks have been marked and denoted in the table below).

Table 3.2: Description of the marked peaks along with expected mode and range of overlayed spectra.

Classification	Group	Bond	Range	Expected mode	Observed values (cm^{-1})
Polyamides	Poly vinylpyrrolidone	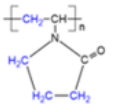	2950-2910	Antisymmetric	2919
			2920-2840	Symmetric	2849
			1490-1420	Deformation	1422
		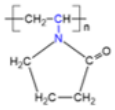	1290-1250	Stretching	1287 &1271
		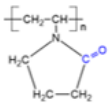	1690-1640	Stretching	1646, 1655
Aliphatic acids	Poly (acrylic acid)	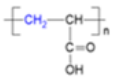	1480-1440	Deformation	1455
		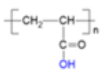	3200-2500	Stretching	3150
		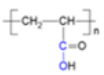	1260-1230	Stretching	1244
			1185-1165	Stretching	1171
		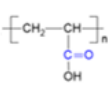	1720-1700	Stretching	1701, 1716

3.2 Investigation of critical micellar concentration of PVP-OD polymer

Fluorescence spectroscopy was used to determine the critical concentration of micelle formation for PVP-OD polymers by Kulikov *et al.* [21]. They used DPHT (diphenylhexatriene) as a fluorescence test indicator owing to its hydrophobic nature thus low solubility in water. It also exhibits a striking feature to fluoresce only in the associated state i.e., upon incorporation into the hydrophobic core of the micelle. The main principle lies in the solubilization of hydrophobic DPHT with polymer particles upon reaching the critical concentration leading to micellization and giving highly intense fluorescence in the associated state. The study was carried out at a certain concentration of DPHT with the help of a spectrophotometer (excitation wavelength λ_{ex} = 366 nm, emission wavelength λ_{em} = 433 nm) (Figure 3.7a).

The research group also analysed the effect of number-average molecular weight on the CMC value of the synthesized polymers containing 18-Carbon octadecyl hydrophobic fragment (table 3.3). The data revealed that the CMC value increases with the number-average molecular weight and reaches an inflection around 12kDa (Figure 3.7b). Moreover, the ability to form micellar structures in the aqueous medium depends on the hydrophilic fragment since the hydrophobic fragment remains unchanged with changing average molecular weight of the PVP-OD polymer. The evidence suggested that the low number-average molecular weight polymers have high emulsifying ability, and so these polymers can be considered a good candidate as solubilizers for the DiI fluorescent dye [21].

Table 3.3. List of PVP based polymers with different number average molecular weight and the corresponding CMC value [21].

Sample name	Number-average molecular weight of amphiphilic polymer, kDa		Hydrophobic fragment	CKM, mmol/L
	titration	elemental analysis		
Amph-40	40200	42015	$C_{18}H_{37}$	0.764
Amph-20	20040	21050	$C_{18}H_{37}$	0.339
Amph-12	12000	12250	$C_{18}H_{37}$	0.095
Amph-6	6100	6200	$C_{18}H_{37}$	0.065
Amph-3	3210	3100	$C_{18}H_{37}$	0.054
Amph-1	1030	980	$C_{18}H_{37}$	0.044

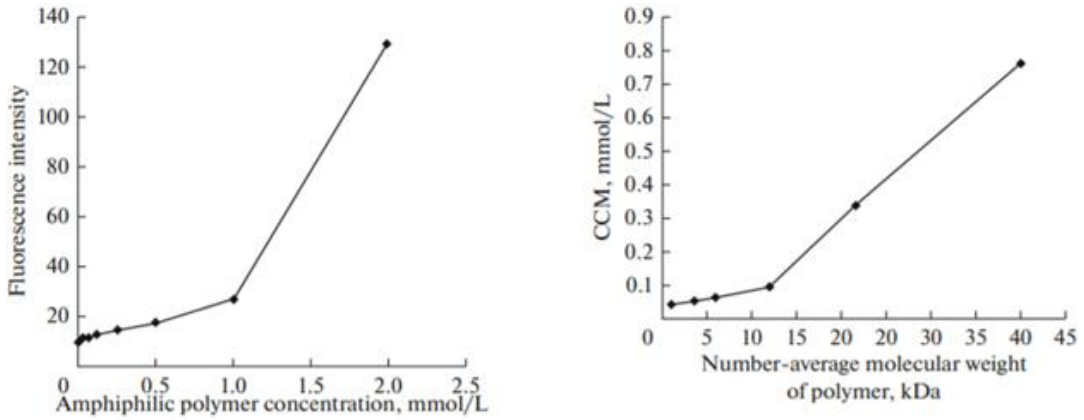

Figure 3.7: (a) Fluorescence intensity of DPHT dye in relation to the polymer concentration and (b) CMC of PVP based polymers as a function of number average molecular weight [21].

3.3 Optimization of solvent for the polymer and conjugation reaction via EDC/NHS chemistry.

The following section provides an insight into solvent optimization for PVP-OD 20%AA polymer along with some additional information about Polymer dynamics with regards to the calculation of concentration regime based on our theoretical consideration of radius of gyration. (described in section 1.3.1)

The polymer used in our study is an acrylic acid modified vinyl-based block copolymer containing thiooctadecyl-terminated block. The hydrophilic nature of this polymer comes from the pyrrolidone ring and the acrylic acid moiety whereas the hydrophobic nature comes from the vinyl part and the thiooctadecyl-terminated block (mentioned in section 1.2.3). In general, PVP is soluble in water and non-aqueous solvents but this modified variation proved to be quite troublesome when it comes to dissolution in water and organic solvents. It has been observed that “PVP is protonated and soluble in water at low values of pH and deprotonated and fairly hydrophobic at pH higher than 4.8” [26].

As a first step, we designed a pH-based solubility test for PVP-OD 20% AA polymer in aqueous medium. We tried dissolving PVP-OD-20%AA in acidic (pH~4), neutral (pH 7) and basic (pH~10) water under constant agitation (via magnetic stirring) and it has to be noted that within the same concentration (1mg/1ml), sample with basic pH appeared to be way less turbid compared to acidic and neutral one. It gave a clear indication that water with basic pH seems more suitable for various experiments with PVP-OD-20%AA. This observation goes against the behaviour of non-modified PVP polymer mentioned above. To have a reference of solubility, we also dissolved PVP-OD without acrylic acid and PVP-OD with 100% carboxylation in the same fashion as for PVP-OD-20%AA and to our surprise, all the samples showed better solubility in water, regardless of the pH.

PVP-OD 20%AA polymer belongs to the polyamide classification containing a tertiary amide group and a carboxylic group. Based on the pH chemistry, PVP-OD 20% AA should be protonated at low pH and deprotonated at higher pH values in water and therefore low pH should be favourable for its dissolution. But it seems like this polymer doesn't prefers aqueous hospitality so we had to exclude water as a potential solvent for polymer dissolution and subsequent, 5-Aminofluorescein dye conjugation reaction.

Consequently, we decided to search for alternative in organic solvents, such as Chloroform, DMSO, DMF, Ethanol and Acetone. Even though chloroform seemed to dissolve PVP-OD-20%AA rather well, it had to be excluded from choice pool, since one of the main chemicals used for conjugation mechanism, namely NHS is completely insoluble in chloroform. For rest of previously mentioned organic solvents we performed an old-fashion solubility test. It showed, that DMSO and DMF are exceptionally good solvents for PVP-OD-20%AA, since only 5ml of DMSO or 2ml of DMF was required to fully solubilize the polymer and even upon significant water addition, both solutions remained transparent until water content reached 61% for DMSO and 41% for DMF. It can be explained by the fact, that DMSO is more polar solvent compared to DMF and therefore it is better miscible with water. In case of ethanol and acetone, even with concentration of 1mg/1ml, both of the solvents couldn't dissolve the polymer at all. Although, addition of 1ml of water to ethanol sample resulted in almost instant and full dissolution of the polymer. Upon further water addition visible turbidity appeared at 77% concentration of ethanol and was increasing until 47%, where polymer almost fully precipitated. Acetone behaved in a very similar manner, where after adding 2ml of water polymer solubilized well, nonetheless at 74% acetone concentration strong turbidity appeared and at 66% polymer was almost fully precipitated. The graph 3.1 summaries the result obtained from the solubility test with organic solvents.

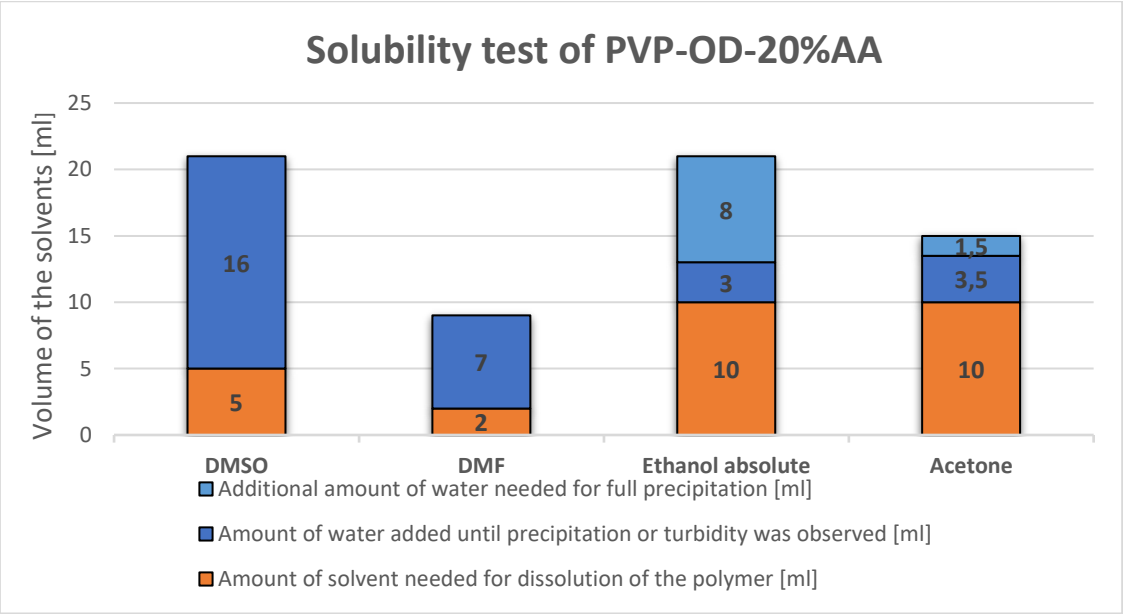

Graph 3.1: Polymer solubility test in various organic solvents.

Based on the solubility test it can be deduced that best solvents for PVP-OD-20%AA are DMF > DMSO > Ethanol > Acetone. Nonetheless, usage of DMF or DMSO implies certain complications, since both solvents are considered as highly toxic and are hard to get rid of by standard laboratory methods. Moreover, DMSO possess a very high dielectric constant with value of 47.24 at 20°C and according to the literature [54], DMSO is not a suitable solvent for EDC/NHS conjugation reaction, since it reacts with EDC and leads to formation of unwanted racemic by-product hindering the efficiency of amidation reaction.

After considering all the complications associated with DMSO/DMF, we started exploring ethanol as a safer and good alternative for polymer dissolution and EDC/NHS amidation reaction. The only concern with ethanol was that it might interfere with the carboxylic group present in the polymer via esterification reaction. So, we performed an FTIR analyses to check the chemical composition of PVP-OD 20% AA after dissolving it in ethanol and subjecting the freeze-dried, ethanol solubilized polymer to FTIR spectroscopy. The result obtained shows no change in the position of C=O stretch associated with the acrylic acid group of the polymer and also all the other characteristic chemical vibrations are present and positionally, well within the range (Figure 3.8).

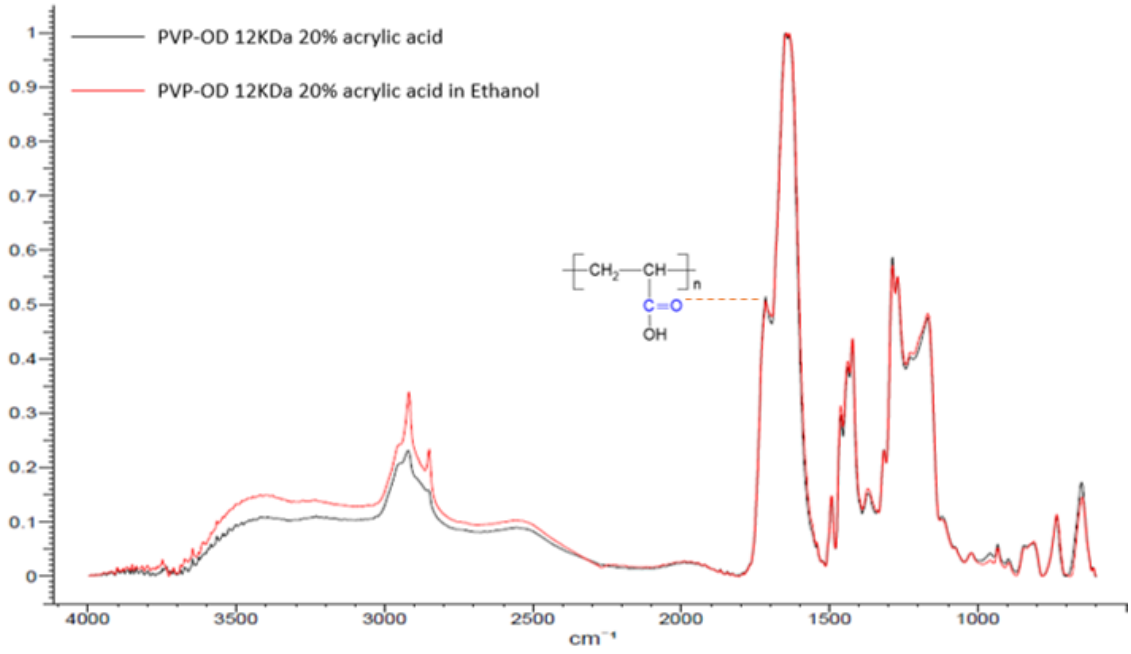

Figure 3.8: Comparative IR spectra of PVP-OD 20% acrylic acid (water) and PVP-OD 20% acrylic acid polymer (ethanol); only the relevant C=O stretch from acrylic acid part of the polymer is marked.

Investigation of Hansen solubility parameter (described in section 1.3.2) leaded to conclusion that ethanol is the most promising solvent for PVP polymer. Using the polymer solvent function in HSPiP software, it is possible to find a list of compatible solvents based

on the principle of *like dissolves like* [55]. The online database suggested ethanol as a most suitable solvent for PVP polymer (Table 3.4).

Table 3.4. Hansen Solubility Parameters components (δD, δP and δH for Dispersion, Polar and Hydrogen-bonding respectively) for ethanol and PVP polymer.

	δD	**δP**	**δH**
PVP	18.1	10	18
Ethanol	15.8	8.8	19.4

3.4 Radius of gyration and concentration regime calculation for PVP-OD-20%AA polymer

Polymers in a solution are dynamic in nature, random coils of the polymer chains interact with other coils leading to entanglement. In a strict thermodynamic sense, even if a polymer is soluble in a given solvent, it might take a long time for a portion of it to actually go into the solution even if dissolution is carried under heavy agitation. Concentration regime comes into picture when we talk about interaction of polymer chains in a solution. It is divided into three broad categories based on the concentration of polymer in solution; dilute, semi-dilute and concentrated (described in section 1.3.1). Usually, polymer dynamics is studied in either dilute regime, where polymer chains are separated from each other or semi-dilute regime in which chains begin to overlap leading to impartment of different thermodynamic properties.

In order to figure out the concentration regime, the **Overlapping Concentration** [28] can be calculated using the equation 1.5, mentioned in section 1.3.1.

$$c^*\left(\frac{4\pi}{3}R_g^{\,3}\right) = \frac{M}{N_A}$$

where M/N_A is the mass of each chain, N_A - Avogadro's number and Rg is the radius of gyration.

This equation is based on a simple approximation that each linear polymer chain occupies a space of a sphere of a linear dimension of radius of gyration R_g, as illustrated below.

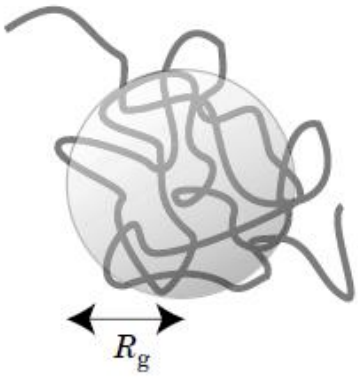

Figure 3.9: Polymer chain has a volume approximately of a sphere of radius R_g [28].

Radius of gyration (R_g) is required in order to calculate the Overlapping concentration. Radius of gyration can be obtained from hydrodynamic radius (R_h) measured with the help of Dynamic light scattering experiment. Based on the theoretical predictions (Dynamic and static light scattering studies), radius of gyration (R_g) is related to hydrodynamic radius (R_h); for a theta solvent $R_h = 0.66\ R_g$, and for a good solvent $R_h = 0.537\ R_g$ [56].

In our study, we have calculated the overlapping concentration based on the DLS results approximation of hydrodynamic radius (R_h) ~ 10 nm and assumption that ethanol is a good solvent for PVP-OD 20%AA polymer. Taking all previously mentioned information into account and applying it to the equations mentioned above, the Overlapping concentration for PVP-OD 20%AA (12KDa) is around 0.6 to 1mg/mL. It is a very important parameter because our EDC/NHS crosslinking reaction calculations for polymer dissolution is based on keeping the Overlapping concentration range in mind. We wanted to operate in the dilute concentration regime, so that the polymer chains would freely move in the solution (avoiding entanglement) which should provide better crosslinking efficiency.

3.5 Conjugation of 5-Aminofluorescein to PVP-OD-20%AA via EDC/NHS chemistry.

After studying the properties of the PVP-OD 20%AA and taking the solvent compatibility and Overlapping concentration into consideration, we evaluated the polymer's conjugation with 5-Aminofluorescin dye in ethanol via the EDC/NHS route. The results obtained with the help of UV-Visible spectroscopy, Fluorescence spectroscopy and FTIR spectroscopy are described in this section along with the relevant discussion associated with solvent and pH dependent behaviour of 5-Aminofluorescein dye and EDC/NHS chemistry.

3.5.1 pH consideration and general reaction mechanism of EDC and NHS chemistry for PVP-OD-20%AA and 5-Aminofluorescein

The pH of reaction environment for EDC-NHS chemistry is crucial parameter for optimization of the amidation reaction. Unfortunately, available literature does not offer universal approach in this regard. General statement is that carbodiimide activation is possible when carbodimide is in protonated state, whereas carboxylate is ionized [43]. Protonation of EDC nitrogen atom results in decrease of electron density at EDC central carbon atom, which leads to more favourable nucleophilic attack by the carboxylate anion [57]. According to the literature [57], pH value in which EDC is protonated and carboxyl groups ionized is in range of 4.5-4.75 and is recommended for O-acylisourea formation. O-acylisourea is an unstable ester, which easily hydrolyse in water and its formation is essential step in order to achieve successful amidation reaction (Figure 3.10)

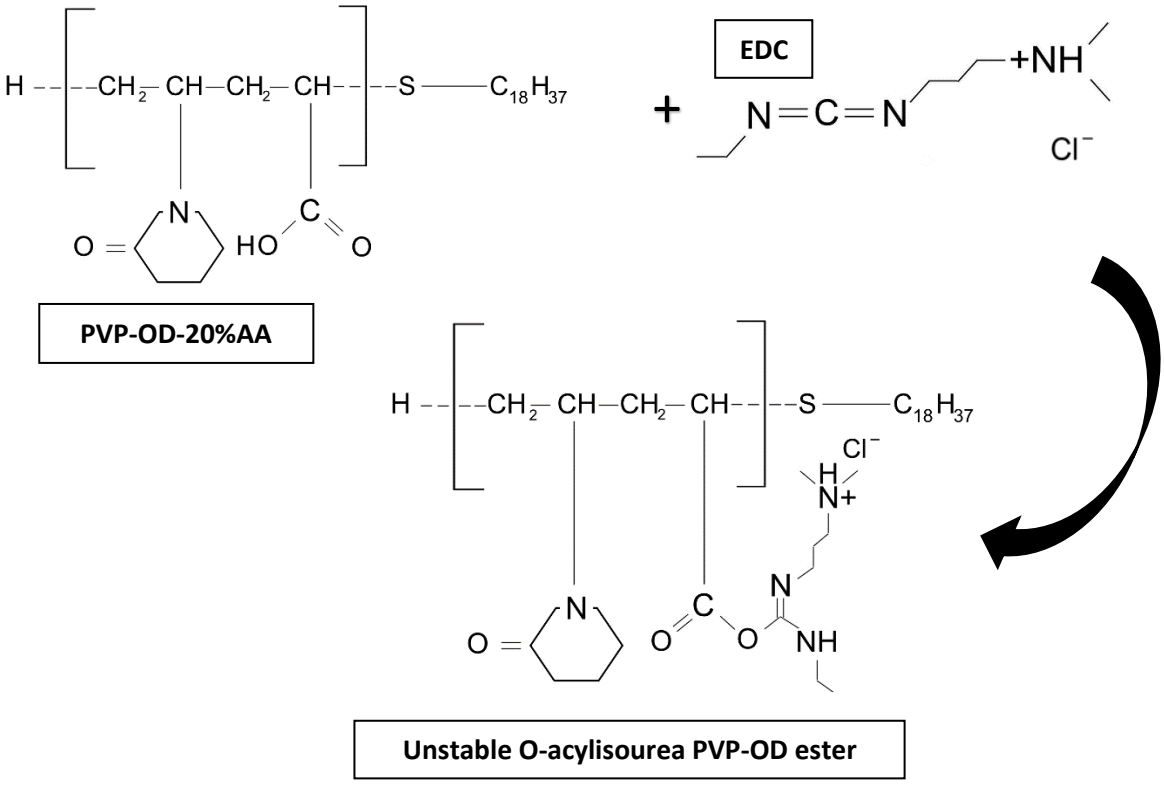

Figure 3.10: Formation of unstable O-acylisourea PVP-OD ester.

In order to improve efficiency of reaction and prevent hydrolysis of O-acylisourea, we decided to carry out two-step amidation with addition of NHS, which in reaction with O-acylisourea ester forms a more stable amine-reactive NHS ester (Figure 3.11)[43].

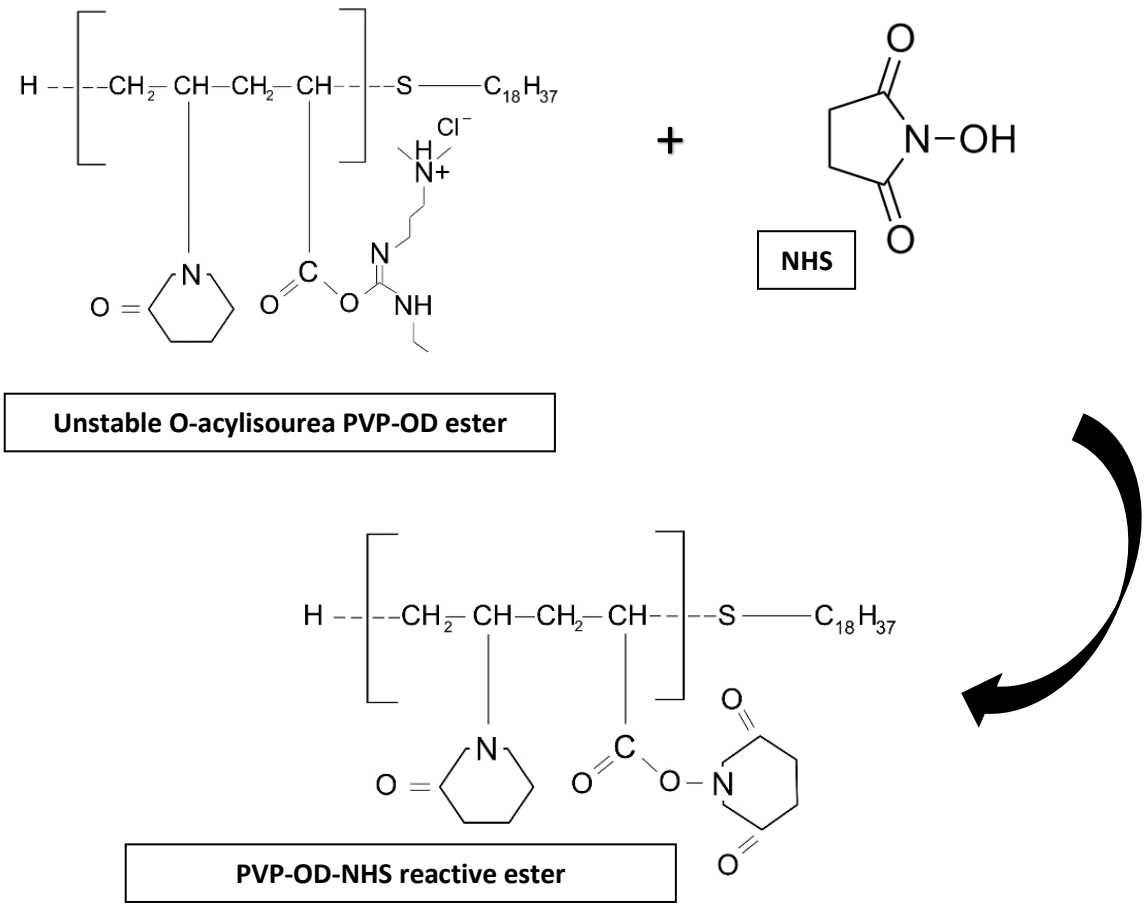

Figure 3.11: Conversion of unstable O-acylisourea PVP-OD ester into PVP-OD-NHS reactive ester.

Unfortunately, the most suitable conditions for ester creation are different for amide bond formation. The reaction of O-acylisourea or NHS-amine reactive ester with primary amine is typical nucleophilic attack [43]. Therefore it important to maintain unprotonated state of 5-Aminofluorescein to preserve its nucleophilicity [58]. Nonetheless, 5-Aminofluorescein is an example of primary amine and in pH range optimal for O-acylisourea formation (pH ~ 4.5) will be protonated. According to [59], the most efficient reaction between NHS-ester and primary amines is at pH>7, which ensures deprotonated form of chosen primary amine.

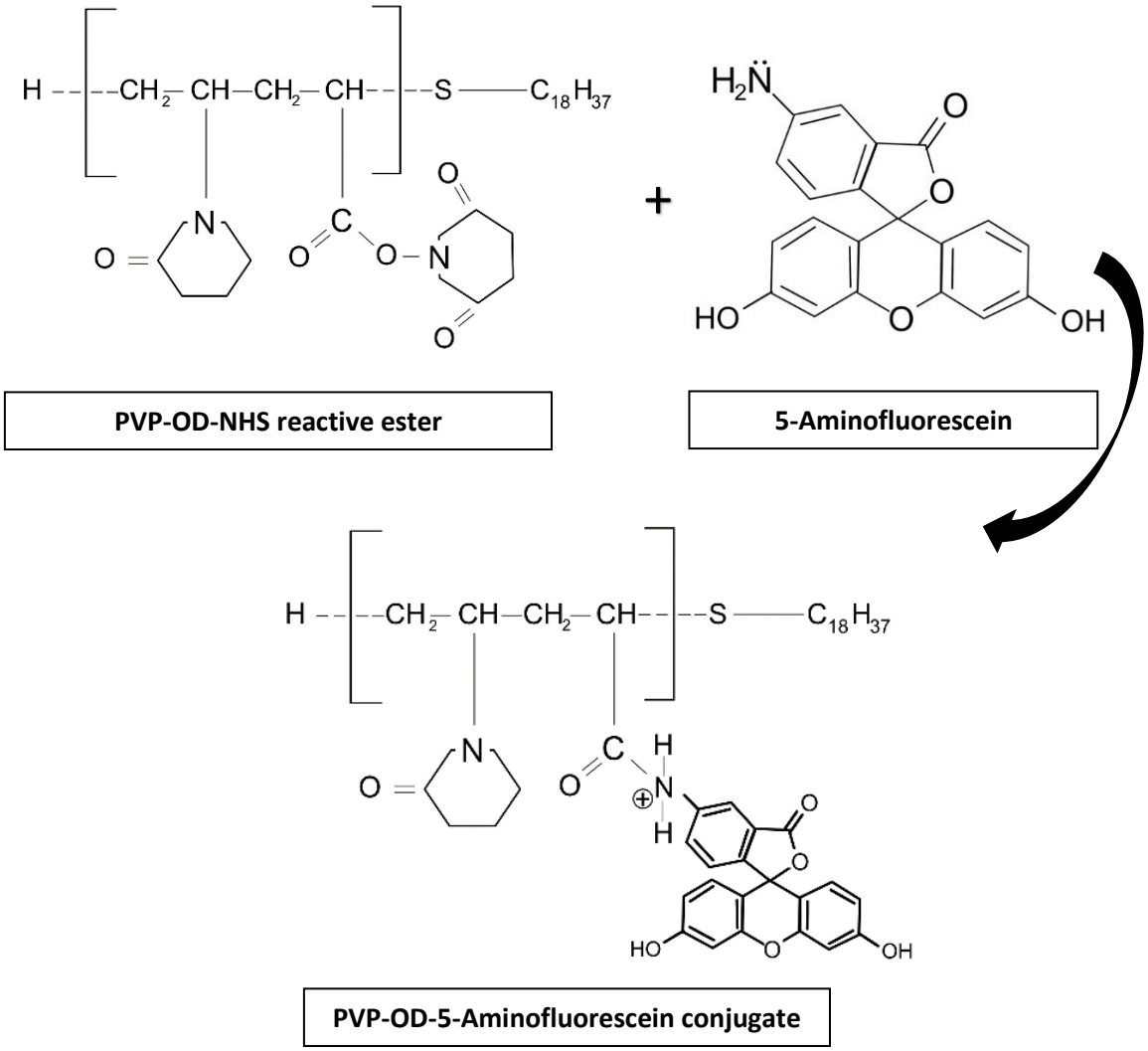

Figure 3.12: Formation of PVP-OD-5-Aminofluorescein conjugate

Consequently, two-step amidation approach was employed, with EDC and NHS activation mechanism in pH 4.5, where O-acylisourea is stable and amidation reaction in highly basic pH to ensure deprotonated state of 5-Aminofluorescein. To provide basic environment for amidation reaction, DIPEA was added to solution of 5-Aminofluorescein (Figure 3.13). DIPEA is a hindered base and poor nucleophile [60], therefore it will not compete in the conjugation reaction with nucleophilic 5-Aminofluorescein. Additional reason for using DIPEA is that during amidation reaction considerable amount of protons is being released, which could decrease the pH of reaction mixture and hinder conjugation mechanism. Presence of DIPEA excludes this possibility, since DIPEA is a proton scavenger commonly used in amidation reactions.

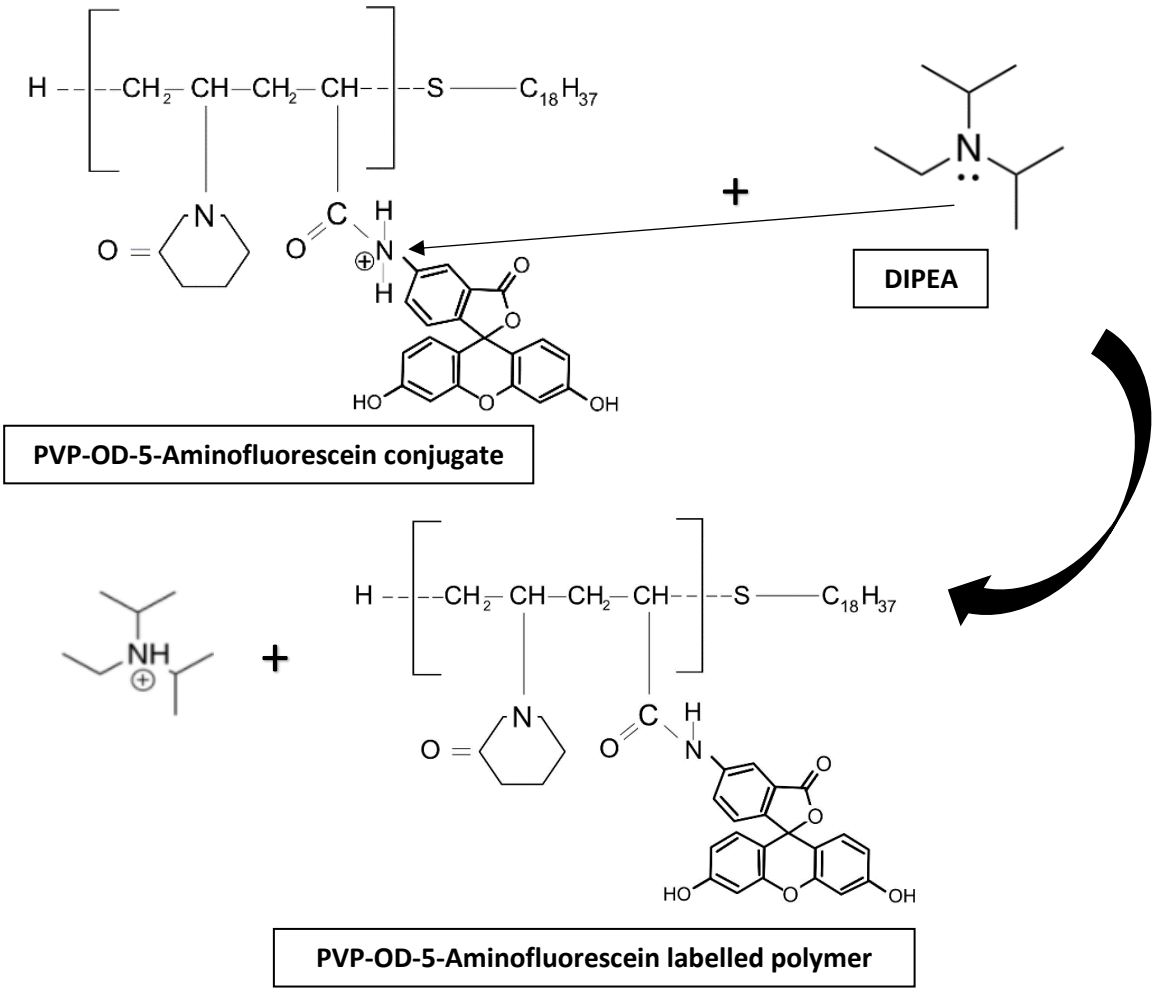

Figure 3.13: Representation of DIPEA influence on conjugation reaction.

Carbodiimide concentration is also a crucial factor to be considered while performing the EDC/NHS chemistry. EDC and NHS respective concentration should be selected carefully to produce efficient amidation reaction with minimal to no formation of unwanted by-products. In our study, we examined three different concentration ratios of EDC/NHS/COOH group (5:2:1,3:3:1 and 2:4:1). Out of the three, 3:3:1 gave the best result whereas 2:4:1 sample showed almost immediate precipitation during dialysis and after freeze drying obtained material was very sticky and not suitable for further analysis. Concentration of 5:2:1 appeared to produce insignificant zeta-potential value and distorted amide band peak in FTIR. This behaviour can be explained by the fact that when EDC concentration is large and NHS low, the amidation reaction kinetics is slow and thus results in the formation of unwanted by-products such as Anhydride and N-acylurea. On the other hand, the equimolar mixture of EDC and NHS results in the formation of desired intermediate O-acylurea and gives promising results from FTIR and UV-Vis spectroscopy [65].

3.5.2 UV-VIS and Fluorescence spectroscopy analysis

UV-Visible and Fluorescence spectroscopy was performed in order to analyse the absorption and emission profile of free and conjugated 5-Aminofluroscein dye in different pH conditions. All the samples were dissolved in water and subjected to UV-Visible and Fluorescence spectrophotometer.

Initially, we evaluated the absorption spectrum of non-conjugated PVP-OD 20%AA polymer in the visible range (400-700 nm) to exclude any interference that can arise due to the polymer. The spectrum doesn't show any significant absorbance (no absorption peak) in the visible range as depicted below in Figure 3.14

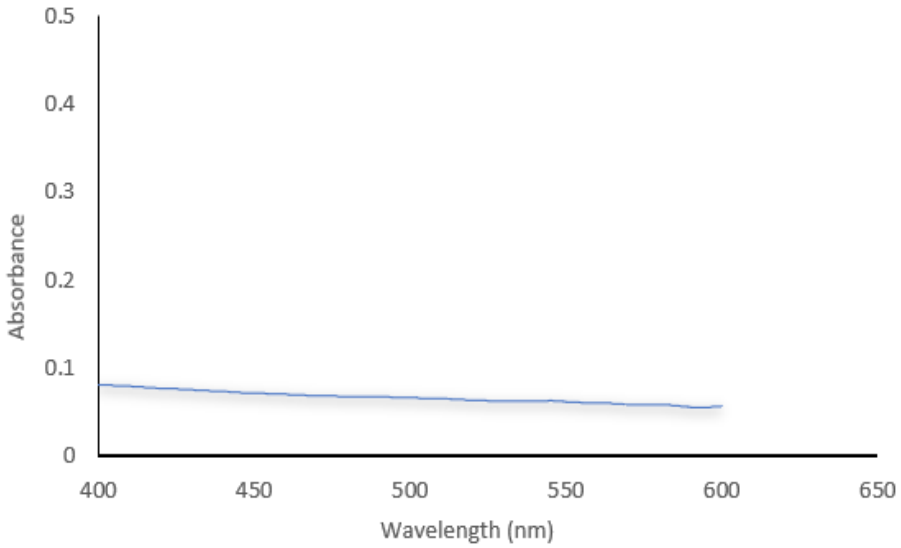

Figure 3.14: UV-Visible spectrum of PVP-OD-20%AA polymer dissolved in water (1mg/1ml).

According to the literature, Fluorescein or derivatized fluorescein dyes are used in many cytological applications due its pH sensitivity and high quantum yield. 5-Aminofluorescein, which is an amine derivative of fluorescein (Figure 3.15) is known to be pH sensitive and is shown to fluoresce at basic pH with high quantum yield [61]. 5-Aminofluorescein exhibits excitation at 490nm and emission at 515nm wavelength [62].

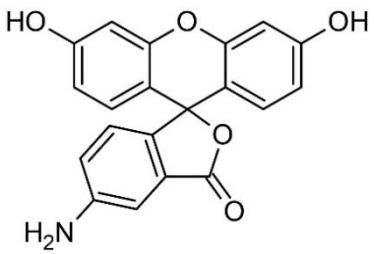

Figure 3.15: Chemical structure depiction of 5-Aminofluorescein dye [62].

Firstly, we investigated the behaviour of free 5-Aminofluorescein dye in different pH conditions and furthermore, we have evaluated the change in the absorption and emission profile of 5-Aminofluorescein dye upon conjugation with PVP-OD 20% AA (as we expect the amine group present in the dye to get converted into amide after the EDC/NHS reaction).

The result obtained from the UV-Visible spectroscopic investigation of free 5-Aminofluorescein dye in different pH conditions revealed that 5-Aminofluorescein shows a dual peak (454 and 477nm) nature with very low absorbance in water at pH 7 (Figure 3.16).

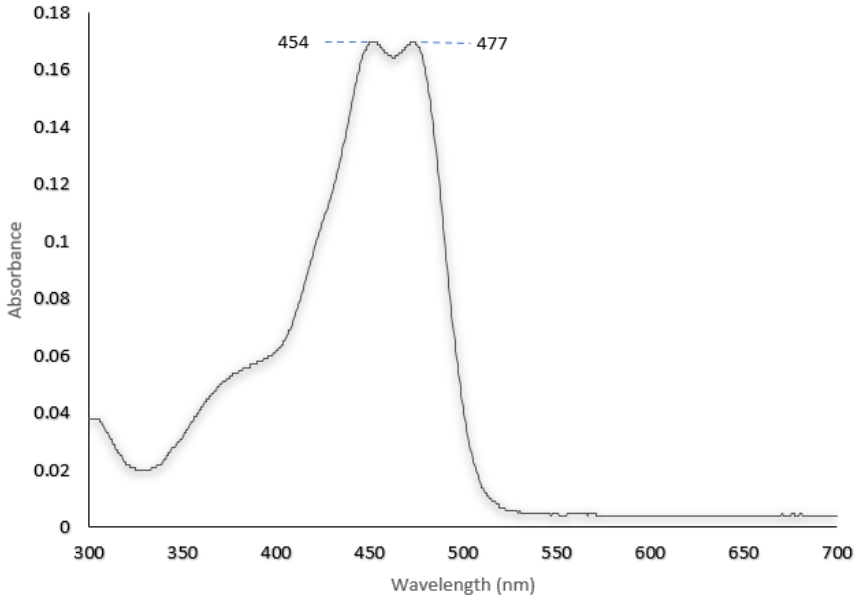

Figure 3.16: UV-Visible spectrum of free 5-Aminofluorescein dye in water (pH 7).

On the other hand, when pH of the sample was shifted to basic it resulted in the appearance of narrow absorption spectrum with a prominent absorption peak at 488nm (Figure 3.17).

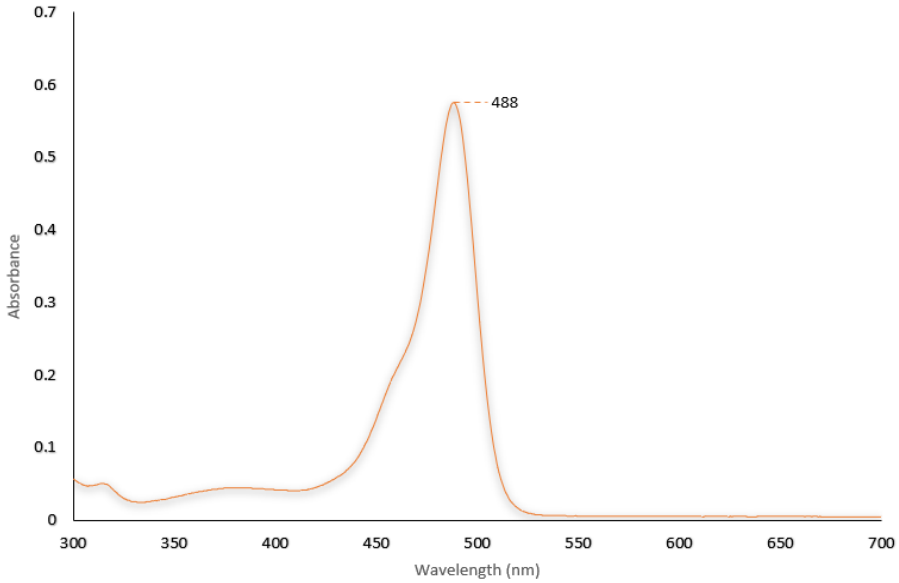

Figure 3.17: UV-Visible spectrum of free 5-Aminofluorescein dye in 0.01M NaOH (pH12).

The results obtained from the Fluorescence spectroscopic analysis of free 5-Aminofluorescein dye in different pH conditions shows slight shift in λ_{max} value from 512nm to 514nm as the pH shifts from 7 to 12 respectively. The result is depicted in Figure 3.18.

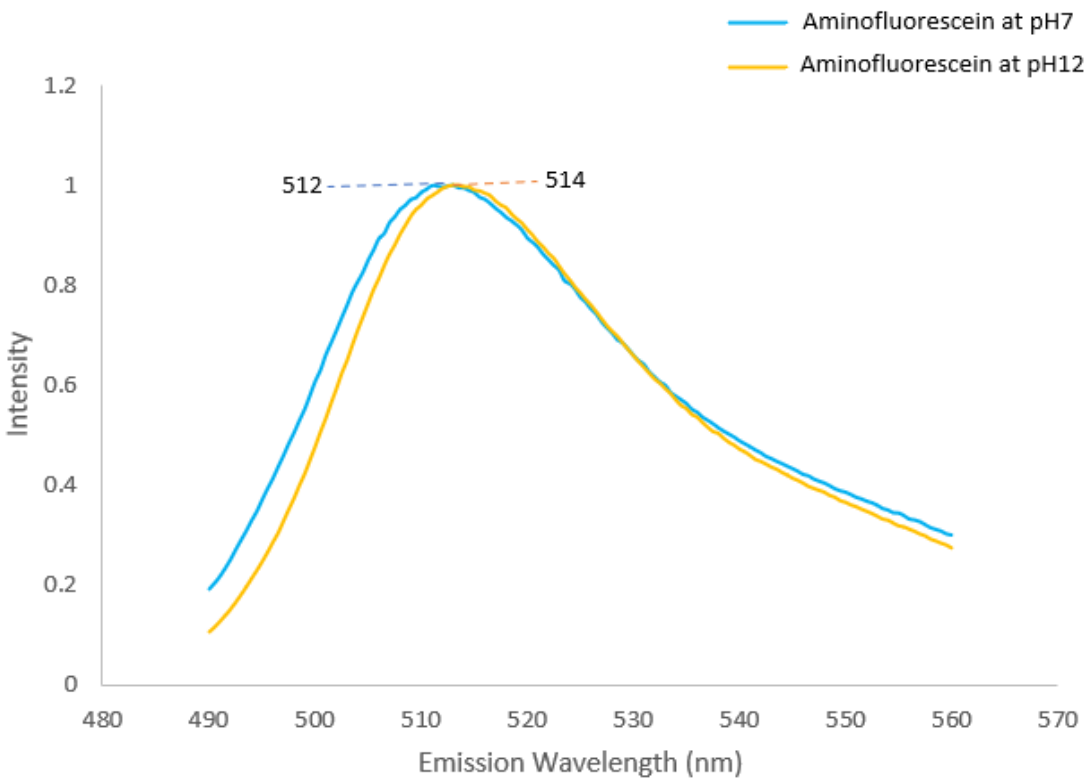

Figure 3.18: Emission spectrum of free 5-Aminofluorescein in different pH conditions (Excitation at 490nm).

The investigation of free 5-Aminofluorescein dye in different pH conditions indicates an overall red shift in λ_{max} value as the pH shifts to basic range. This behaviour can be understood by the chemical nature of 5-Aminofluorescein dye in solution (ionization and pH sensitivity). 5-Aminofluorescein is a derivative of Fluorescein dye and thus belong to the diprotic acid group, designated as H_2R. It has a tendency to ionize in solutions to form anions, HR^- and R^{2-} whereas in acidic medium, H_3R^+ cations are formed (depicted in the equation 3.1).

$$H_2R \rightleftarrows HR^- + H^+$$
$$HR^- \rightleftarrows R^{2-} + H^+ \quad (3.1)\ [61]$$

5-Aminofluorescein remains in protonated state (protonation of the aromatic amine) in acidic conditions (pH 3.2-4.6) and once deprotonation comes into play, the nitrogen lone pair is available for quenching [61]. The double charged anionic state R^{2-} is the preferred

state as the molecule exhibit strong fluorescence in aqueous media under basic conditions (deprotonation).

Based on the information gathered from the analysis of free 5-Aminofluorescein dye, we examined the nature of conjugated 5-Aminofluorescein dye with PVP-OD 20% AA (EDC/NHS chemistry). We employed a similar approach of measuring the absorption and emission profile of conjugated dye in different pH conditions. The results obtained from UV-Visible spectroscopy measurement shows no apparent peak in the case of conjugated dye at pH 4, whereas the shift in the pH to basic side results in the appearance of a prominent absorption peak at 492nm. The result is shown in Figure 3.19

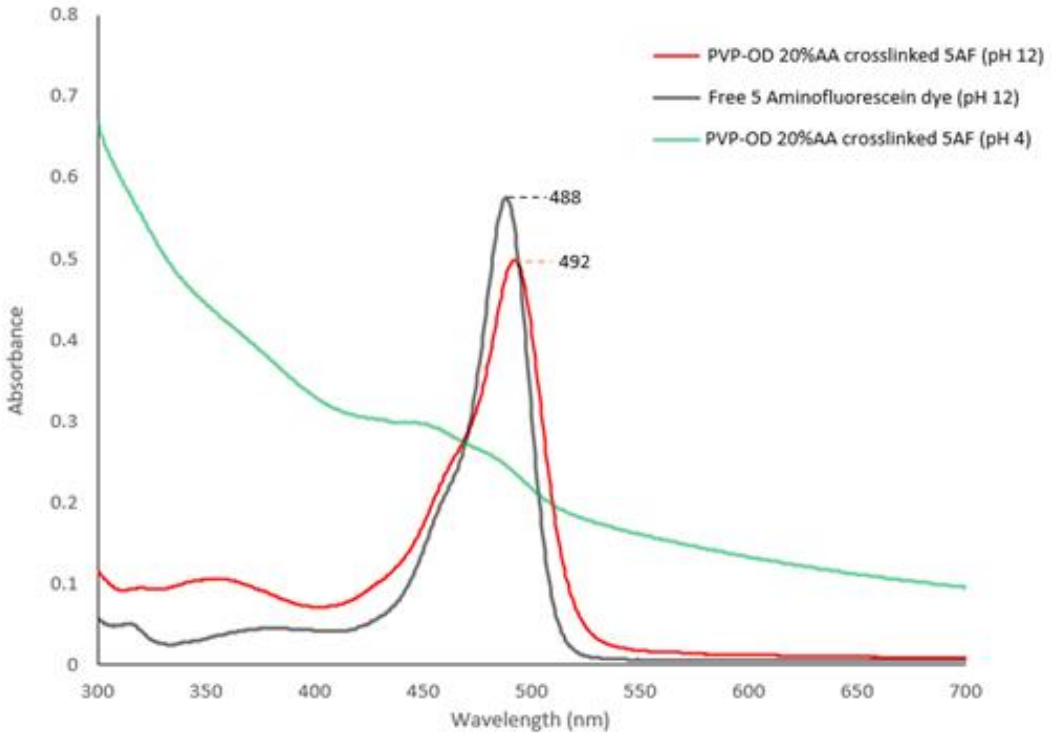

Figure 3.19: Overlay UV-Visible spectra of free 5-Aminofluorescein dye (pH 12) and PVP-OD 20%AA crosslinked with 5-Aminofluroscein (pH 4) and PVP-OD 20% AA crosslinked with 5-Aminofluroscein (pH 12)

The results obtained from the Fluorescence spectroscopic analysis of conjugated 5-Aminofluorescein dye in different pH conditions shows a peak shift in λ_{max} value from 512nm to 525nm as the pH shifts from 4.1 to 12 respectively. Upon comparison of free 5-Aminofluorescein dye with the conjugated one, it is evident that the amine group present in the dye is fluorescently affected, which is indicated by the red shift. The results are depicted in Figure 3.20 and 3.21.

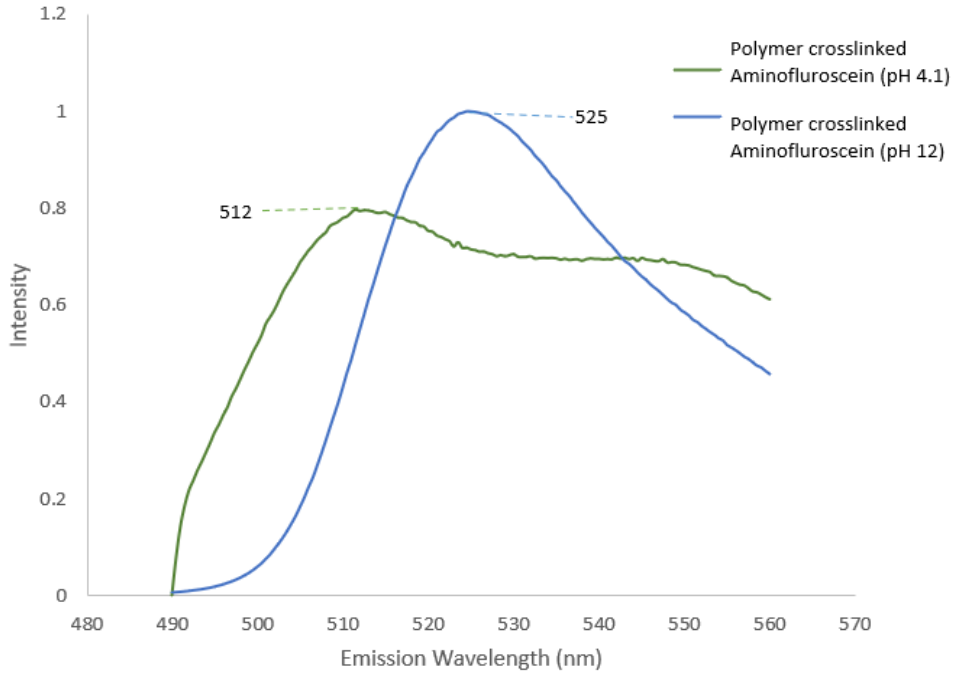

Figure 3.20: Emission spectrum of polymer crosslinked with 5-Aminofluorescein in different pH conditions (Excitation at 490nm).

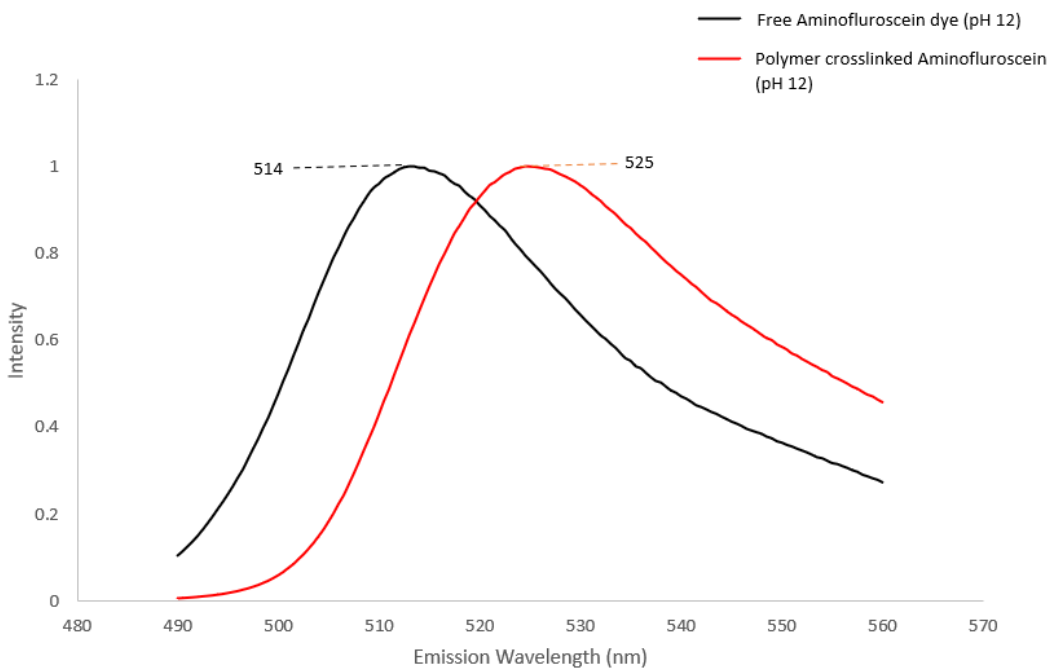

Figure 3.21: Overlay emission spectra of free 5-Aminofluorescein dye (pH 12) and PVP-OD-20%AA crosslinked with 5-Aminofluorescein (pH 12) with excitation wavelength of 490nm.

This spectral behaviour of conjugated 5-Aminofluroscein dye can be explained by studying the fluorescence mechanism and the factors that influence the fluorescent properties of 5-Aminofluorescein.

The non-modified 5-Aminofluorescein dianion gives a low quantum yield fluorescence in water. It has been reported that functionalization of amine group (NH2 → NHCOR), present in the 5-Aminofluorescein dye leads to full restoration of fluorescence property exhibiting high quantum yield [63]. This remarkable ability allows 5-Aminofluorescein to act as an indicator by controlling the fluorescence through the electronic influence of the nitrogen electron lone pair. "A typical amide derivatization can result in fluorescence enhancement in excess of 50-fold (Table 3.5). In these derivatives, electron withdrawal by oxygen of the carbonyl or sulfonyl group makes the amide nitrogen a much poorer source of electrons than the amine nitrogen and, therefore, decreases the intramolecular resonance with the -electron system of the ring as well as the participation in excited-state transfer processes." [61].

Table 3.5: Relative Fluorescence Emission Intensities of Fluorescein and its derivatives [61].

no.	R	concn (m × 10^{-6})[a]	λ_{max} (nm)	I_0 (K_{cps})[b]	ϕ
1	H	5.00	490	607	0.85[18]
2	NH_2	4.27	486	10.5	0.015
3	SCN	4.44	490	541	0.76
	Amide				
4	$CH_2CHCONH$	5.68	490	544	0.76
5	C_6H_5CONH	5.40	490	566	0.79
6	$(CH_3)_2CHCH_2CONH$	4.77	490	585	0.82
7	*p*-$CH_3OC_6H_4CONH$	3.39	490	625	0.88
	Nitrobenzamide Derivatives				
8	*o*-$NO_2C_6H_4CONH$	4.76	492	31.5	0.044
9	*m*-$NO_2C_6H_4CONH$	5.00	492	160	0.224
10	*p*-$NO_2C_6H_4CONH$	5.16	492	11	0.015

3.5.3 FTIR analysis for EDC and NHS conjugation.

FTIR spectroscopy was performed in order to get a clear indication and confirmation of the successful crosslinking results obtained from UV-Visible and Fluorescence spectroscopy. We have compared three distinct FTIR spectra (PVP-OD without acrylic acid, PVP-OD 20%AA and PVP-OD 100% acrylic acid) with the main crosslinking spectrum under investigation (PVD-OD 20% AA crosslinked 5-Aminofluorescein). All the polymer samples were subjected to FTIR instrument in ATR mode and the spectra were processed and analysed with the help of Bio-Rad Know It All software (section 2.2.4). The results obtained from the comparison of these FTIR spectra are depicted in Figures 3.22 – 3.24.

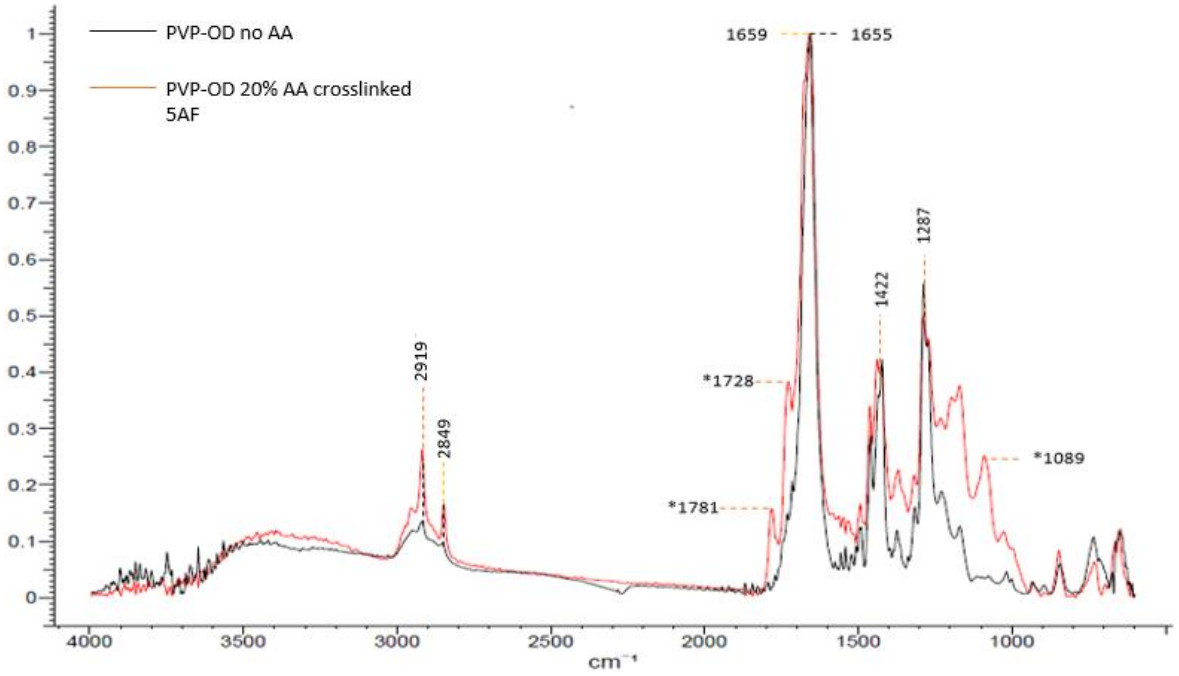

Figure 3.22: Overlay spectra of PVP-OD without acrylic acid and PVP-OD 20% crosslinked 5-Aminofluorescein (all the significant peaks have been marked; refer to table below)

Table 3.6: Description of the marked peaks along with expected mode and range of overlayed spectra.

	Type	Bond	Range (cm^{-1})	Mode	Comment
1.Polymer reference (Bio-Rad database)	PVP	CH_2 CH_2 C=O CH_2 CN	2950-2910 2920-2840 1690-1640 1490-1420 1290-1250	Anti-symmetric Symmetric Stretching Deformation Stretching	The tertiary amide poly (vinyl pyrrolidone), PVP, shows a strong C=O absorption band near 1660 cm^{-1}. Other characteristic features are the medium intensity CH_2 deformation bands near 1420 cm^{-1} and the C-N doublet near 1280 cm^{-1}.

	Type	Expected Bond	Observed value (cm^{-1})	Expected mode	Comment
2.Polymer measured **[Fig. 3.22]**	PVP-OD no AA (12KDa)	CH_2 CH_2 **C=O** CH_2 CN	2918 2894 **1655** 1422 1287	Anti-symmetric Symmetric Stretching Deformation Stretching	All the characteristic chemical vibrations are present and positionally, well within the range provided in the reference.
	Type	**Expected Bond**	**Observed value (cm^{-1})**	**Expected mode**	**Comment**
3.Polymer measured **[Fig. 3.22]**	PVP-OD 20% AA crosslinked 5-Aminofluorescein (12KDa)	CH_2 CH_2 **C=O** CH_2 CN	2918 2894 **1659** 1422 1287	Anti-symmetric Symmetric Stretching Deformation Stretching	The main C=O stretch from pyrrolidone ring is slightly shifted compared to PVP-OD no AA (Highlighted)

The result obtained from the comparison of PVP-OD no AA and PVP-OD 20% AA crosslinked 5-Aminofluorescein reveals that the C=O stretch associated with the pyrrolidone ring shows a very slight positional shift towards higher wavenumber. Apart of this, all the other characteristic chemical vibrations are present and positionally, well within the range provided in the PVP reference.

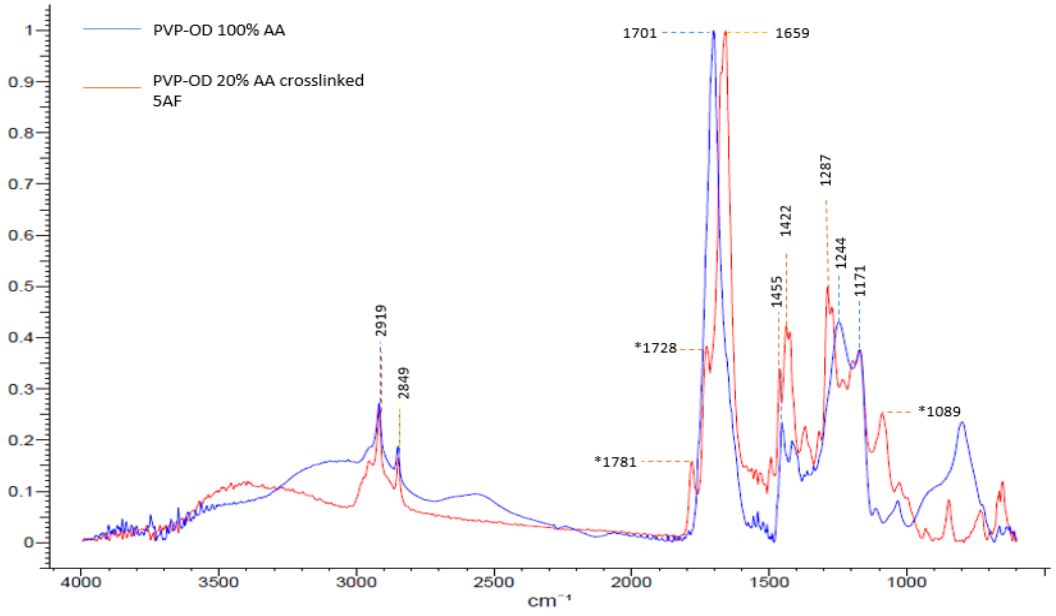

Figure 3.23: Overlay spectra of PVP-OD 100% acrylic acid and PVP-OD 20% crosslinked 5-Aminofluorescein (all the significant peaks have been marked; refer to table below).

Table 3.7: Description of the marked peaks along with expected mode and range of overlayed spectra.

	Type	**Bond**	**Range (cm^{-1})**	**Mode**	**Comment**
1. Polymer reference (Bio-Rad database)	Poly (acrylic acid)	OH C=O CH2 C-O C-O	3200-2500 1720-1700 1480-1440 1260-1230 1185-1165	Stretching Stretching Deformation Stretching Stretching	This spectrum is dominated by the intense C=O stretching mode absorption band near 1710 cm^{-1}. The broad hydrogen-bonded carboxylic acid -OH stretching band extending from about 3500 to 2400 cm^{-1} is another very characteristic feature.
	Type	**Expected Bond**	**Observed value (cm^{-1})**	**Expected mode**	**Comment**
2. Polymer measured **[Fig. 3.23]**	PVP-OD 100%AA (12KDa)	OH C=O CH2 **C-O** **C-O**	3150 1701 1455 **1244** **1171**	Stretching Stretching Deformation Stretching Stretching	The OH stretch appears as a shoulder not an intense peak due to the masking effect of water present in the sample.
	Type	**Expected Bond**	**Observed value (cm^{-1})**	**Expected mode**	**Comment**
3. Polymer measured **[Fig. 3.23]**	PVP-OD 20% AA crosslinked 5-Aminofluorescein (12KDa)	OH **C=O** CH2 **C-O** **C-O**	------ ------ 1455 ------ **1171**	Stretching Stretching Deformation Stretching Stretching	The main C=O stretch associated with acrylic acid group seems to be affected drastically. One of the expected C-O stretching is missing at 1244 cm^{-1} and the peak structure near C-O stretch 1171 cm^{-1} is slightly distorted.

The results obtained from comparison of PVP-OD 100% acrylic acid and PVP-OD 20% crosslinked 5-Aminofluorescein shows that the main C=O stretching band associated with acrylic acid group (1701-1720 cm^{-1}) seems to be drastically affected. Two of the expected C-O stretching bands related to acrylic acid group also appears to be different. The C-O stretching band at 1244 cm^{-1} is not present in the crosslinked polymer sample and the C-O

stretching band near 1171 cm^{-1} in crosslinked polymer sample shows a slightly distorted peak structure.

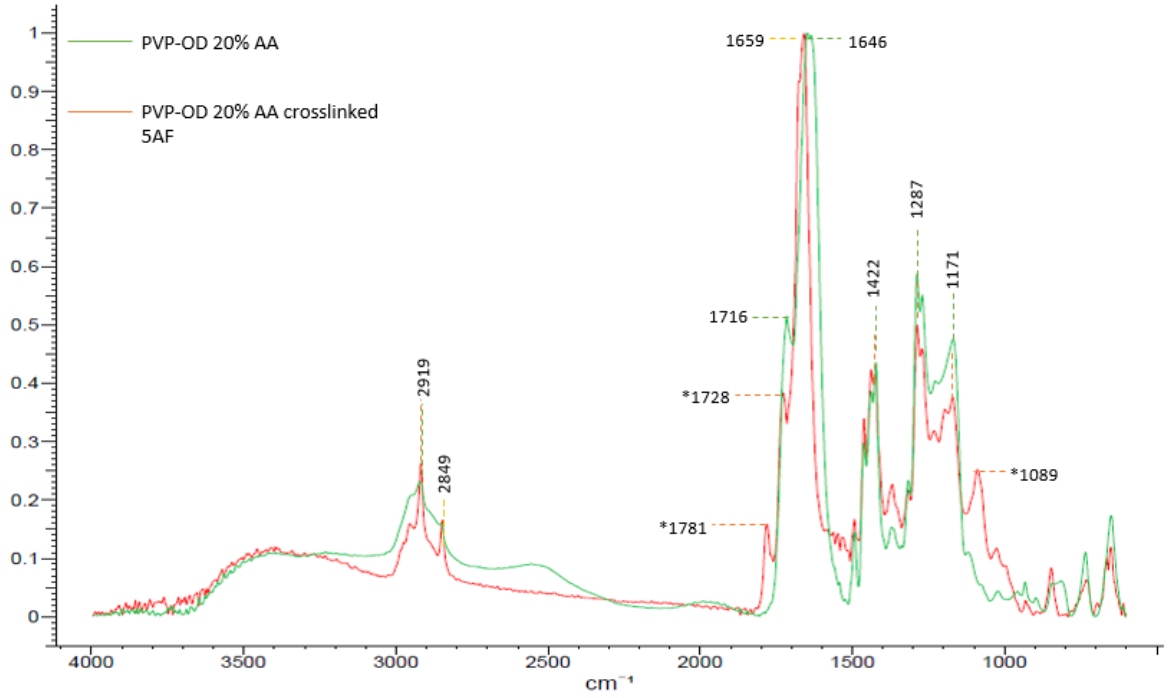

Figure 3.24: Overlay spectra of PVP-OD 20% acrylic acid and PVP-OD 20% crosslinked 5-Aminofluorescein (all the significant peaks have been marked; refer to table below)

Table 3.8: Description of the marked peaks along with expected mode and range of overlayed spectra.

	Type	Bond	Range (cm^{-1})	Mode	Comment
1. Polymer reference (Bio-Rad database)	PVP	CH_2 CH_2 C=O CH_2 CN	2950-2910 2920-2840 1690-1640 1490-1420 1290-1250	Anti-symmetric Symmetric Stretching Deformation Stretching	The tertiary amide poly (vinyl pyrrolidone), PVP, shows a strong -C=O absorption band near 1660 cm^{-1}. Other characteristic features are the medium intensity CH_2 deformation bands near 1420 cm^{-1} and the C-N doublet near 1280 cm^{-1}.

	Type	**Expected Bond**	**Observed value (cm^{-1})**	**Expected mode**	**Comment**
2. Polymer measured **[Fig. 3.24]**	PVP-OD 20%AA (12KDa)	CH_2 CH_2 **C=O** CH_2 CN	2919 2849 **1646** 1422 1287	Anti-symmetric Symmetric Stretching Deformation Stretching	All the characteristic chemical vibrations are present and positionally, well within the range provided in the PVP reference. * Appearance of small peak at 1716 cm^{-1} comes from C=O stretch present in acrylic acid group of PVP-OD 20%AA.
	Type	**Expected Bond**	**Observed value (cm^{-1})**	**Expected mode**	**Comment**
3. Polymer measured **[Fig. 3.24]**	PVP-OD 20%AA crosslinked 5-Aminofluorescein (12KDa)	CH_2 CH_2 **C=O** CH_2 CN	2919 2849 **1659** 1422 1287	Anti-symmetric Symmetric Stretching Deformation Stretching	* The main C=O stretch shows a peak shift compared to PVP-OD 20%AA spectrum. * The small peak at 1716 cm^{-1} associated with acrylic acid in PVP-OD 20%AA sample is affected drastically.

The results obtained from comparison of PVP-OD 20% acrylic acid and PVP-OD 20% crosslinked 5-Aminofluorescein provides following information:

- The C=O stretching band related to the acrylic acid group (refer to FTIR analysis discussion above) at 1716 cm^{-1} in PVP-OD 20% AA spectrum is drastically affected
- The main C=O stretching band associated with the pyrrolidone ring shows a significant peak shift
- All the other absorption bands (CH_2 antisymmetric, symmetric and deformation, CN doublet stretching band) are present in the crosslinked polymer spectrum and positionally, overlaps with the PVP-OD 20% AA spectrum

The appearance of three new characteristic peaks (*1780, *1728 and *1089) and the significant peak shift of the stretching band (1659 cm^{-1}) in the PVP-OD 20% crosslinked 5-Aminofluorescein spectrum needs further clarification and explanation. We have correlated the measured PVP-OD 20% crosslinked 5-Aminofluorescein spectrum with the reported spectral information available in the literature related to FTIR study of EDC/NHS amidation reactions involving poly (acrylic acid) polymer.

The characteristic infrared bands assigned in the Table 3.9 denotes NHS-ester band near ~1740 cm^{-1} and 1780 cm^{-1} and amide associated band at 1660 cm^{-1} [42].

Table 3.9: Infrared Peak Assignments in the Carbonyl Stretching Region from 1500 to 2000 cm^{-1} [42].

1740	ν_{as} (imidyl C=O)	NHS-ester C=O antisymmetric stretch
1780	ν_{s} (imidyl C=O)	NHS-ester C=O symmetric stretch
1815	ν (ester C=O)	NHS-ester carbonyl stretch
1760	ν_{as} (anhydride C=O)	anhydride antisymmetric C=O stretch
1804	ν_{s} (anhydride C=O)	anhydride symmetric C=O stretch
1733	ν (ester C=O)	ester C=O stretch of tert-butyl ester, N-acylurea; L-leucine methyl ester[a]
1710	ν (acid C=O)	carboxylic acid C=O stretch
1660	ν (amide C=O)	peptide C=O stretch (amide I)

Based on the information provided in the Table 3.9, the peak shift of the stretching band (1659 cm^{-1}) in the PVP-OD 20% crosslinked 5-Aminofluorescein when compared to PVP-OD 20% AA peak position of C=O stretch at 1646 cm^{-1} can be explained by the positioning of peptide C=O stretch (amide I) at 1660 cm^{-1}. The appearance of the peak at 1728 cm^{-1} and 1780 cm^{-1} can be associated with the NHS-ester C=O antisymmetric stretch and the NHS-ester C=O symmetric stretch as mentioned in the table. According to [64], peak at 1089 cm^{-1} corresponds to asymmetric stretch of C-O-C present in the structure of 5-Aminofluorescein.

3.5.4 Characterization of produced nanocarriers via microelectrophoresis

Zeta-potential of polymeric micelles produced from different polymer samples (PVP-OD without acrylic acid, PVP-OD 20%AA, PVP-OD 100%AA and PVP-OD 20%AA crosslinked with 5-Aminofluorescein dye) was measured as the indication of system stability with the help of Zetasizer instrument (described in section 2.2.7).

It is a well-known fact that Zeta-potential is hugely influenced by pH conditions and concentration of colloidal particles as described in section 1.8.4. Based on this information, we designed an experiment to measure the zeta-potential behaviour of various PVP-OD based polymer samples with different pH and concentration conditions. The results obtained from these measurements are depicted in Figure.

Initially, we measured the Zeta-potential of PVP-OD polymer sample with varying pH conditions in water to evaluate the charge distribution without the presence of acrylic acid moiety in the polymer. The result is illustrated in Figure 3.25.

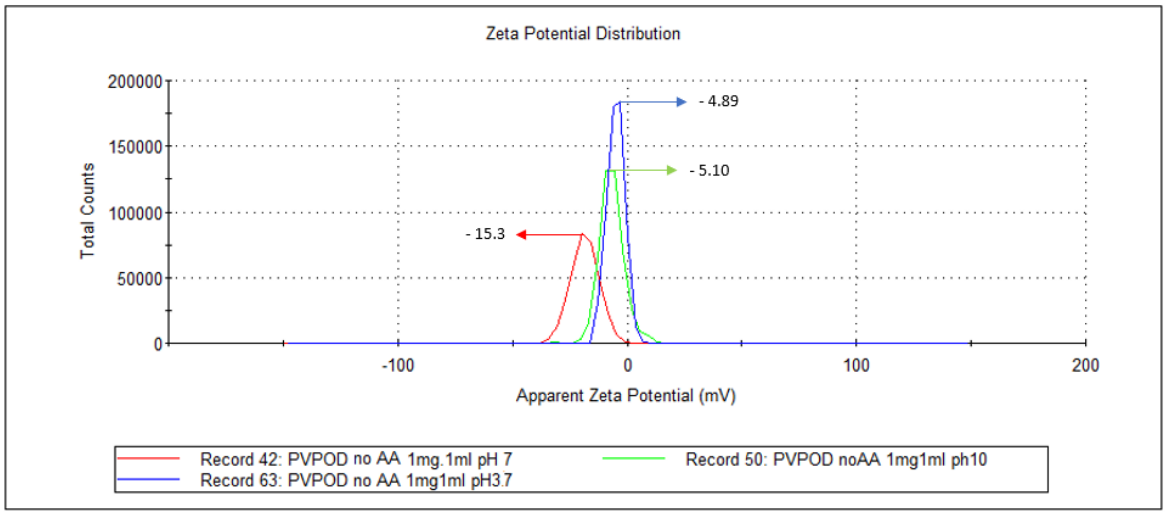

Figure 3.25: Zeta-potential distribution of PVP-OD without acrylic acid across a varying pH range (pH ~4, pH ~7 and pH ~10).

The result obtained from the Zeta-potential measurement of PVP-OD without acrylic acid shows a value of -4.89mV at pH ~4, -5.10mV at pH ~10 and significant shift in the value at pH~7 (-15.3mV).

Furthermore, we measured the Zeta-potential value of PVP-OD 20%AA and PVP-OD 100% AA with varying pH conditions in water. The results obtained from these measurements are illustrated in Figures 3.26 and 3.27

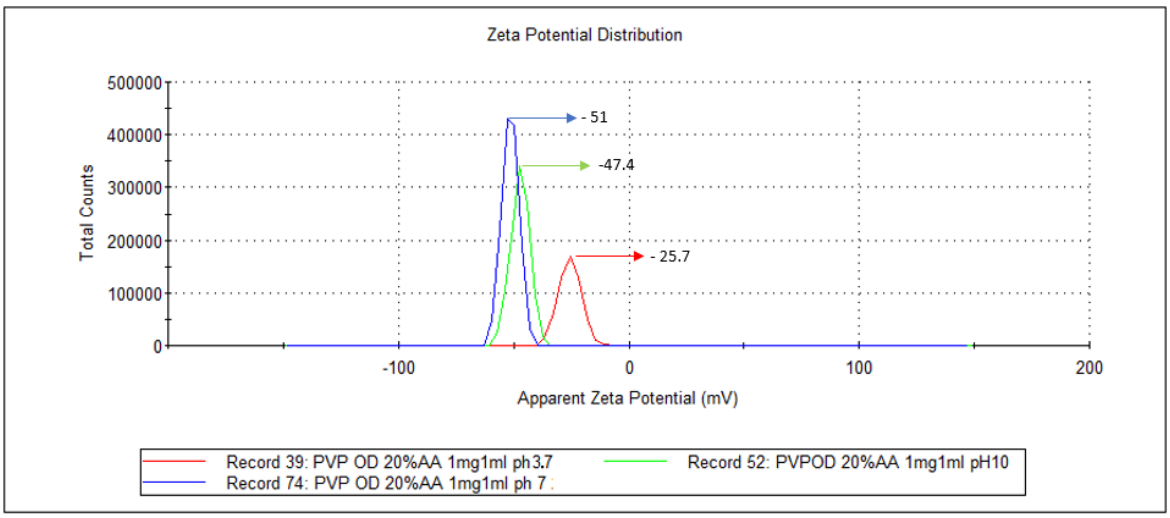

Figure 3.26: Zeta-potential distribution of PVP-OD without acrylic acid across a varying pH range (pH ~4, pH ~7 and pH ~10).

The result obtained from the Zeta-potential measurement of PVP-OD 20%AA shows a value of -25.7mV at pH ~4, -47.4mV at pH ~10 and significant shift in the value at pH~7 (-51mV).

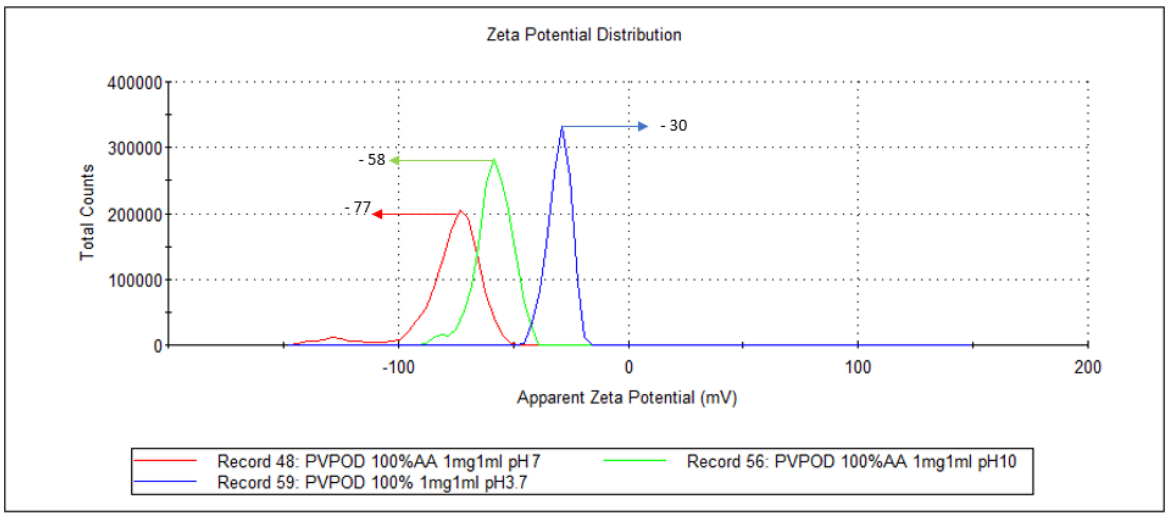

Figure 3.27: Zeta-potential distribution of PVP-OD 100%AA across a varying pH range (pH ~4, pH ~7 and pH ~10).

The result obtained from the Zeta-potential measurement of PVP-OD 20%AA shows a value of -30mV at pH ~4, -58mV at pH ~10 and significant shift in the value at pH~7 (-77mV).

Finally, we analysed the Zeta-potential value of PVP-OD 20%AA crosslinked with 5-Aminofluorescein dye with varying pH conditions in water. The results obtained from these measurements are illustrated in Figure 3.28.

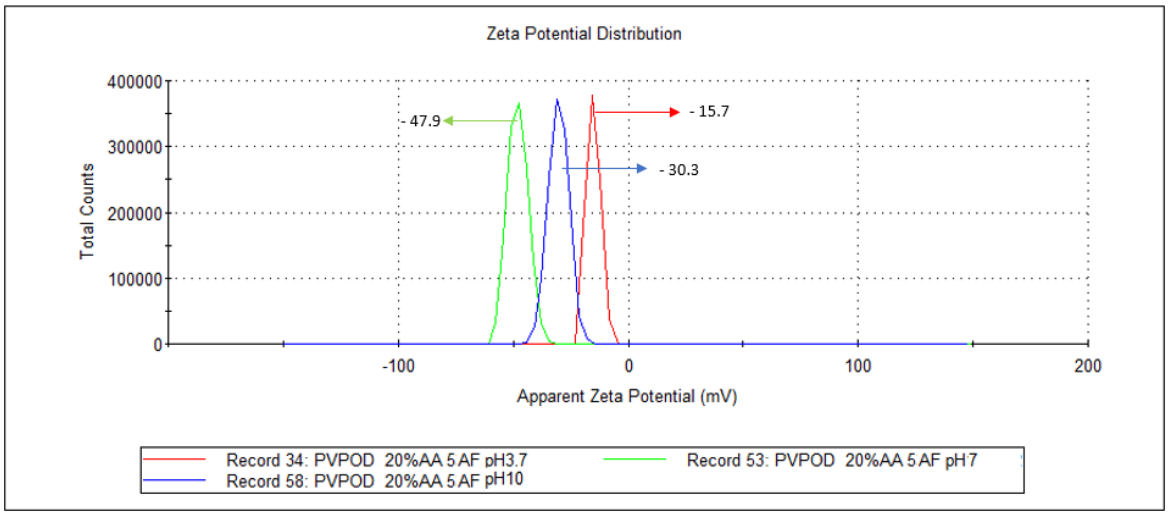

Figure 3.28: Zeta-potential distribution of PVP-OD 20%AA crosslinked with 5-Aminofluorescein dye across a varying pH range (pH ~4, pH ~7 and pH ~10).

The charge distribution obtained from the Zeta-potential measurement of PVP-OD 20%AA crosslinked with 5-Aminofluorescein shows a value of -15.7mV at pH ~4, -30.3mV at pH ~10 and significant shift in the value at pH~7 (-47.9mV). Table 3.10 summarises the results obtained from Zeta-potential measurement of PVP based polymer samples.

Table 3.10: Zeta-potential values obtained from PVP based samples across a varying pH range (4-10)

Material	Zeta potential value [mV]		
	pH 3.7	**pH 7**	**pH 10**
PVP-OD	-4.89	-15.3	-5.10
PVP-OD-20% AA	-25.7	-51	-47.4
PVP-OD-100% AA	-30	-77	-58
PVP-OD-20%AA-5AF	-15.7	-47.9	-30.3

Following observations can be extrapolated from a comparative study of the Zeta-potential values obtained from the measurement of various PVP based samples:

- Zeta-potential value at pH~7 seems to be the highest among all the polymer samples under investigation
- There is significant change in the Zeta-potential value as we move from acidic to neutral pH range across all the polymer samples under analyses
- The presence of acrylic acid moiety obviously, provides extra negative potential to the polymeric entity in water (PVP-OD no AA vs carboxylated PVP samples)

- Upon comparison of charge distribution values between non-conjugated PVP-OD 20%AA and PVP-OD 20%AA crosslinked 5-Aminofluorescein dye reveals a significant drop in the Zeta-potential value of the crosslinked sample (Figure 3.29)

These trends obtained from Zeta-potential analyses reflects the fact that pH titration studies are very important in order to get a realistic picture about the charge distribution of colloidal particles. One of the key observations extracted from this measurement is the change is charge distribution of non-conjugated and conjugated PVP-OD 20%AA sample. It might be an indicator that amide bond is present in the sample thus imparting a positive charge $-NH^{+}$ group (Figure 3.29) and therefore reducing the overall charge distribution.

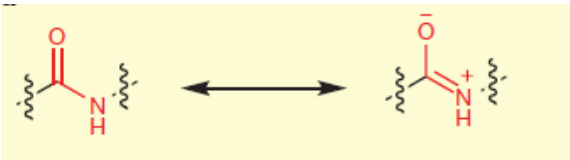

Figure 3.29: Illustration of resonance structures of an amide group [66].

Apart from the pH factor, we also evaluated the effect of concentration on Zeta-potential values. The results obtained can be found in the Appendix A.1 as they didn't reflect any significant influence on the Zeta-potential value. Irrespective of this, it is quite important to analyse the concentration factor when it comes to Zeta-potential evaluation of complex molecules such as polymers. The zeta-potential values obtained from high sample concentration might not be realistic due to the viscosity factor. For example, "Polyurethane Complex samples probably exhibit non-Newtonian behaviour and, therefore, it is uncertain which viscosity value is the most appropriate to use for the conversion of the electrophoretic mobility data into zeta potential values" [67].

3.5.5 DLS analysis of produced nanocarriers

For obtaining information about size and polydispersity index (PdI) of produced nanocarriers, DLS measurment was performed on Zetasizer instrument. Preparation of all samples that were subjected to DLS is described in section 2.2.6. All measurments were repeated three times and their averaged values are presented in Table 3.11

Table 3.11: Results obtained from DLS measurement of produced nanocarriers

	Preparation method	Average hydrodynamic diameter [nm]	PdI	Presence of large aggregates	Comment
PVP-OD-20%AA	*Cosolvent evaporation*	***234,6***	***0,357***	+	*Nanocarriers with desired size were absent*
	Dialysis	***173,4***	***0,219***	+	*Desired size of nanoaggregates was obtained*
PVP-OD-5-Aminofluorescein	*Direct dissolution*	***97,43***	***0,530***	+	*Sample refer to quality report*
	Cosolvent evaporation	***168,6***	***0,114***	+	*Desired size of nanocarrierss was obtained*
	Dialysis	***105,6***	***0,172***	+	*Desired size of nanoacarriers was obtained*

Nanocarriers prepared by direct dissolution method.

After conjugation mechanism, obtained PVP-OD-5-Aminofluorescein polymer, in contrast to its not crosslinked variation, was well soluble in water. Since direct dissolution method could not be employed for original PVP-OD-20%AA, we decided to examine possibility of creating polymeric micelles from fluorescently labelled polymer via direct dissolution method. According to the literature [5], direct dissolution is regarded as ineffective method for polymers with long hydrophobic part, although ultrasonic treatment might allow micelle formation by this approach. Although, even after sonication and filtration of obtained polymer solution through 0,2 μm cellulose filter, direct dissolution method resulted in formation of nanoaggregates with size of 172,2nm and a small fraction of 28,32nm (see appendix X) with relatively high PdI value of 0,530. According to DLS Zetasizer software, samples with such PdI value is regarded as polydispersed and entire measurement was referred to quality report. Based on obtained information it can be deduced that nanoaggregates based on PVP-OD-5-Aminofluorescein produced by direct dissolution method are highly unstable and tend to aggregate, which is in accordance with literature [5] and therefore excludes them from potential drug delivery application. Consequently, we employed dialysis and cosolvent evaporation method as a gentler alternative for micelle production.

Cosolvent evaporated nanocarriers

In order to overcome complications related to direct dissolution method, cosolvent evaporation was chosen as subsequent approach for polymeric micelles production. Implementation of this method resulted in formation of nanoaggregates with average hydrodynamic diameter of 168,6nm and 173,4nm for PVP-OD-5-Aminofluorescein and PVP-OD-20%AA respectively. Even though average size of nanocarriers was higher than expected, fraction of desired nanocarriers with size around 70nm was observed for both polymers used. Moreover, both samples exhibited satisfactory PdI value, which was the lowest of all employed methods and indicates a monodisperse size distribution desired in formation of nanoparticles. Nonetheless, regardless the sonication and filtration of the samples with 0,2 µm cellulose filter, particles with size over 200nm were still present. For both PVP-OD-5-Aminofluorescein and PVP-OD-20%AA intensity distribution obtained from DLS was manifested by a very broad peak, therefore number distribution was chosen as a more realistic representation of results (Figure 3.30 and 3.31).

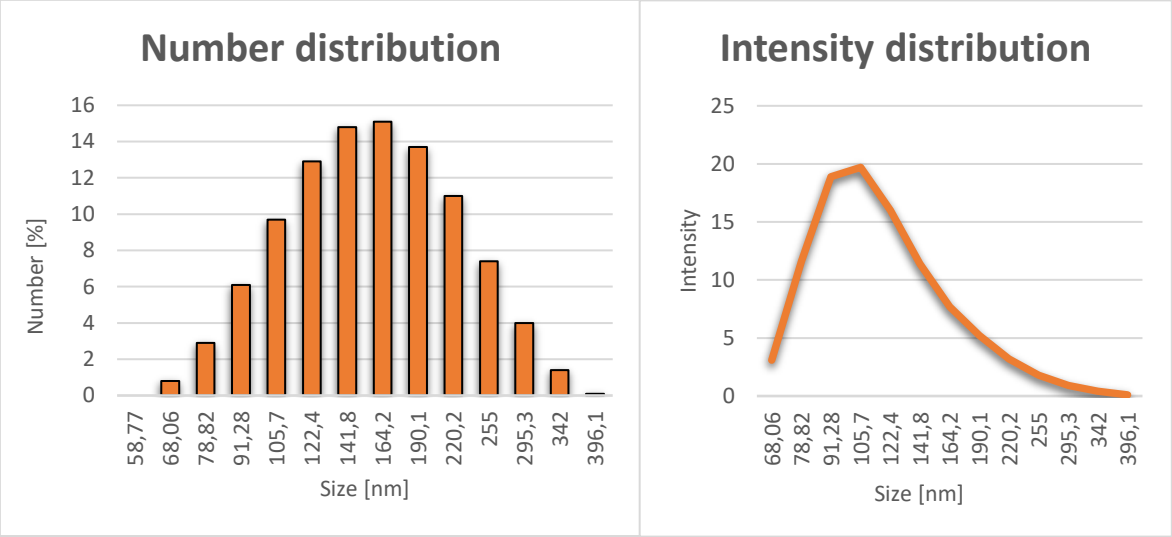

Figure 3.30: (left) Number size distribution and (right) Intensity size distribution of PVP-OD-5-Aminofluorescein Dil loaded nanocarriers prepared via cosolvent evaporation method.

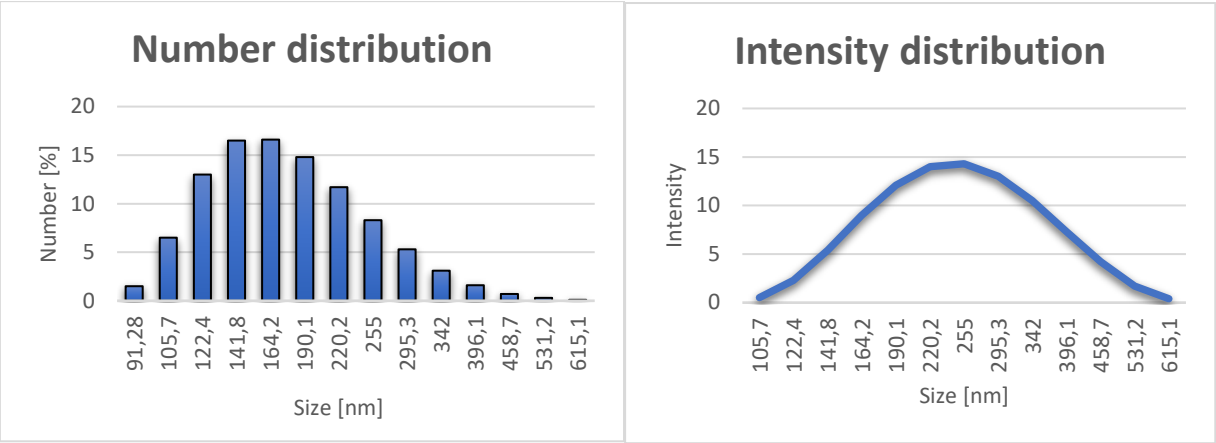

Figure 3.31: (left) Number size distribution and (right) Intensity size distribution of PVP-OD-20%AA-Dil loaded nanocarriers prepared via cosolvent evaporation method.

According to [5], for some of the polymers with long hydrophobic tail, cosolvent evaporation method might result in non-equilibrium micelles which tend to aggregate. After extensive study and analyses related to the physical and chemical properties of our polymer, it can be said that it requires very long solvation time. Our polymer is partially soluble in water, it might take a long time for a portion of it to actually go into the solution even if under constant heavy agitation (via magnetic stirring). Apart from this , it was also observed that even after extensive evaporation, our polymer samples still contained low amount of ethanol. In order to overcome these complications, dialysis of obtained solution could be implemented.

Nanocarriers prepared by dialysis method

According to the literature [5], dialysis method is probably the most suitable approach for polymeric micelle formation from polymers with considerable hydrophobic segment. Our results confirm this statement, since nanocarriers produced by dialysis method exhibited the lowest average hydrodynamic diameter with value of 105,6nm for PVP-OD-5-Aminofluorescein and 173,4nm for PVP-OD-20%AA (Figure 3.32 and 3.33). For modified polymer, PdI value was higher than the one obtained from cosolvent evaporation method, although in terms of PVP-OD-20%AA opposite trend was observed. Nonetheless, for both of the materials PdI value was not exceeding 0,22, indicating a monodisperse size distribution. Nanocarriers produced from PVP-OD-5-Aminofluorescein via dialysis method exhibited the biggest fraction of desired sized particles in range of ~50 to 80nm with smallest contribution of >100nm aggregates. It can be explained by a fact, that during dialysis water gradually replaces the organic solvent and triggers self-assembly process in more controlled fashion that is in the case of cosolvent evaporation method.

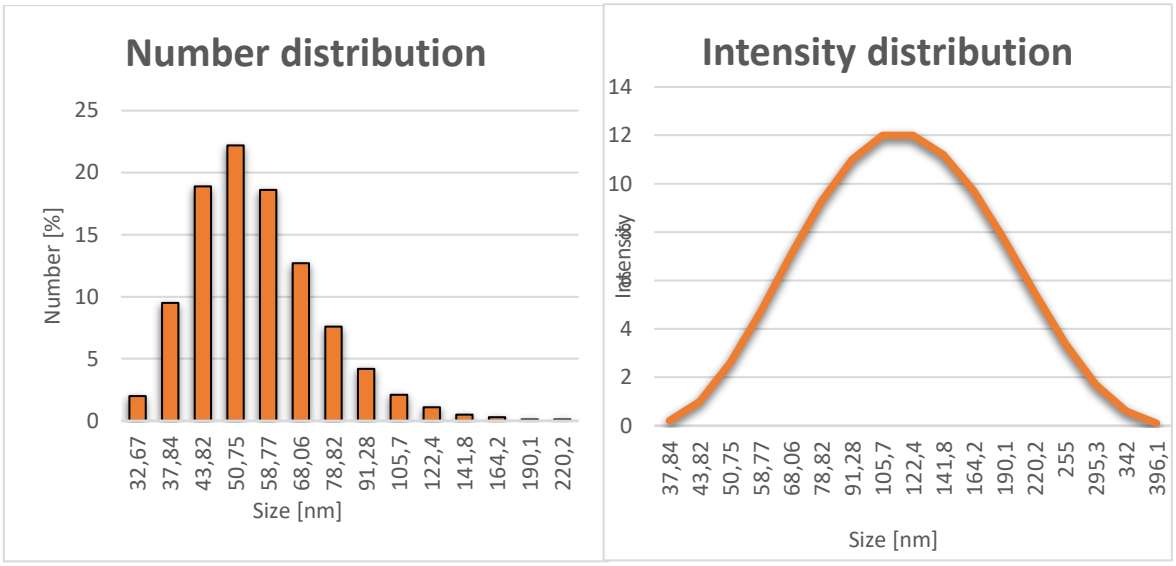

Figure 3.32: (left) Number size distribution and (right) Intensity size distribution of PVP-OD-5-Aminofluorescein Dil loaded nanocarriers prepared via dialysis method.

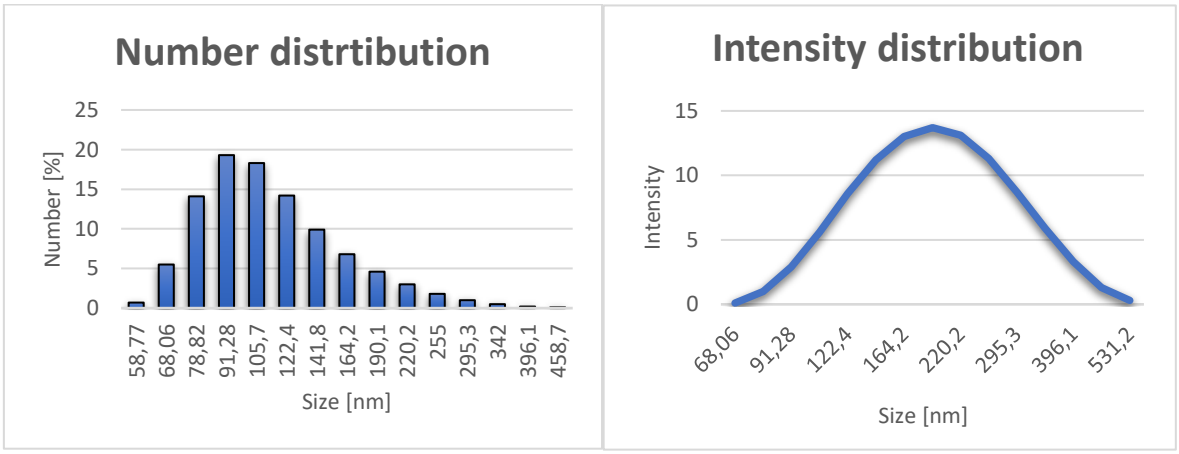

Figure 3.33: (left) Number size distribution and (right) Intensity size distribution of PVP-OD-20%AA Dil loaded nanocarriers prepared via dialysis method.

Regardless the preparation method and used polymer, large aggregates (>200nm) which could pass through 0,2 µm cellulose filter were present in all the samples. One of possible scenarios might be that smaller particles tend to aggregate after passing the filter. Moreover, information about polymer molecular weight distribution was not provided by the research group from which we received the polymer samples and most likely PVP-OD-20%AA is highly polydispersed, which could possibly explain the presence of large aggregates in DLS results.

3.5.6 Fluorescence microscopy results

In order to evaluate the possibility of studying the uptake mechanisms of the produced polymeric micelles in mammalian cells, we performed mammalian cell culture followed by Fluorescence microscopy imaging with the help of our student colleague Miquel Santos Llinàs under the guidance and supervision of Associate Professor Pablo Pennissi (mentioned in section 3.2.8.). The results obtained shows appearance of huge aggregates with no to fluorescence signal, depicted in Figure 3.34

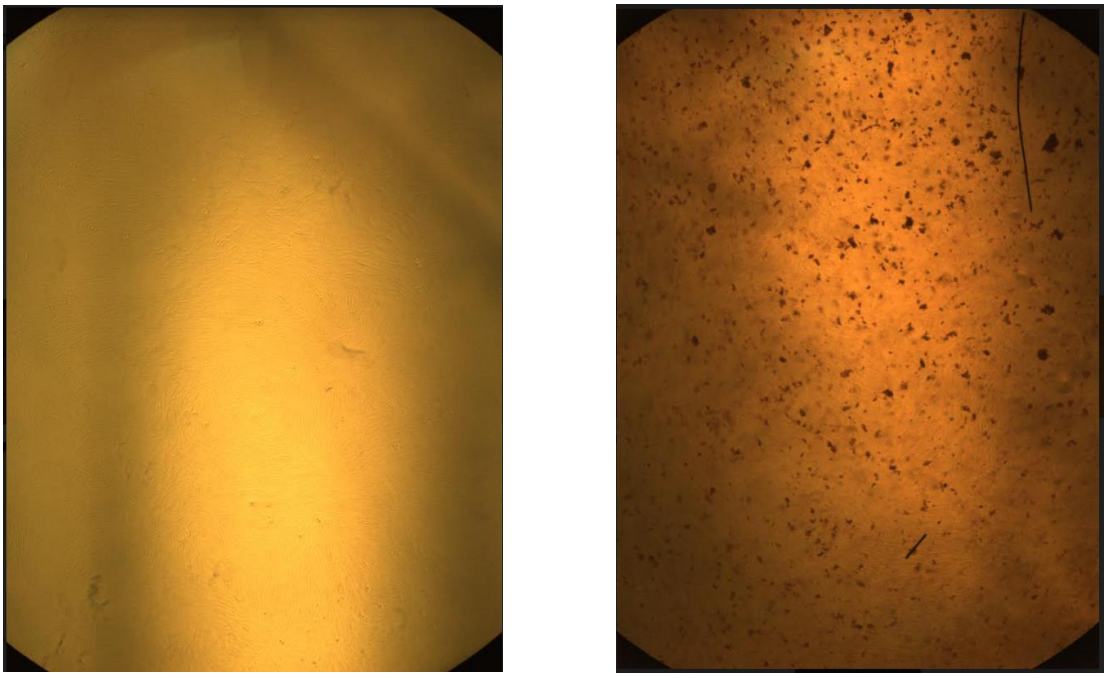

Figure 3.34: Fluorescence microscopy imaging before incubation of polymeric micelles (left) and after incubation PVP-OD-5-AF+DiI micelles produced by co-solvent evaporation method (right)

Due to the inconclusive nature of the results obtained from fluorescence microscopy imaging of the produced polymeric micelles loaded with DiI dye, we decided to exclude the images obtained from dye labelled polymeric micelles by different approaches (all the other images related to mammalian cell study can be found in Appendix A.2)

4. Conclusion

In this master thesis, we studied different aspects of amphiphilic block copolymer poly-N-vinyl-2-pyrrolidone modified with acrylic acid (PVP-OD AA 12kDa) containing thiooctadecyl-terminated block. We delved into the polymer chemistry/dynamics to understand the physical and chemical properties associated with the amphiphilic nature of our polymer. FT-IR spectroscopy was performed in order to analyse the different chemical groups present in the polymer with varying degree of carboxylation (PVP-OD with 0%, 20% and 100% acrylic acid). The most crucial finding of this FT-IR anlayses was that the C=O stretch at 1716 cm^{-1} in PVP-OD 20% AA is associated with acrylic acid part of the polymer. Later in the study, this information was used to evaluate the presence of peptide (amide I) strectch in PVP-OD 20%AA crosslinked 5-Aminofluorescein sample.

The solvent compatibility evaluation with water and various other oragnic solvents was performed with the help of simple solubiltiy test and the information from Hansen solubility parameter. The results obtained from the solvent compatibility study revealed that ethanol is the best solvent for our polymer's dissolution and its futher modfication via EDC/NHS chemistry. In order to operate at the optimum conditons for the polymer crosslinking reaction dissolved in ethanol, we used radius of gyration (obtained from DLS approximation results) to calculate the Overlap concentration which was around 0.6 to 1mg/mL. The information acquired from the study of polymer chemistry/dynamics helped us to design suitable reaction conditions for PVP-OD20%AA while performing the EDC/NHS conjugation reaction. The results obtained from UV-Visible and Fluorescence spectroscopy revealed that the amine group present in the dye is fluorescently affected, which is indicated by the red shift [comparison of free 5-Aminofluorescein dye (λ_{abs} 488nm, λ_{em}514nm) with the conjugated one (λ_{abs} 492nm, λ_{em}525nm)]. The FT-IR analyses of the PVP-OD 20%AA crosslinked 5-Aminofluorescein cemented the successful EDC/NHS chemistry by the evaluation of the appearance of three new characteristic peaks (*1780, *1728 and *1089) and the significant peak shift of the stretching band (1659 cm^{-1}).

Polymeric micelles were produced by three different methods (direct dissolution, co-solvent evaporation and dialysis method) and their size and charge distribution were determined with the help of Zetasizer instrument. The zeta-potential was evaluated taking the influence of pH and concentration of particles into account. The results obtained from DLS and zeta-potential revealed that some fraction of the polymer produced micellar like aggregates (50 -60 nm) whereas a major portion of it appeared as large aggregates. This was evident in the Fluorescence microscopy study of the fluorescently labelled DiI loaded polymeric micellar aggregates.

PVP based polymeric micelles can be used to elucidate the uptake mechanism, as the polymer can be fluorescently labelled so its fate upon cellular uptake can be studied

independently from that of the hydrophobic load, which can be modelled with a hydrophobic fluorescent dye such as DiI, imparting a different emission profile to the inner-core of the polymeric micelle. Nonetheless, strategy to exclude unwanted aggregates has to be developed in order to efficiently use these PVP based polymeric micelles for investigation of uptake mechanism by mammalian cells.

5. Bibliography

1. Nishiyama, N., & Takemoto, H. (2021). Encyclopedia of Polymeric Nanomaterials. *Encyclopedia of Polymeric Nanomaterials*, 1–7. https://doi.org/10.1007/978-3-642-36199-9
2. Luo, Y., Yao, X., Yuan, J., Ding, T., & Gao, Q. (2009). Preparation and drug controlled-release of polyion complex micelles as drug delivery systems. *Colloids and Surfaces. B, Biointerfaces*, *68*(2), 218—224. https://doi.org/10.1016/j.colsurfb.2008.10.014
3. Dobrawa, R., & Würthner, F. (2005). Metallosupramolecular approach toward functional coordination polymers. *Journal of Polymer Science, Part A: Polymer Chemistry*, *43*(21), 4981–4995. https://doi.org/10.1002/pola.20997
4. Xu, W., Ling, P., & Zhang, T. (2013). Polymeric Micelles, a Promising Drug Delivery System to Enhance Bioavailability of Poorly Water-Soluble Drugs. *Journal of Drug Delivery*, *2013*(1), 1–15. https://doi.org/10.1155/2013/340315
5. Kapse, A., Anup, N., Patel, V., Saraogi, G. K., Mishra, D. K., & Tekade, R. K. (2019). Polymeric micelles: A ray of hope among new drug delivery systems. In *Drug Delivery Systems*. https://doi.org/10.1016/B978-0-12-814487-9.00006-5
6. Adams, M. L., Lavasanifar, A., & Kwon, G. S. (2003). Amphiphilic block copolymers for drug delivery. *Journal of Pharmaceutical Sciences*, *92*(7), 1343–1355. https://doi.org/10.1002/jps.10397
7. Jhaveri, A. M., & Torchilin, V. P. (2014). Multifunctional polymeric micelles for delivery of drugs and siRNA. *Frontiers in Pharmacology*. https://doi.org/10.3389/fphar.2014.00077
8. Savić, R., Eisenberg, A., & Maysinger, D. (2006). Block copolymer micelles as delivery vehicles of hydrophobic drugs: micelle-cell interactions. *Journal of drug targeting*, *14*(6), 343–355. https://doi.org/10.1080/10611860600874538
9. Gaucher, G., Dufresne, M. H., Sant, V. P., Kang, N., Maysinger, D., & Leroux, J. C. (2005). Block copolymer micelles: preparation, characterization and application in drug delivery. *Journal of controlled release : official journal of the Controlled Release Society*, *109*(1-3), 169–188. https://doi.org/10.1016/j.jconrel.2005.09.034
10. Burt, H. M., Zhang, X., Toleikis, P., Embree, L., & Hunter, W. L. (1999). Development of copolymers of poly(D,L-lactide) and methoxypolyethylene glycol as micellar carriers of paclitaxel. *Colloids and Surfaces B: Biointerfaces*, *16*(1–4), 161–171. https://doi.org/10.1016/S0927-7765(99)00067-3
11. Plapied, L., Duhem, N., des Rieux, A., & Préat, V. (2011). Fate of polymeric nanocarriers for oral drug delivery. *Current Opinion in Colloid and Interface Science*, *16*(3), 228–237. https://doi.org/10.1016/j.cocis.2010.12.005
12. Mccarthy, W. (2016). Polymeric Drug Delivery Techniques. *Aldrich Material Science*, (5), 2–5.
13. Rapoport, N. (2007). Physical stimuli-responsive polymeric micelles for anti-cancer drug delivery. *Progress in Polymer Science (Oxford)*. https://doi.org/10.1016/j.progpolymsci.2007.05.009

14. Gothwal, A., Khan, I., & Gupta, U. (2016). Polymeric Micelles: Recent Advancements in the Delivery of Anticancer Drugs. *Pharmaceutical Research*. https://doi.org/10.1007/s11095-015-1784-1
15. Danhier, F., Feron, O., & Préat, V. (2010, December 1). To exploit the tumor microenvironment: Passive and active tumor targeting of nanocarriers for anti-cancer drug delivery. *Journal of Controlled Release*, Vol. 148, pp. 135–146. https://doi.org/10.1016/j.jconrel.2010.08.027
16. Kuskov, A. N. et al. Preparation and characterization of amphiphilic poly-N-vinylpyrrolidone nanoparticles containing indomethacin. J. Mater. Sci. Mater. Med. (2010).
17. Kulthe, S. S., Choudhari, Y. M., Inamdar, N. N. & Mourya, V. Polymeric micelles: Authoritative aspects for drug delivery. Designed Monomers and Polymers (2012).
18. Zhang, Y., Huang, Y. & Li, S. Polymeric micelles: Nanocarriers for cancer-targeted drug delivery. AAPS PharmSciTech (2014).
19. Qu, G., Yao, Z., Zhang, C., Wu, X. & Ping, Q. PEG conjugated N-octyl-O-sulfate chitosan micelles for delivery of paclitaxel: In vitro characterization and in vivo evaluation. Eur. J. Pharm. Sci. (2009).
20. Woo, E. M. & Chang, L. Tacticity in Vinyl Polymers. in Encyclopedia of Polymer Science and Technology (2011).
21. Kulikov, P. P., Kuskov, A. N., Goryachaya, A. V., Luss, A. N. & Shtil'man, M. I. Amphiphilic poly-n-vinyl-2-pyrrolidone: Synthesis, properties, nanoparticles. Polym. Sci. - Ser. D (2017).
22. Luss, A. L. et al. Nanosized carriers based on amphiphilic poly-N-vinyl-2-pyrrolidone for intranuclear drug delivery. Nanomedicine (2018).
23. Kariduraganavar, M. Y., Kittur, A. A. & Kamble, R. R. Polymer Synthesis and Processing. in Natural and Synthetic Biomedical Polymers (2014).
24. Koczkur, K. M., Mourdikoudis, S., Polavarapu, L. & Skrabalak, S. E. Polyvinylpyrrolidone (PVP) in nanoparticle synthesis. Dalt. Trans. (2015).
25. Chari, K. & Lenhart, W. C. Effect of polyvinylpyrrolidone on the self-assembly of model hydrocarbon amphiphiles. J. Colloid Interface Sci. (1990).
26. Prochazka, K., Martin, T. J., Webber, S. E. & Munk, P. Onion-type micelles in aqueous media. Macromolecules (1996).
27. Pleštil, J. et al. Small-angle neutron scattering study of onion-type micelles. Macromol. Chem. Phys. (2001).
28. Tera, I. *POLYMER SOLUTIONS An Introduction to Physical Properties* (2002).
29. Chanda, M. *Introduction to Polymer Science and Chemistry*. *Introduction to Polymer Science and Chemistry* (2013).
30. Polymer chemistry: introduction to an indispensable science. Choice Rev. Online (2004).
31. Hansen, C. M. Solubility parameters - an introduction. in *Hansen Solubility Parameters: A Users Handbook, Second Edition* (2007).
32. Allan F.M. Barton, CRC Handbook of Solubility Parameters and Other Cohesion Parameters, Second Edition (1991).
33. Polymer properties database. Available at: https://www.polymerdatabase.com/polymer. (Accessed: 12th February 2021)
34. Batrakova, E. V., Bronich, T. K., Vetro, J. A., & Kabanov, A. V. (2006). Polymer micelles as drug carriers. *Nanoparticulates as Drug Carriers*, 57–93. https://doi.org/10.1142/9781860949074_0005

35. Hussain, M. A., Muhammad, G., Haseeb, M. T., & Tahir, M. N. (2019). *Quince Seed Mucilage: A Stimuli-Responsive/Smart Biopolymer*. https://doi.org/10.1007/978-3-319-95990-0_19
36. Liu, J., Xiao, Y., & Allen, C. (2004). Polymer-drug compatibility: a guide to the development of delivery systems for the anticancer agent, ellipticine. Journal of pharmaceutical sciences, 93(1), 132–143. https://doi.org/10.1002/jps.10533
37. Yang, L., Wu, X., Liu, F., Duan, Y., & Li, S. (2009). Novel biodegradable polylactide/poly(ethylene glycol) micelles prepared by direct dissolution method for controlled delivery of anticancer drugs. Pharmaceutical Research, 26(10), 2332–2342. https://doi.org/10.1007/s11095-009-9949-4
38. Chen, Q., Zheng, J., Yuan, X., Wang, J., & Zhang, L. (2018). Folic acid grafted and tertiary amino based pH-responsive pentablock polymeric micelles for targeting anticancer drug delivery. Materials science & engineering. C, Materials for biological applications, 82, 1–9. https://doi.org/10.1016/j.msec.2017.08.026
39. Woraphatphadung, T., Sajomsang, W., Rojanarata, T., Ngawhirunpat, T., Tonglairoum, P., & Opanasopit, P. (2018). Development of Chitosan-Based pH-Sensitive Polymeric Micelles Containing Curcumin for Colon-Targeted Drug Delivery. AAPS PharmSciTech, 19(3), 991–1000. https://doi.org/10.1208/s12249-017-0906-y
40. Yang, X., Li, Z., Wang, N., Li, L., Song, L., He, T., … Gong, C. (2015). Curcumin-encapsulated polymeric micelles suppress the development of colon cancer in vitro and in vivo. *Scientific Reports*, *5*(April), 1–15. https://doi.org/10.1038/srep10322
41. Fischer, M. J. E. Amine coupling through EDC/NHS: a practical approach. Methods Mol. Biol. (2010).
42. Wang, C., Yan, Q., Liu, H. B., Zhou, X. H., & Xiao, S. J. (2011). Different EDC/NHS activation mechanisms between PAA and PMAA brushes and the following amidation reactions. Langmuir, 27(19), 12058–12068. https://doi.org/10.1021/la202267p
43. Madison, S. A., & Carnali, J. O. (2013). PH optimization of amidation via carbodiimides. Industrial and Engineering Chemistry Research, 52(38), 13547–13555. https://doi.org/10.1021/ie401724m
44. Mourdikoudis, S., Pallares, R. M. & Thanh, N. T. K. Characterization techniques for nanoparticles: Comparison and complementarity upon studying nanoparticle properties. *Nanoscale* (2018).
45. Ronson. Uv/Vis/Ir Spectroscopy Analysis of Nanoparticles. *nanoComposix* (2012).
46. Rani, S., Mishra, S., Sharma, M., Nandy, A. & Mozumdar, S. Solubility and stability enhancement of curcumin in Soluplus® polymeric micelles: a spectroscopic study. J. Dispers. Sci. Technol. (2020).
47. Kumar, A., & Dixit, C. K. (2017). Methods for characterization of nanoparticles. *Advances in Nanomedicine for the Delivery of Therapeutic Nucleic Acids*, 44–58. https://doi.org/10.1016/B978-0-08-100557-6.00003-1
48. Stetefeld, J., McKenna, S. A., & Patel, T. R. (2016). Dynamic light scattering: a practical guide and applications in biomedical sciences. *Biophysical Reviews*, *8*(4), 409–427. https://doi.org/10.1007/s12551-016-0218-6
49. Bhattacharjee, S. (2016). DLS and zeta potential - What they are and what they are not? *Journal of Controlled Release*, *235*, 337–351. https://doi.org/10.1016/j.jconrel.2016.06.017

50. Malvern Panalytical Ltd. (2018). Dynamic light scattering: An introduction in 30 minutes. Tecnical note (MRK656-01). *Technical Note MRK656-01*, 1–8. Retrieved from https://www.malvernpanalytical.com/en/learn/knowledge-center/technical-notes/TN101104DynamicLightScatteringIntroduction
51. Kim, K. M., Kim, H. M., Lee, W. J., Lee, C. W., Kim, T. I., Lee, J. K., Jeong, J., Paek, S. M., & Oh, J. M. (2014). Surface treatment of silica nanoparticles for stable and charge-controlled colloidal silica. International journal of nanomedicine, 9 Suppl 2(Suppl 2), 29–40. https://doi.org/10.2147/IJN.S57922
52. Park, K., Kim, Y. & Lee, K. J. Analysis of deuterated water contents using FTIR bending motion. J. Radioanal. Nucl. Chem. 322, 487–493 (2019).
53. Ryu, S. R., Noda, I. & Jung, Y. M. Positional fluctuation of IR absorption peaks: Frequency shift of a single band or relative intensity changes of overlapped bands? Am. Lab. 43, 40–43 (2011).
54. MacLennan, M. S., Tie, C., Kovalchik, K., Peru, K. M., Zhang, X., Headley, J. V., & Chen, D. D. Y. (2016). Potential of capillary electrophoresis mass spectrometry for the characterization and monitoring of amine-derivatized naphthenic acids from oil sands process-affected water. *Journal of Environmental Sciences (China)*, *49*, 203–212. https://doi.org/10.1016/j.jes.2016.06.019
55. Available at: https://www.hansen-solubility.com/HSPiP/. (Accessed: 25th March 2021)
56. Linegar, K. L., Adeniran, A. E., Kostko, A. F. & Anisimov, M. A. Hydrodynamic radius of polyethylene glycol in solution obtained by dynamic light scattering. *Colloid J.* **72,** 279–281 (2010).
57. Kuo, J. W., Swarm, D. A., & Prestwich, G. D. (1991). Chemical Modification of Hyaluronic Acid by Carbodiimides. *Bioconjugate Chemistry*, *2*(4), 232–241. https://doi.org/10.1021/bc00010a007
58. Nakajima, N.; Ikada, Y. Mechanism of amide formation by carbodiimide for bioconjugation in aqueous media. Bioconjugate Chem. 1995, 6, 123−130.
59. Ko, Y. G.; Ma, P. X. Surface-grafting of phosphates onto a polymer for potential biomimetic functionalization of biomaterials. J. Colloid Interface Sci. 2009, 330,77−83
60. Dunetz, J. R., Magano, J., & Weisenburger, G. A. (2016). Large-Scale Applications of Amide Coupling Reagents for the Synthesis of Pharmaceuticals. *Organic Process Research and Development*, *20*(2), 140–177. https://doi.org/10.1021/op500305s
61. Munkholm, C., Parkinson, D. R. & Walt, D. R. Intramolecular Fluorescence Self-Quenching of Fluoresceinamine. *J. Am. Chem. Soc.* 112, 2608–2612 (1990).
62. McHedlov-Petrossyan, N. O. *et al.* 5-Aminofluoresceins Versus Fluorescein: Peculiarity of Fluorescence. *J. Phys. Chem. A* 123, 8860–8870 (2019).
63. McHedlov-Petrossyan, N. O., Cheipesh, T. A., Roshal, A. D., Doroshenko, A. O. & Vodolazkaya, N. A. Fluorescence of 5-Aminofluoresceins as an indicative process allowing one to distinguish between micelles of cationic surfactants and micelle-like aggregates. *Methods Appl. Fluoresc.* 4, (2016).
64. Defeyt, C., Langenbacher, J., & Rivenc, R. (2017). Polyurethane coatings used in twentieth century outdoor painted sculptures. Part I: Comparative study of various systems by means of ATR-FTIR spectroscopy. *Heritage Science*, *5*(1), 1–11. https://doi.org/10.1186/s40494-017-0124-7

65. Sam, S. et al. Semiquantitative study of the EDC/NHS activation of acid terminal groups at modified porous silicon surfaces. Langmuir 26, 809–814 (2010).
66. Pattabiraman, V. R. & Bode, J. W. Rethinking amide bond synthesis. *Nature* 480**,** 471–479 (2011).
67. Kaszuba, M., Corbett, J., Watson, F. M. N. & Jones, A. High-concentration zeta potential measurements using light-scattering techniques. in Philosophical Transactions of the Royal Society A: Mathematical, Physical and Engineering Sciences 368, 4439–4451 (2010).

6. Appendix

A1. Additional Zeta potential distribution (Concentration factor)

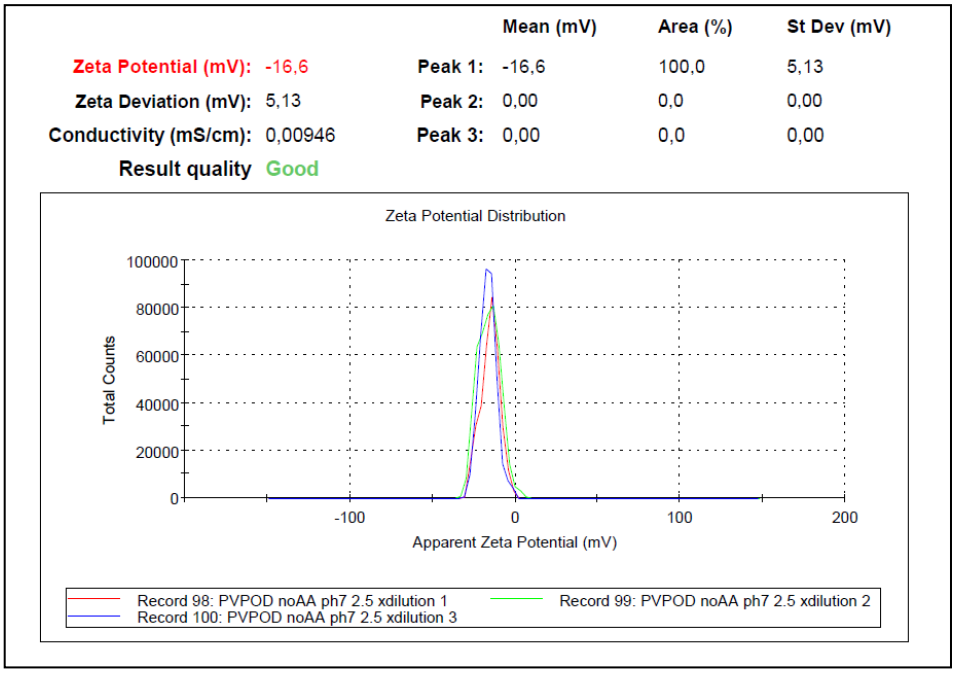

Figure A: Zeta-potential distribution of PVP-OD without acrylic acid in water (Initial concentration 1mg/mL, Sample diluted 2.5 times)

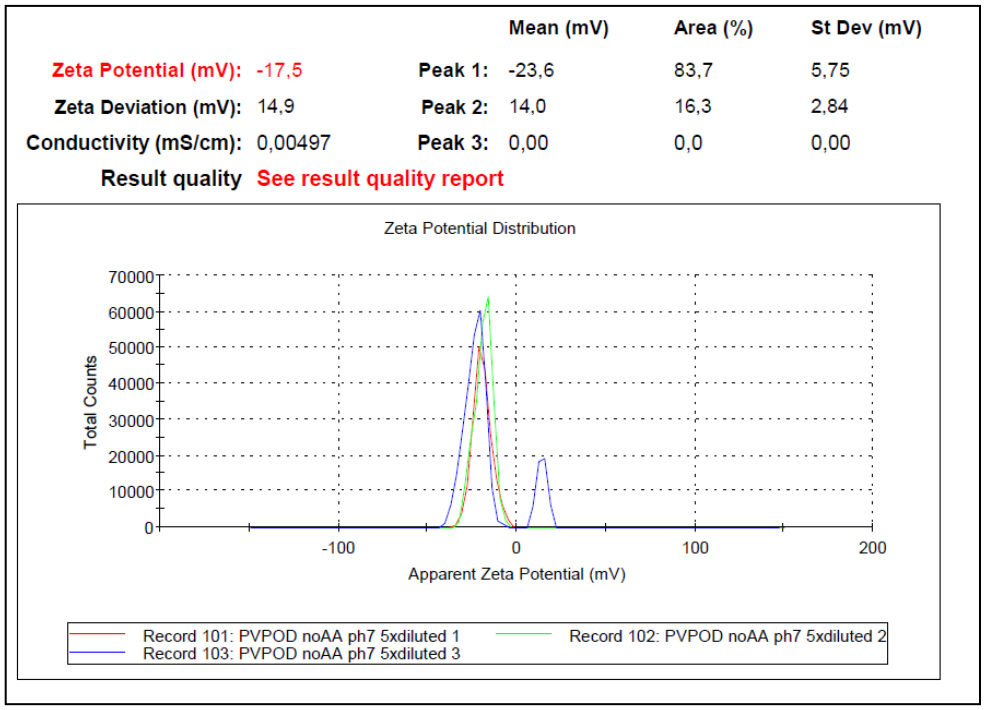

Figure B: Zeta-potential distribution of PVP-OD without acrylic acid in water (Initial concentration 1mg/mL, Sample diluted 5 times)

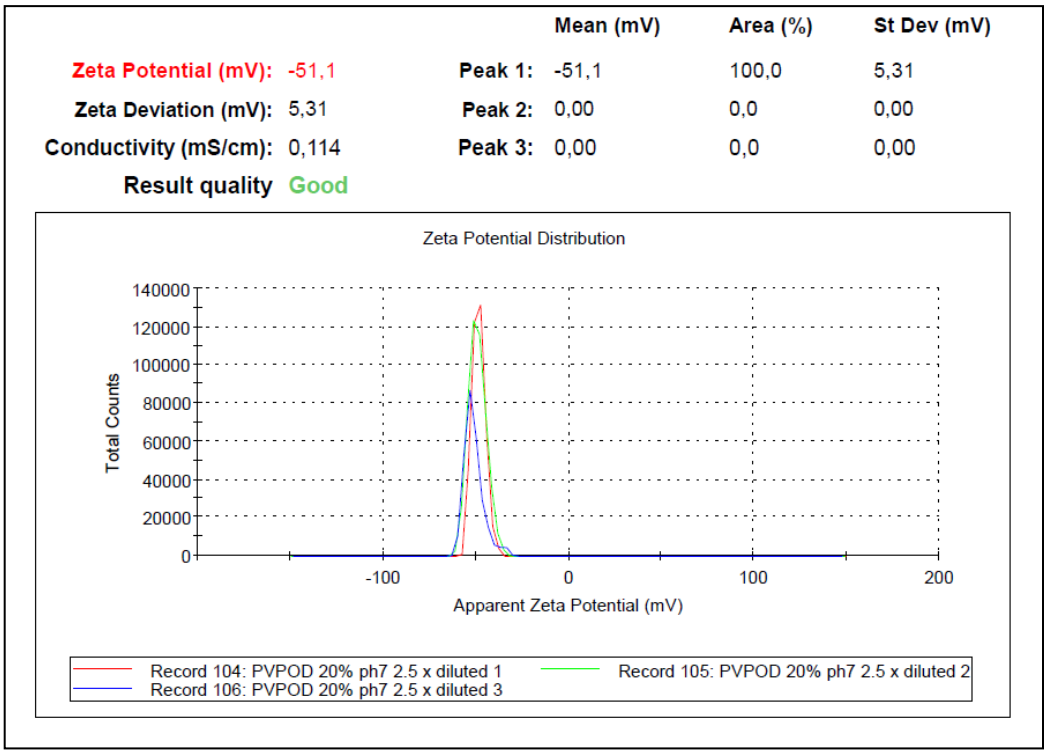

Figure C: Zeta-potential distribution of PVP-OD 20%AA in water (Initial concentration 1mg/mL, Sample diluted 2.5 times)

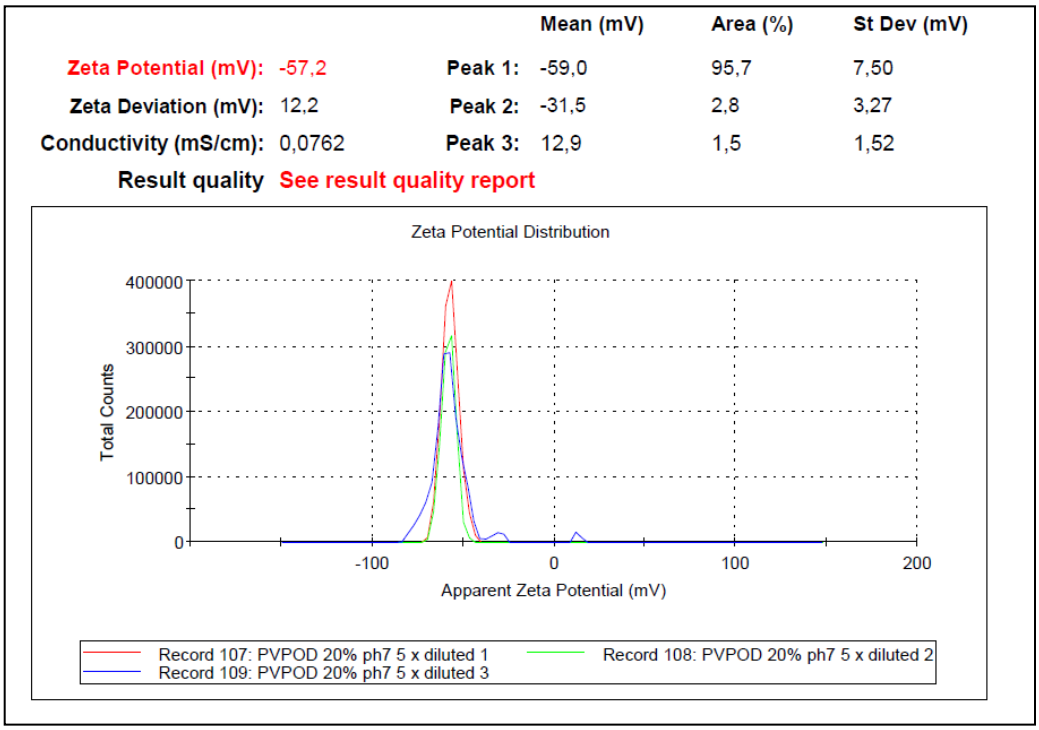

Figure D: Zeta-potential distribution of PVP-OD 20%AA in water (Initial concentration 1mg/mL, Sample diluted 5 times)

A2. Uptake possibility of produced polymeric micelles in mammalian cells

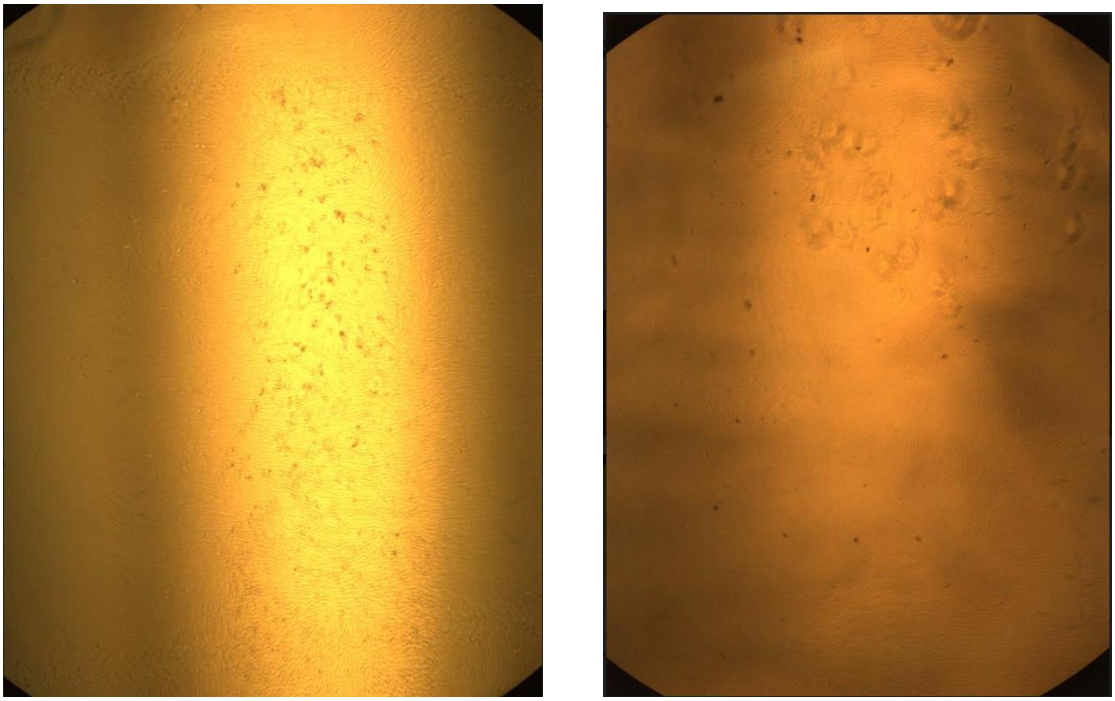

Figure E: Fluorescence microscopy imaging before incubation of polymeric micelles (left) and after incubation PVP-OD-5-AF+DiI micelles produced by dialysis method (out of focus) (right)

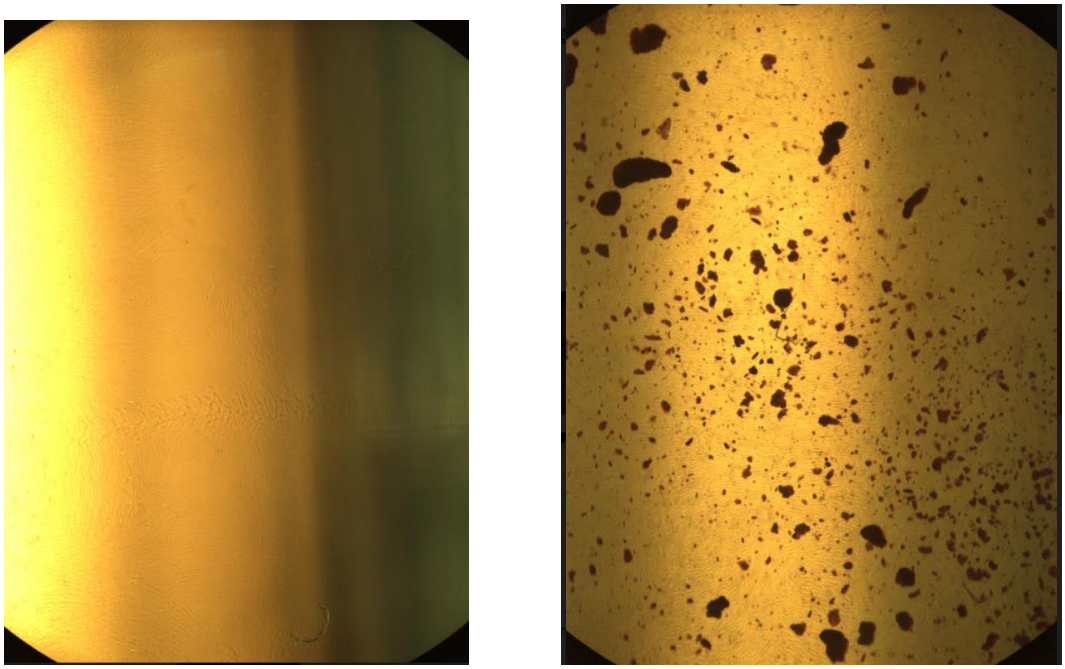

Figure F: Fluorescence microscopy imaging before incubation of polymeric micelles (left) and after incubation PVP-OD-5-AF+DiI micelles produced by co-solvent evaporation method (right)